PARAMETRIC STUDIES ON THE STABILITY OF STRINGER AND RING REINFORCED CIRCULAR SHELLS

A THESIS

Presented to

The Faculty of the Division of Graduate

Studies and Research

by

Joseph Scott Ford II

In Partial Fulfillment

of the Requirements for the Degree

Doctor of Philosophy

in the School of Aerospace Engineering

Georgia Institute of Technology

November 1970

PARAMETRIC STUDIES ON THE STABILITY

OF STRINGER AND RING REINFORCED

CIRCULAR SHELLS

Approved:

Chairman

Date approved by Chairman: 3 December 1970

ACKNOWLEDGMENTS

The contribution of Professor Wilfred H. Horton to this research is gratefully acknowledged. His timely advice and unselfish donation of time and talents provided the guidance and encouragement necessary for the successful completion of this work.

The author also wishes to express his appreciation to those research assistants who contributed to this work through the manufacture of test specimens and apparatus. It is hoped that the experience gained here will be of benefit to them in future experimental projects.

Finally, the sponsorship of the United States Air Force, and in particular Colonel Philip J. Erdle of the United States Air Force Academy, is acknowledged for providing the opportunity and support for me to undertake this program of study at the Georgia Institute of Technology.

TABLE OF CONTENTS

		Page
ACKNOWLEDGMENTS		ii
LIST OF TABLES		v
LIST OF FIGURES		vi
NOMENCLATURE		ix
SUMMARY		xi
Chapter		
I.	INTRODUCTION	1
II.	THEORETICAL CONSIDERATIONS	10
	Selection of Theory for Comparison to Experimental Results	
	The Southwell Plot	
	Harmonic Analysis	
III.	DESIGN OF THE EXPERIMENT	16
	Shell Classification System	
	Shell Manufacture	
	Test Fixture Design and Construction	
	Displacement Transducer Design	
	Strain Gage Installations	
	Data Acquisition System	
IV.	EXPERIMENTAL PROGRAM	48
	Axial Load Distribution	
	Test Procedures	
	Shells 0300 through 0500	
	Shells 0601 through 0608	
	Shells 0701 through 0911	
	Shells 1000 through 1008	
V.	DISCUSSION OF RESULTS	57
VI.	CONCLUSIONS AND RECOMMENDATIONS	91

Page

Appendices

A. BUCKLING EQUATIONS 93

B. DATA ACQUISITION PROGRAM 96

C. TEST DATA 102

LITERATURE CITED 140

VITA 144

LIST OF TABLES

Table		Page
1.	Summary of Stiffened Shell Test Programs	4
2.	Ring Thickness - Shell 06XX	28
3.	Ring Thickness - Shell 08XX	29
4.	Ring Thickness - Shell 09XX	30
5.	Ring Thickness - Shell 10XX	31
6.	Southwell Data Obtained from Displacements along Generators on Shell 0601	65
7.	Uniform Ring Configurations	81
8.	Repeated Buckling Tests for Shell 10XX	84
9.	Non-Uniform Ring Configurations	87

LIST OF FIGURES

Figure		Page
1.	Stringer Geometry and Section Properties, Shells 0300 through 0500 and Shell 08XX	20
2.	Stringer Geometry and Section Properties, Shell 06XX and Shell 0701	21
3.	Stringer Geometry and Section Properties, Shell 09XX and Shell 10XX	22
4.	Ring Forming Fixture in Oven	23
5.	Installation of End Ring Reinforcement	25
6.	End Stiffening Construction	26
7.	Ring Geometry - Fixed Ring Shells	27
8.	Ring Geometry - Shell 06XX	28
9.	Ring Geometry - Shell 08XX	29
10.	Ring Geometry - Shell 09XX	30
11.	Ring Geometry - Shell 10XX	31
12.	Details of Shell Skin/Stringer Construction before End Ring Installation	32
13.	Application of Additional Ring Stiffener to Test Specimen	32
14.	Detail of Shell Upper Endplate Loading System	34
15.	Completed Shell Specimen in Test Machine	34
16.	End Shortening Transducer Mount	37
17.	High Compliance Wall Motion Transducer Mount	37
18.	Vertical Transducer Array	38
19.	Circumferential Transducer Array	38

Figure		Page
20.	Test Specimen and Instrumentation Installed in Test Machine	39
21.	Hickson Self Adhesive Strain Gage Located on Shell .	41
22.	Calibration Beam for Hickson Strain Gages	41
23.	Data Acquisition System Flow Diagram	44
24.	Digital Data Acquisition System	46
25.	Disassembled Buckle Depth Restraining Mandrel . . .	53
26.	Highlighted Diamond Buckles on Shell 1006	54
27.	Buckles Covering Approximately 75% of Shell 1006 . .	54
28.	Scanning System for determining Initial Shape of Shell 1000	56
29.	Initial Out-of-Roundness, and Radial Displacement Versus Circumferential Position for Three Loads Shell 1000	58
30.	Radial Displacements versus Circumferential Position for Three Loads - Shell 1002	59
31.	Wall Motion along Longitudinal Generator for Three Loads at Station 36, Shell 0601	61
32.	Wall Motion along Longitudinal Generator for Three Loads at Station 44, Shell 0601	62
33.	Wall Motion along Longitudinal Generator for Six Ring Configurations at Station 56, Shell 06XX . . .	63
34.	Southwell Plot at Station 36, Shell 0601	66
35.	Southwell Plot at Station 44, Shell 0601	66
36.	Wall Motion along Longitudinal Generator for Six Loads at Station 44, Shell 0608	67
37.	Harmonic Spectrum and Southwell Plot, Shell 0803 . .	69
38.	Harmonic Spectrum and Southwell Plot, Shell 0813 . .	70
39.	Harmonic Spectrum and Southwell Plot, Shell 0608 . .	71

Figure		Page
40.	Harmonic Spectrum and Southwell Plot, Shell 0608 . .	74
41.	P_{SW} and P_{cr} Versus Ring Stiffness, Shell 06XX . . .	75
42.	P_{SW} and P_{cr} Versus S_R, Uniform Rings, Shell 08XX . .	78
43.	P_{SW} and P_{cr} Versus S_R, Uniform Rings, Shell 09XX . .	79
44.	P_{cr} and P_{SW} Compared to Experimental Loads, Shell 10XX	82
45.	Skin Wrinkling on Shell 0300	85
46.	Panel Buckling on Shell 0300	85
47.	Buckling in Second Longitudinal Mode - Shell 1006 .	86
48.	Buckling in Third Longitudinal Mode - Shell 1008 . .	86
49.	P_{SW} Versus S_R, Non-Uniform Rings, Shell 09XX	89
50.	P_{SW} Versus S_R, Non-Uniform Rings, Shell 08XX	90
51.	Harmonic Analysis Flow Diagram	100
52.	Data Acquisition Flow Diagram	101
53 - 89.	Harmonic Spectrum and Southwell Plot, Shells 0600 through 1006	103

NOMENCLATURE

A	cross-sectional area of stiffener
A_n	coefficient of the nth sine component
B_n	coefficient of the nth cosine component
D_x, D_y	bending stiffnesses of orthotropic plate in longitudinal and circumferential directions, respectively
D_{xy}	twisting stiffness of orthotropic plate
E	Young's modulus
E_x, E_y	extensional stiffnesses of orthotropic plate in longitudinal and circumferential directions, respectively
G	shear modulus
G_{xy}	in-plane shear stiffness of orthotropic plate
I_o	moment of inertia of stiffener about middle surface of shell
J	torsional constant for stiffener
M_x, M_y, M_{xy}	bending and twisting moments in orthotropic shell
N_x, N_y, N_{xy}	normal and shearing forces in orthotropic shell
$\bar{N}_x, \bar{N}_y$	applied compressive loads per unit length
P	applied compressive load
$_nP_{cr}$	critical load for the nth mode
R	radius of cylinder to middle surface of orthotropic shell
X_n	power spectral density for the nth mode
a	length of stiffened cylinder
d	stringer spacing
ℓ	ring spacing

m	number of half waves in cylinder buckle pattern in longitudinal direction
n	number of full waves in cylinder buckle pattern in circumferential direction
u,v,w	displacements in x, y, and z directions, respectively, of a point in middle surface of shell
x,y,z	orthogonal curvilinear coordinates with origin lying in middle surface of shell
$\bar{z}$	distance from centroid of stiffener to middle surface of shell, positive if stiffener lies on external surface of shell
δ	deflection normal to applied load P
$n\delta_o$	nth modal component of the initial irregularity
μ_x, μ_y	Poisson's ratio for bending of orthotropic plate in longitudinal and circumferential directions respectively
μ'_x, μ'_y	Poisson's ratio for extension of orthotropic plate in longitudinal and circumferential directions respectively
S_R	ring stiffness parameter, represents total number of 0.030 inch layers of ring material on shell
M	harmonic magnitude

Subscripts:

s,r	denote properties of stringers (longitudinal stiffening, parallel to x-axis), and rings (transverse stiffening, parallel to y-axis), respectively
x,y	longitudinal and circumferential directions, respectively

SUMMARY

This thesis outlines the results obtained from testing eight 15 inch diameter ring and stringer stiffened cylindrical shells. Individual shells were tested with a series of different ring configurations. The work provides substantial confirmation of the small deflection linear theory for stiffened shells. The usefulness of acrylic plastics in the manufacture of test specimens for this type of structure is shown. The Southwell process of data analysis is shown to be useful in parametric test studies on stiffened shells.

CHAPTER I

INTRODUCTION

The ring and stringer stiffened cylindrical shell has wide use in modern aircraft systems. Guided missile and space launch vehicle designers also rely on this mode of construction for high strength, lightweight structures. The use of a combination of ring and stringer stiffeners in aerospace structures is, in fact, so widespread that this configuration has earned the designation "conventional", as opposed to the less commonly used shell reinforcing methods employing rings only, stringers only, or waffle stiffening. In spite of such widespread application over an extended time, there is no universally accepted design or analysis procedure for ring and stringer stiffened shell structures either in compression or in flexure.

The failure of stiffened cylindrical shells under axial compression or bending often occurs in the form of an instability. Initial instability may be followed immediately by large deformations and a permanent reduction in the strength of the structure. Such a catastrophic collapse can rarely, if ever, be tolerated. Thus the knowledge of the load at which instability will occur is of prime importance to the designer.

The four types of buckling associated with the stiffened cylindrical shell are: local, skin wrinkling, panel, and general instability. Local instability is the buckling of the unsupported areas of the

stiffener cross-sections and is therefore an important consideration in the selection of the stiffener geometry. Skin wrinkling represents buckling of the skin bounded by the stiffening elements. Panel instability involves a buckling mode in which only the skin and stringers between adjacent rings participate. Finally, general instability is defined by an instability mode in which rings as well as the skin and stringers are involved in the buckling distortion.

The problem of the instability of stiffened shells has been studied by many investigators over the past 40 years. A comprehensive survey of the early work in the field is included in a report prepared by the Guggenheim Aeronautical Laboratory of the California Institute of Technology in 1943 (1). An excellent historical sketch covering the development of the subject through 1958 is given by Becker (2).

Early investigators replaced the stiffened shell by an equivalent orthotropic structure. More recent treatments have included the effect of eccentricity or "one-sidedness" of the stiffeners. The potential importance of eccentricity had been mentioned by Flügge (3) as early as 1932 and were included in a quantitative analysis in 1947 by Van der Neut (4). Eccentricity effects are recognized today as being real and large enough to warrant consideration in design of stiffened cylinders.

A small deflection linear theory incorporating the effect of eccentricity was proposed by Baruch and Singer (5) in 1963 for hydrostatic loading of stiffened shells. This theory was generalized by Block et al (6) to encompass orthotropic skins and various loading conditions. The theory is classical in that prebuckle deformations

are neglected and only small deflections are considered. Stiffener properties are "smeared" or distributed over the surface, with consideration given to the eccentricity or one-sidedness of the reinforcement.

Closely stiffened shells are usually analyzed by such a linear theory. Fairly good agreement between theory and experiment prevails for shells with moderate to heavy stiffening. In the case of sparse stiffening experimental agreement with the linear theory has generally been poor (7). Knowledge of the range of stiffener geometries and spacing which will qualify a shell as closely stiffened has by no means been determined by the tests performed to date. Such bounds can only be conclusively determined by further testing.

Linear theories which account for effects of discrete ring stiffeners have recently been developed (8, 9). In these the ring stiffeners are treated as linear discontinuities represented by a Dirac delta function. Such discrete theory is considerably more involved in application than a smeared theory. The discreteness effect is often considered to be small (6). The results of reference 8, however, suggest that discreteness can be a factor which considerably reduces the instability load of the shell.

A summary of test programs which have been conducted on stiffened cylindrical shells is given in Table 1. The references in this table contain the bulk of available test data from which an assessment of theoretical predictions can be made. As can be seen from the table, the greatest number of test results are available on ring stiffened only, or stringer stiffened only, shells. Noticeably missing from this listing

Table 1. Summary of Stiffened Shell Test Programs

Test Class	Principal Investigator	Date	Number of Tests	Test Description	Reference Number
RING STIFFENED					
	Peterson	1956	25	Moderate scale specimens Panel instability predominated	10
	Singer	1969	18	Small scale machined shells Panel and general instability	7
	Tenerelli and Horton	1969	9	Small scale machined shells Program included limited wall motion studies	11
	Singer, Arbocz, and Babcock	1970	13	Small scale machined shells Program included extensive mapping of initial imperfections and wall motion under axial load	12
CORRUGATED					
	Dickson	1966	5	Ring stiffened large scale cylinders	13
	Peterson	1966	5	Ring stiffened large scale cylinders Testing in bending	14
	Anderson	1966	2	Ring stiffened large scale cylinders Inside and outside rings evaluated	15

Table 1. Summary of Stffened Shell Test Programs (continued)

Test Class	Principal Investigator	Date	Number of Tests	Test Description	Reference Number
STRINGER STIFFENED					
	Peterson	1959	6	Large scale, riveted construction	16
	Peterson	1963	17	Forty-eight inch diameter, riveted construction	17
	Card	1966	12	Integral milled and riveted stiffeners Both inside and outside stiffeners tested	18
	Weller, Singer and Nachmani	1970	86	Small scale machined specimens	19
	Singer, Arbocz, and Babcock	1970	3	Small scale machined specimens, part of larger program on ring stiffened shells	12
RING AND STRINGER STIFFENED					
	Card	1964	7	Large scale shells tested in bending Skin wrinkling preceded general instability	20
	Lockheed (Missiles & Space Co.)	1965	10	Data not available in open literature Photographs show general instability on only one shell	21

Table 1. Summary of Stiffened Shell Test Programs (continued)

Test Class	Principal Investigator	Date	Number of Tests	Test Description	Reference Number
NON-REPRESENTATIVE TESTS					
	Milligan	1965	51	Small scale machined shells Excessive skin thickness variation and closely spaced, low eccentricity stiffeners	22
	Lakshmikantham	1965	6	Similar specimens to reference 22	23
	Katz	1965	21	Skin wrinkling preceded general instability Low deflectional stiffness of reinforcement did not provide nodes in this pattern	24
EARLY TESTS					
	Hoff	1944	13	Riveted shells not representative of contemporary construction	25
	Dunn	1947	174	Riveted shells not representative of contemporary construction Results of these tests formed the basis for the "Shanley Criterion"	26

are large numbers of tests on ring and stringer stiffened shells of contemporary design. Even for the tests listed in this category, namely those of Card (20) and the Lockheed tests (21), there is some question as to the applicability of the results. Skin wrinkling preceded general instability on the shells tested by Card (20), necessitating the use of an empirically determined reduced skin modulus for the comparison of these test results to theoretical predictions (27). Results of the Lockheed tests (21) are not available in the open literature, however, post-buckling photographs of these shells show general instability occurred in only one specimen.

The early tests of Hoff (25), which are no longer considered representative of contemporary design, are important historically in that these tests represented the only data available to designers for many years. The shells tested by Dunn (26) in 1947 are also not considered representative of modern construction. It is significant to note, however, that these tests formed the basis for the "Shanley Criterion" (28), a design technique for rings which is still in use.

A "sequential" concept is normally employed in the design of stiffened cylinders. In this process, the stringers are spaced as widely as skin stability will permit. The ring spacing is then determined as the widest possible which will prevent panel instability. The ring size is then determined to preclude general instability. A technique often used for sizing the rings is the semi-empirical "Shanley Criterion", which, as previously mentioned, is based upon the tests of Dunn.

This sequential design process assumes implicitly a lack of

coupling between various modes of buckling. There is indeed practically no coupling between skin wrinkling and panel or general instability so that the widest possible stringer spacing is best. The question of possible interaction between panel and general instability is not as clear. Additional experimental results on more representative specimens than those upon which the "Shanley Criterion" is based are required to demonstrate the effects of ring spacing and size.

A further question to be answered through experiment is the effect of discreteness. Although stringer spacing which will preclude skin wrinkling is such that the shell may be treated as a continuum in the circumferential direction, such is not always the case for rings.

The present experimental program was conceived in the interest of obtaining additional insight into the problem of the instability of ring and stringer stiffened cylindrical shells. The objectives of the program were threefold: First, to provide experimental data to supplement the limited quantity of test results previously available for such structures. Second, to demonstrate bounds on the range of applicability of the simple "smeared" theory. Third, to provide basic data to aid in the development of a rational design procedure for ring stiffeners.

To accomplish these objectives a series of stiffened shells was designed and constructed having a wide range of stringer and ring geometries. Equipment and techniques for testing these shells in axial compression were developed. Non-destructive testing techniques, utilizing wall motion data obtained from the shells prior to buckling,

were developed for comparison of effects of ring parameter variations on particular skin/stringer combinations. Test results were compared to theoretical predictions using a smeared linear theory (6). The questions of scale and the influences of manufacturing technique were not considered in the present tests. These problems are to be included in a longer range test program on large scale shells.

CHAPTER II

THEORETICAL CONSIDERATIONS

Selection of Theory for Comparison to Experimental Results

The small displacement linear theory which Block et al (6) developed by generalization of the earlier work of Baruch and Singer (5) was used exclusively in this study. The pertinent stability equation is given as Equation (3) in Appendix A. It is representative of the more advanced buckling equations currently used for predicting the stability loads of stiffened shells. One-sidedness of the stiffening element is accounted for and buckling is assumed to occur from a membrane state of stress. An important underlying assumption is the form of the displacements which are taken to satisfy the simple support boundary conditions of classical buckling theory, that is,

$$w = M_x = N_x = v = 0.$$

Generally, the boundary conditions for stiffened shells do not fulfill these requirements. However, ring and stringer stiffened cylinders appear to be relatively insensitive to such influences. Experimental results obtained on a wide range of stiffened shells has provided much confidence in the adequacy of this theory (27). However, it has not been validated for all important conditions.

The Southwell Plot

In the past structural stability theories were generally developed for ideal bodies with perfect loading and boundary restraint conditions. Today there is a tendency to deviate from this and consider the imperfect body. Historically, structural testing, in so far that it has been done from a research aspect, has tended to follow similar lines. Great effort has been expended on the design of ideal restraints and in loading in a readily definable manner. An alternate approach is to test the structure in a way which accounts for deviations from ideal. A process, popularized by Southwell, is useful in this regard. This process associates deflection or strain and load for an imperfect structure with the critical load level for the ideal. The analytical basis for this method reaches back into history. Young (29), the celebrated philosopher and physician was aware of the relationship and Aryton and Perry (30) used it during the latter part of the 19th century. Westergaard (31) made a very detailed study in 1922 of this type of behavior for linear systems. Starting with the Lagrangian expressed in generalized co-ordinates he considered not only initial geometric variations but also nonhomogeniety and eccentricities of loading. Using the theory of minimum potential he derived a relationship between the applied load, the critical loads for the several modes, and the modal components of the initial irregularity in the form

$$\delta = \sum_{n=1}^{\infty} \frac{1}{P_{cr_n} - P} \; n\delta_o \qquad (1)$$

This law, as subsequent research has shown, is applicable to a very wide range of structural problems (32). It is, however, well to recognize that it is true if and only if the system is completely linear. Practical difficulties also arise when the eigenvalues $_nP_{cr}$ are closely spaced.

The Southwell method has been studied extensively for the column. In this case it is clear that there is wide separation of the eigenvalues and, provided the observations are made at an appropriate point, all terms beyond the first in the Westergaard expression are small. Many researchers have made use of the relationship. Flügge (33), in his text on shells, directed attention to the potential of the method for unstiffened shells, and several recent papers have shown application to stiffened shells (7, 11, 19, 34). It is true that there is an element of doubt when the method is used to interpret data on shells, since several values of Southwell load can frequently be derived for one shell under a particular critical condition. Physically this is to be expected since experience has shown that shell failures in instability, particularly in compression, tend to be localized rather than gross. In other words the stability is not critical at all points simultaneously. Previous investigators (7, 19, 34), using strain gage techniques, have obtained reasonable consistency between Southwell loads computed for stations located on a circumferential line. From this experience it would be expected that Southwell values computed from displacement data obtained about a circumferential line should also be in fair agreement. However, it is to be emphasized that in accordance with the Westergaard equation there are multi-mode issues of concern. This question of

separation or determination of other than the first eigenvalue was first mentioned by Donnell (35). The problem was faced by Tuckerman (36) for rods and by Craig (37) for shells.

Harmonic Analysis

Harmonic analysis is used extensively for the evaluation of data obtained in this program. Such analysis is often used by experimentalists to evaluate spectral distributions. It is a powerful tool which the analyst can use for the classification and refinement of data. With it he can bring together a large number of discrete data into a single form for evaluation. On the other hand he can adapt the process to effectively filter his information. It is in this way that it is used in this work. The need for harmonic analysis arises because the wall motions of stiffened shells in axial compression contain unwanted components viz. the inevitable Poisson expansion and the rigid body displacement inherent in the test machine.

The application of any mathematical tool in evaluation of experimental data, particularly one such as harmonic analysis, requires a degree of caution; not only must one understand the manner in which idealized data will be processed, but perhaps more important, what is the sensitivity of the process to irregularities of the form and magnitude associated with the real system. Errors associated with the application of a harmonic analysis to a discrete set of data can be broken into three catagories (38); aliasing, finite term error, and computational round off. Aliasing, or the folding back of higher frequency components, and the subsequent confusion in the lower modes,

may be a problem when an equal spaced measurement scheme is employed. Such aliasing was not considered to be a serious problem here, since the bending stiffness of the shell wall virtually eliminates the shorter wave lengths. Certainly, if there are short wave length components present in the deformation, they are of insignificant magnitude. The structural "filter" cannot, however, remove the short wave length noise due to the instrumentation. In this program the prime instrumentation noise was due to a $\pm$ 0.0001 inch uncertainty in the voltmeter reading. A worst case condition was evaluated by superimposing a 0.0002 inch peak to peak distortion having a wave length equal to two stringer spacings onto a 0.010 inch peak to peak distortion with a wave length equal to one-fifth of the shell circumference. These displacements are representative of the instrumentation noise and a typical shell distortion respectively. The result of a harmonic analysis of this displacement field was compared to a harmonic analysis of the five wave displacement field alone. The effect of the "noise" was a change in the fifth harmonic coefficient of less than one per cent.

The error associated with the finite series results from the practical necessity of choosing a finite number of measuring stations. The sensitivity of the lower harmonics, specifically the zeroth through the seventh, to this finite series effect was investigated by performing a harmonic analysis first on a set of 63 data points, and subsequently on 31 points representing alternate points of the first set. The results are included in a later chapter and indicate no change in the predicted buckling load.

Computational round off errors are fixed by the particular scheme used for computing the coefficients of the harmonic series, and depend upon the numerical processes used. The computational technique here is a standard numeric scheme taken from Ralston and Wilf (39). The magnitudes of the complex series are presented while the phase angles are neglected as they are related entirely to the choice of spatial coordinate origin. This phase information is of little value in the present analysis. In terms of the real sine and cosine series, the power spectral density is given by

$$X_n = \sqrt{A_n^2 + B_n^2} \qquad (2)$$

where A_n and B_n are the sine and cosine coefficients. Obviously the sine and cosine coefficients will vary with choice of coordinate origin on the shell. The expression above can, however, be shown to be invariant.

CHAPTER III

DESIGN OF THE EXPERIMENT

Shell Classification System

A numbering system was established for the shells to identify the various specimens for discussion and to provide for indexing of the data. A four digit code was used, the first two digits representing a particular skin/stringer combination and the last two digits representing the specific ring configuration. Skin/stringer combinations, when referred to alone, will contain a XX in the ring designation positions. With the exception of four shells tested early in the program each shell skin/stringer combination was tested with a number of different ring combinations.

Shell Manufacture

The principal reason for the scarcity of test data for ring and stringer stiffened shells has been the difficulty and expense of fabricating specimens. Therefore, the choice of a suitable material and manufacturing technique for the shells to be tested was of primary concern. Typical manufacturing techniques for large test shells have been conventional riveting, metal to metal bonding, and integral milling with auxiliary bonding or riveting. None of these processes were suitable for the relatively small scale test specimens envisioned for this program. Previous tests on small scale stiffened cylinders have been on specimens with machined rings (7, 11, 12), machined stringers (12, 19),

and integral milled waffle stiffeners (40). Additionally, machined shells which included both ring and stringer stiffening in the same specimen have been tested by Milligan (24), however, obtaining such specimens with sufficient tolerances is very difficult. Whatever the stiffening form, machine shells are expensive and are not easily modified in the test machine.

After evaluating the various manufacturing techniques used by other investigators, it was clear that a different type of specimen was necessary to meet the proposed objectives. The final choice of material and a construction method was made after extensive evaluation of materials. Commercial acrylic plastic was selected, and conventional ring and stringer shells were designed using this material. The selection of a plastic to simulate structures which are typically manufactured from metals appeared quite radical at first. An evaluation of the necessary mechanical properties required to achieve a proper simulation shows such an initial reaction to be unfounded. Acrylics, rather uniquely among the common plastics, possess a linear stress/strain relation up to a yield point of approximately 6000 pounds per square inch and are isotropic. The material is available in a minimum standard sheet thickness of .030 inch and as 0.25 inch square bar stock. A very important advantage of the material is the ease with which high strength joining can be achieved. High strength welded joints are attained by placing the surfaces to be joined in intimate contact and thoroughly wetting. Excess solvent evaporates from free surfaces without causing damage. Drying time is a matter of minutes if the surfaces are smooth and a minimum of solvent flows into the contact area.

Viscoelastic behavior under load, and crack propagation in the plastic created some difficulties in the early stages of the test program. These problems, and the manner in which they were treated are discussed fully in Chapter IV.

Measurements of variations in thickness were made on each sheet of plastic. These measurements showed individual sheets to have uniform thickness to within ± 0.001 inch with a variation between different sheets of ± 0.002 inch from the manufacturers specification of .030 inch. To minimize the thickness variation within a single test specimen, each shell was made from a single sheet of the material.

Manufacturers' specifications on acrylic plastics show a wide variation in modulus, with values ranging from 3.9×10^5 pounds per square inch to 4.6×10^5 pounds per square inch (41). Tensile tests on the material from a single manufacturer resulted in a range of moduli from 4.47×10^5 to 4.54×10^5 pounds per square inch. From these tests a representative modulus of 4.5×10^5 pounds per square inch was chosen.

Shell skins were cut from a single sheet of plastic, using a holding fixture to insure parallel edges. Cutting of the material was carried out by deeply scoring the surface of the sheet with a single edge razor blade and breaking the material over the edge of the cutting table. Rough edges which resulted from the cutting operation were removed with a file. Stringers were manufactured from the 0.25 inch square stock of the same acrylic plastic as the skin, or built up from narrow strips of the 0.030 inch thick sheet. Various stringer shapes

were milled from the square stock using either a six inch cutter or end mill in a standard machine. Coolant was applied during the operation to prevent distortion of the plastic. A complete description of the stringer geometries for each shell is shown in Figures 1 through 3.

End rings for the shells were formed from the 0.25 inch square stock using the slotted mold shown in Figure 4. Ring material was inserted into the slot of the mold and placed into an oven at 350 degrees Fahrenheit for approximately 20 minutes. Natural shrinkage of the material when heated resulted in the ring assuming the shape of the inner surface of the mold. The mold was removed from the oven and spacers were placed between the outer surface of the mold and the ring to maintain circularity as the plastic cooled. As rings formed in this manner were incomplete circles, short additional sections were required when the ring was installed on the shell.

Stringers were positioned on the shell skin using fixtures to insure uniform spacing. Bonding of the stringers to the skin was accomplished by inserting solvent, with a hypodermic syringe, along the stringer/skin junction. The transparent material permitted visual inspection of the degree to which the solvent penetrated the joint. Care was exercised to insure complete penetration on the first application as voids could not be filled by subsequent solvent application. Stringer/skin combinations were rolled into cylindrical form and a seam formed using the standard solvent bonding technique. Care was exercised to insure that precise circumferential dimensions were maintained.

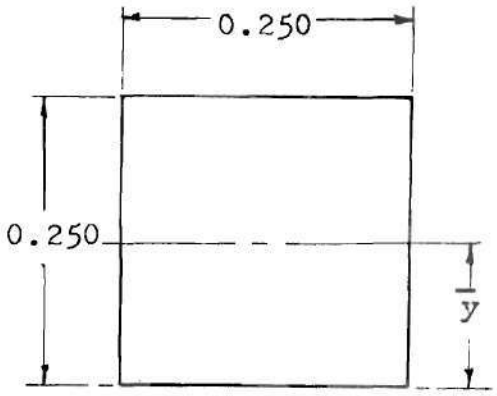

Shells 0300 through 0500

$A_s = 0.063\ in^2$

$\bar{y} = 0.125\ in$

$I_1 = 0.000325\ in^4$

$J_1 = 0.000046\ in^4$

Stringer Pitch = 1.000 in

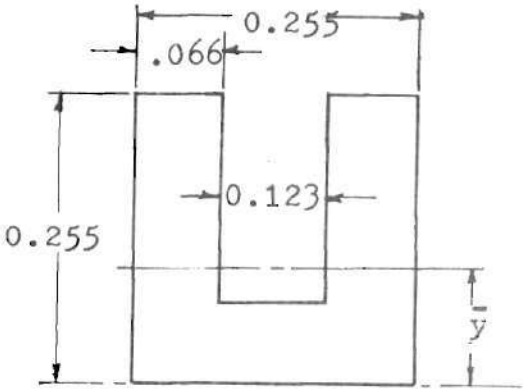

Shell 08XX

$A_s = 0.0404\ in^2$

$\bar{y} = 0.110\ in$

$I_1 = 0.0002\ in^4$

$J_1 = 0.000074\ in^4$

Stringer Pitch = 1.021 in

Figure 1. Stringer Geometry and Section Properties, Shells 0300 through 0500 and Shell 08XX.

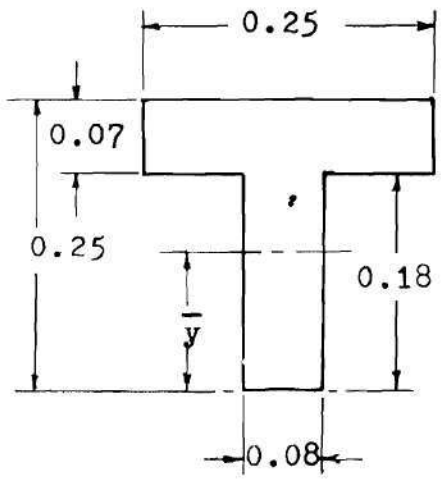

Shell 06XX

$A_s = 0.032 \text{ in}^2$

$\bar{y} = 0.158 \text{ in}$

$I_1 = 0.00017 \text{ in}^4$

$J_1 = 0.000060 \text{ in}^4$

Stringer Pitch = 0.773 in

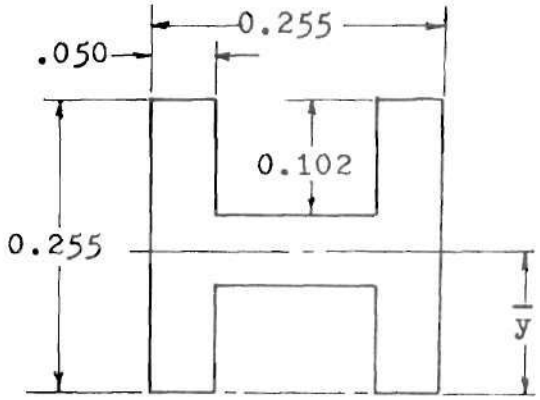

Shell 0701

$A_s = 0.033 \text{ in}^2$

$\bar{y} = 0.123 \text{ in}$

$I_1 = 0.00013 \text{ in}^4$

$J_1 = 0.000028 \text{ in}^4$

Stringer Pitch = 1.03 in

Figure 2. Stringer Geometry and Section Properties, Shell 06XX and Shell 0701.

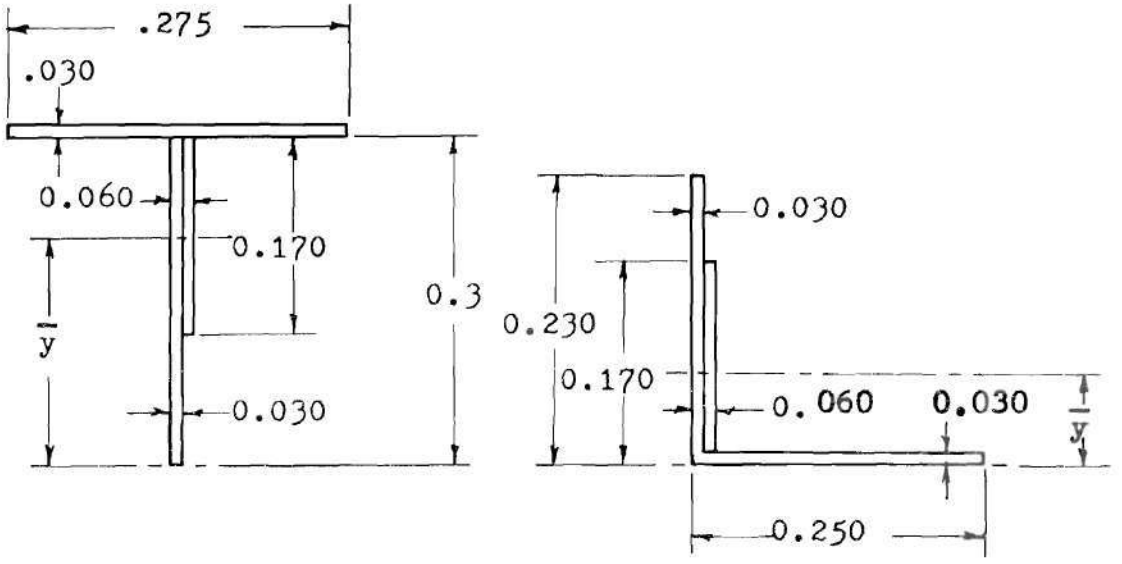

Shell 09XX

$A_s = 0.0206 \text{ in}^2$

$\bar{y} = 0.209 \text{ in}$

$I_1 = 0.00015 \text{ in}^4$

$J_1 = 0.00000517 \text{ in}^4$

Stringer Pitch = 0.650 in

Shell 10XX

$A_s = 0.0177 \text{ in}^2$

$\bar{y} = 0.0742 \text{ in}$

$I_1 = 0.000078 \text{ in}^4$

$J_1 = 0.00000380 \text{ in}^4$

Stringer Pitch = 0.650 in

Figure 3. Stringer Geometry and Section Properties, Shell 09XX and Shell 10XX.

Figure 4. Ring Forming Fixture in Oven.

Circularity of the shell depended to a great extent on the quality of the end reinforcement. This construction is shown in Figures 5 and 6. Two solid rings were formed for each end as previously described. A 0.50 inch load diffuser strip of the 0.030 inch material was bonded to the skin immediately above the outer ring. A similar strip 0.75 inch wide was bonded to the inner surfaces of the stringers at each end of the shell, and the inner ring, formed to the proper diameter, was bonded to this strip.

Intermediate rings were of three types. Formed rings of the 0.25 inch square plastic were used for specimens tested early in the program. Shell 0701 was tested with a milled and formed ring section. All other shells employed rings built up from layers of the 0.030 inch plastic cut into 0.25 inch widths. Buildup was made with the specimen in the test machine as described in a later chapter. A complete description of ring geometries for all shells is given in Figures 7 through 11, and Tables 2 through 5. A skin/stringer combination prior to installation of the rings and the addition of a ring to a test specimen are illustrated in Figures 12 and 13 respectively.

Test Fixture Design and Construction

Tests were conducted in a standard 120,000 pound capacity Baldwin screw jack universal test machine equipped with a strain gage load cell. A voltage divider network driven by the test machine indicator system was constructed to provide test load output to a data acquisition system. Output of this network was linear to within one per cent over the full indicator range. Accuracy of the test machine

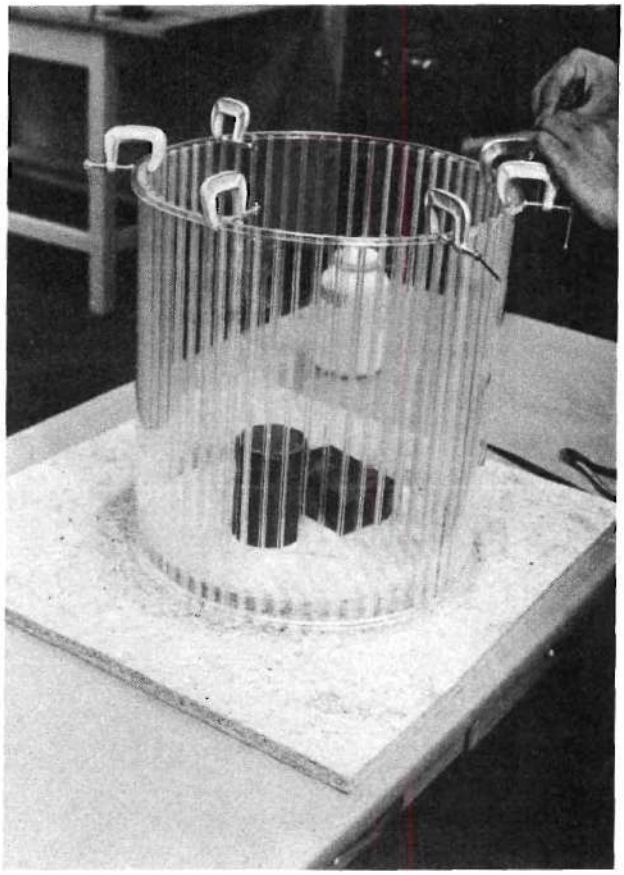

Figure 5. Installation of End Ring Reinforcement.

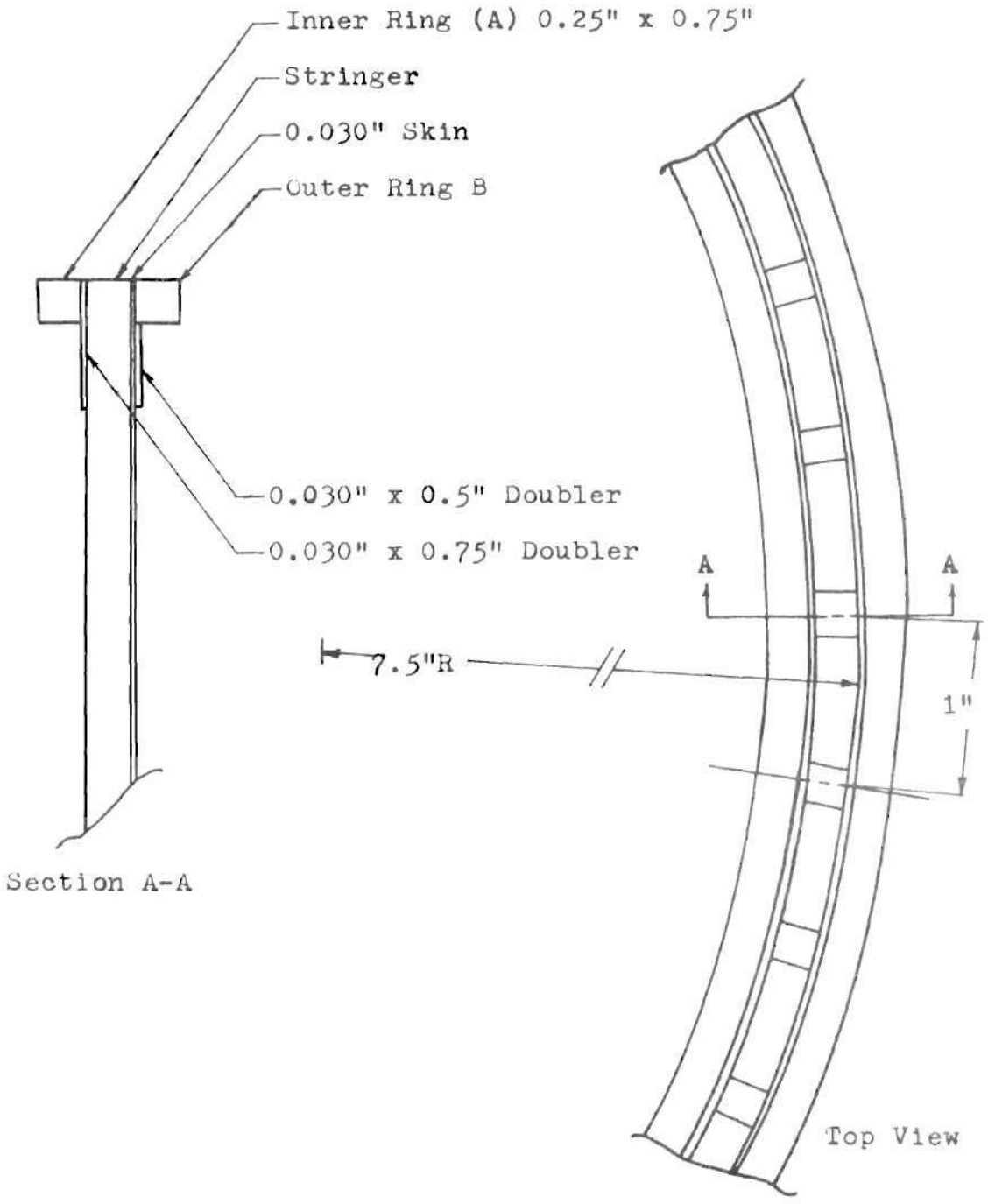

Figure 6. End Stiffening Construction, Shell 0300. Typical For Other Shells Except For Stringer Geometry And Spacing.

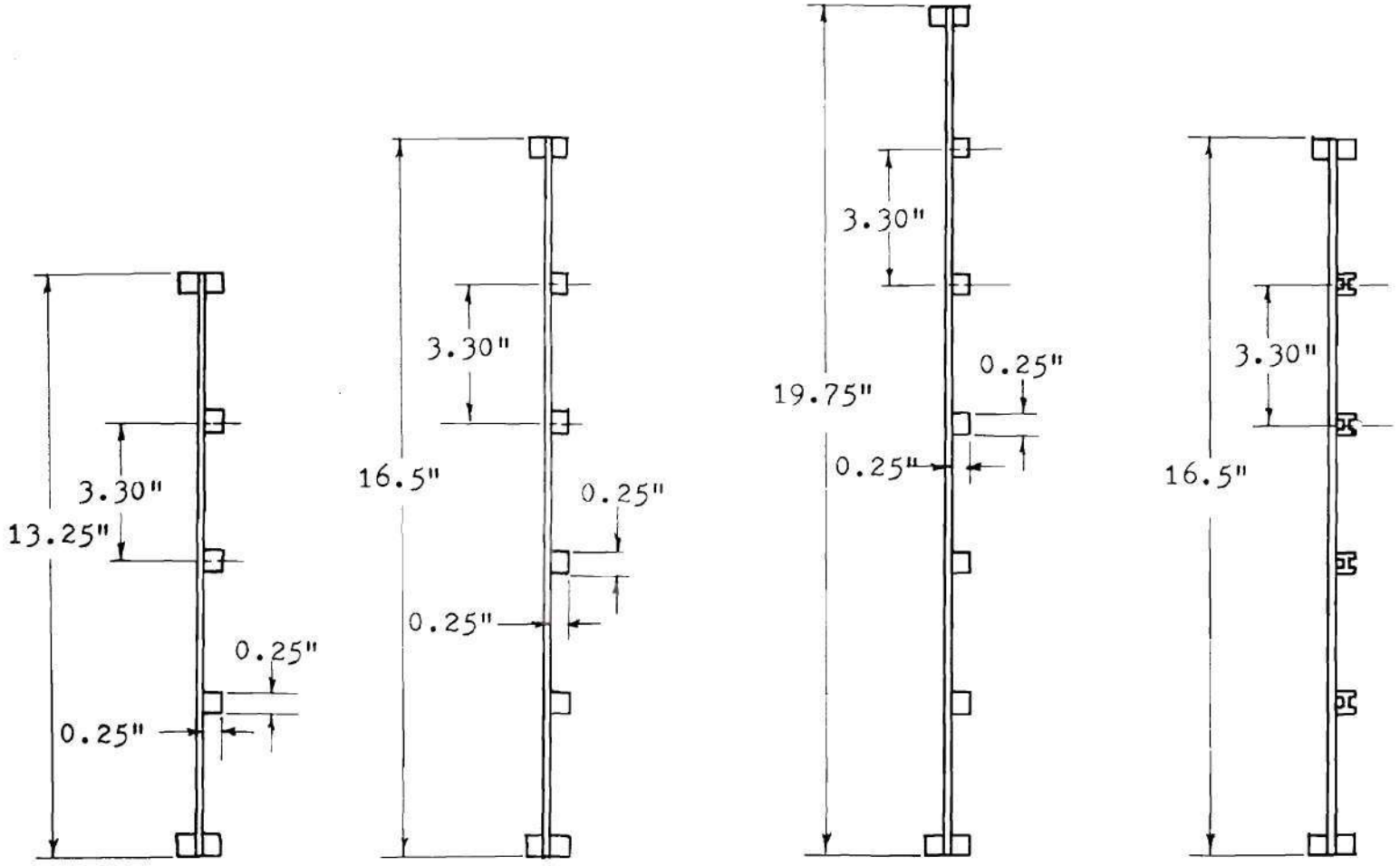

Figure 7. Ring Geometry - Fixed Ring Shells.

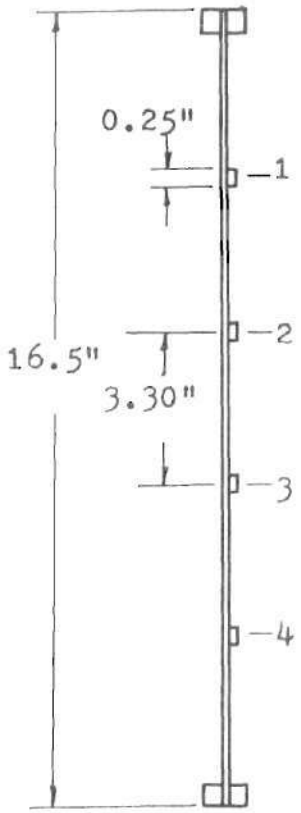

Figure 8. Ring Geometry - Shell 06XX.

Table 2. Ring Thickness - Shell 06XX

Shell Number	Layers of 0.030" Ring at Indicated Position			
	1	2	3	4
0601	1	1	1	1
0602	2	2	2	2
0603	3	3	3	3
0604	4	4	4	4
0605	5	5	5	5
0606	6	6	6	6
0607	7	7	7	7
0608	8	8	8	8

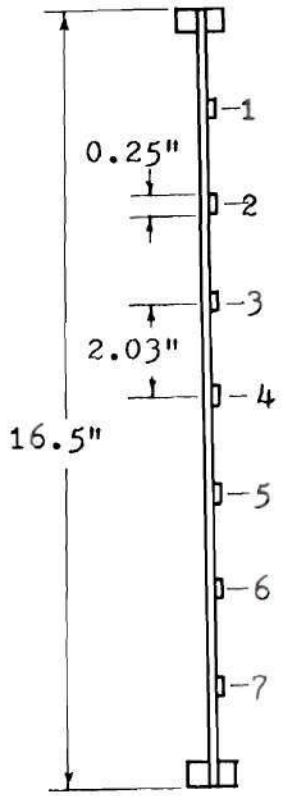

Figure 9. Ring Geometry - Shell 08XX.

Table 3. Ring Thickness - Shell 08XX

Shell Number	Layers of 0.030" Ring at Indicated Position						
	1	2	3	4	5	6	7
0800	0	0	0	0	0	0	0
0801	0	0	0	1	0	0	0
0802	0	1	0	1	0	1	0
0803	1	1	1	1	1	1	1
0804	1	1	1	2	1	1	1
0806	1	2	1	2	1	2	1
0807	2	2	2	2	2	2	2
0808	2	2	2	3	2	2	2
0809	2	3	2	3	2	3	2
0810	3	3	3	3	3	3	3
0811	3	3	3	4	3	3	3
0812	3	4	3	4	3	4	3
0813	4	4	4	4	4	4	4
0814	0	4	0	4	0	4	0

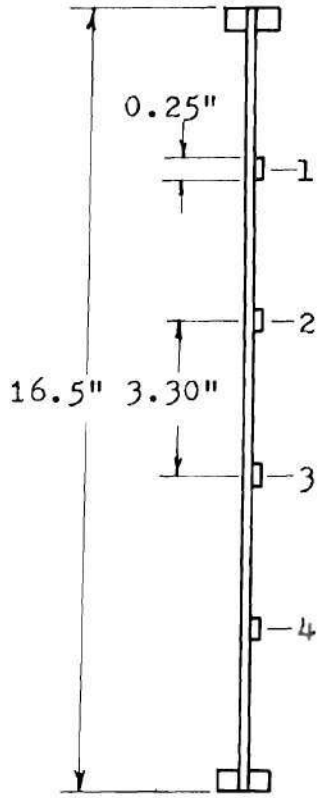

Figure 10. Ring Geometry - Shell 09XX.

Table 4. Ring Thickness - Shell 09XX

Shell Number	Layers of 0.030" Ring at Indicated Position			
	1	2	3	4
0901	1	1	1	1
0902	1	2	2	1
0903	2	2	2	2
0904	3	2	2	3
0905	3	3	3	3
0906	3	4	4	3
0907	4	4	4	4
0908	5	4	4	5
0909	5	5	5	5
0910	6	5	5	6
0911	6	6	6	6

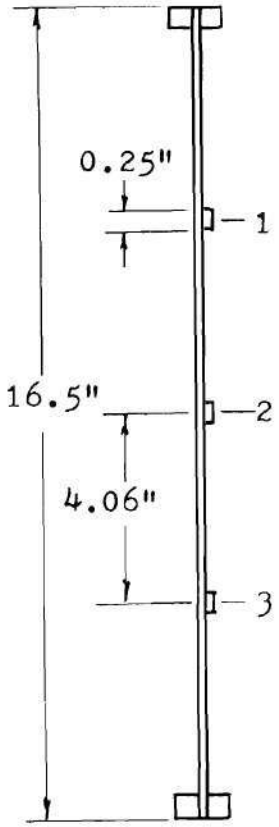

Figure 11. Ring Geometry - Shell 10XX.

Table 5. Ring Thickness - Shell 10XX

Shell Number	Layers of 0.030" Ring at Indicated Position		
	1	2	3
1000	0	0	0
1002	0	2	0
1006	2	2	2
1008	4	2	4

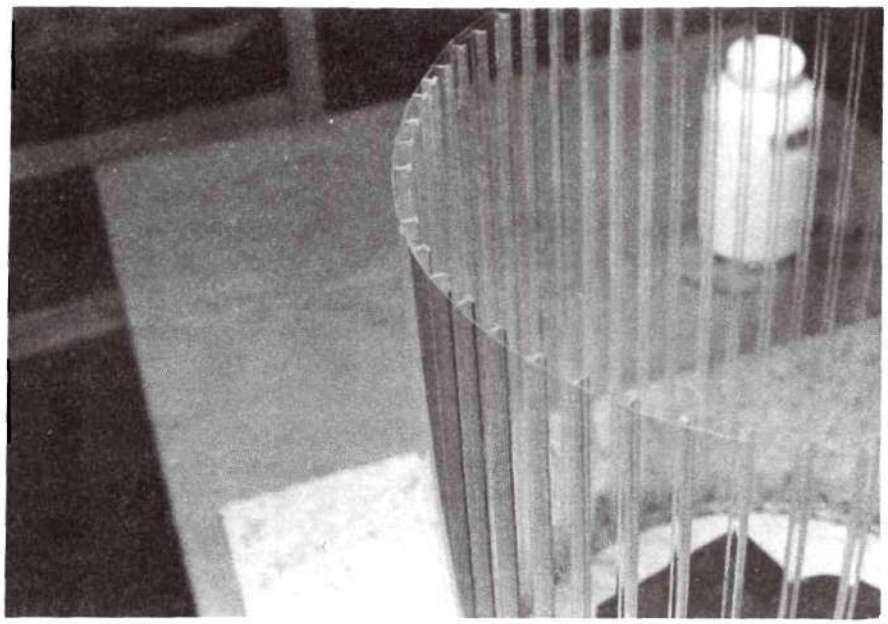

Figure 12. Details of Shell Skin/Stringer Construction Before End Ring Installation.

Figure 13. Application of Additional Ring Stiffener to Test Specimen.

indicator system is rated by the manufacturer at one division on the particular scale in use. On the 6000 pound range, which was used for most of these tests, a maximum error of eight pounds was experienced at any given load.

Shells were mounted in the test machine between two 18 inch square by one inch thick ground steel plates. A liquid epoxy layer was placed on each plate in the area of contact prior to positioning the shell end on the ground steel surface. Silicone release agent was applied to each end plate to facilitate removal of the shell. The epoxy was cured for 24 hours at room temperature prior to loading. The primary purpose of this epoxy layer was to assist in attaining a uniform load distribution on the shell ends by eliminating the effects of minor irregularities. A secondary purpose of the epoxy was to prevent slipping of the end plates on the shell ends between successive loadings. Also the liquid epoxy flowed into the voids between the inner and outer end rings and provided an additional path for load diffusion into the skin and stringers.

The lower end plate rested directly on the table of the test machine. Load application to the upper end plate was through a spherical bearing positioned under the upper loading platten of the test machine. A 12 inch diameter two inch thick steel disc was placed between the spherical bearing and the upper end plate. Safety cables were attached between the upper end plate and the machine crosshead to prevent the end plate and load disc from falling when a shell was tested to failure. Details of the upper loading fixtures are shown in Figures 14 and 15.

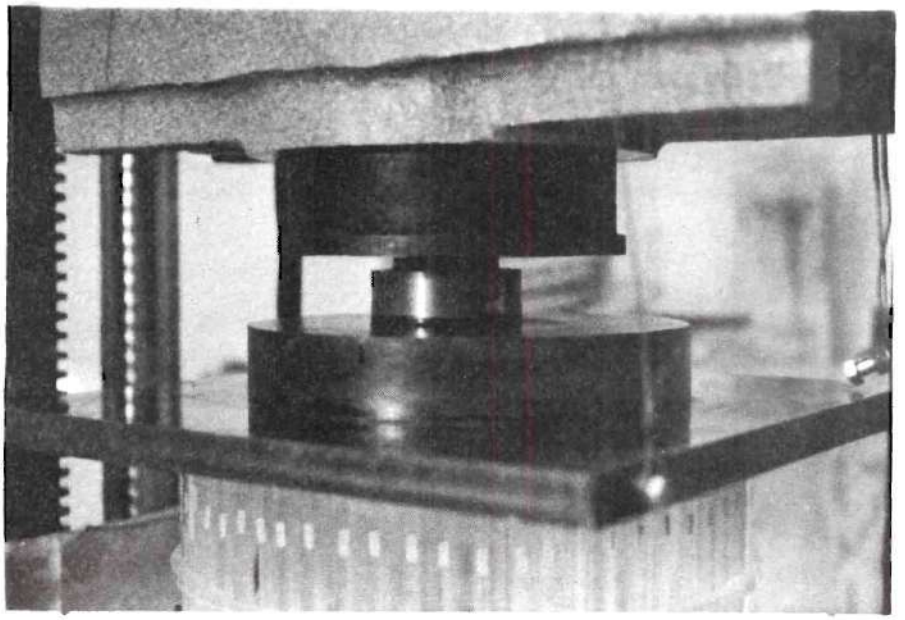

Figure 14. Detail of Shell Upper Endplate Loading System.

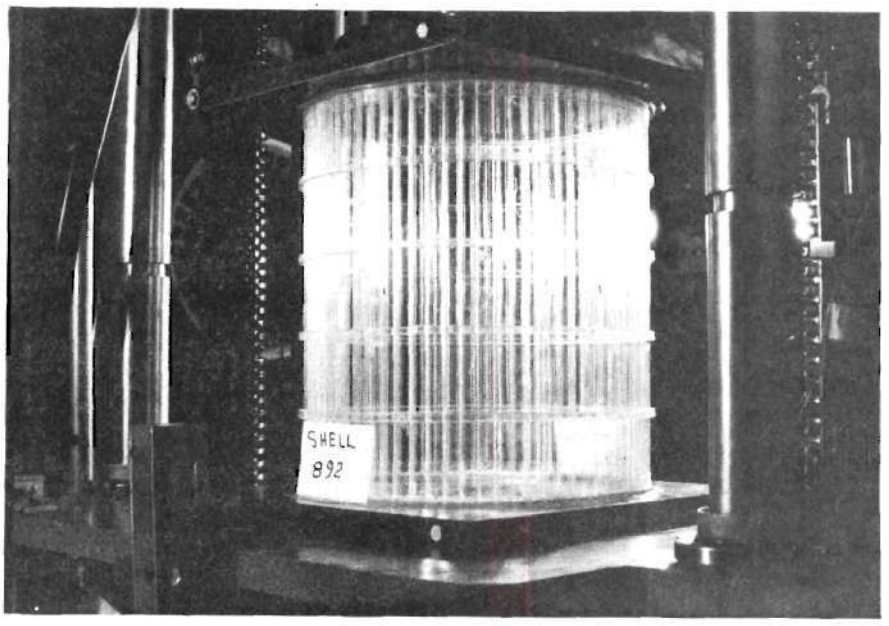

Figure 15. Completed Shell Specimen in Test Machine.

Displacement Transducer Design

A crucial part of the experimental system was the arrangements for transducing and recording the wall motions of the shell. Basically there are two classes of displacement transducers, those which sense displacement without contact and those for which intimate contact is necessary. The choice between these two classes of transducers for a particular test program is dependent upon many factors, the interference between the transducer and the transduced usually being the most important. This is certainly true when the test specimen is a thin wall unstiffened shell. Thus, investigators of such bodies (37, 42, 43) have by necessity used non-contacting devices. In the case of stiffened shells, particularly for those with the dimensions considered here, non-contacting systems are not essential. The present plastic shells had relatively low wall compliance, and those difficulties of using non-contacting probes, such as non-linear output, low level output, and electrical drift, could be avoided through the use of suitable high compliance contacting probes. Thus a system of linear variable differential transformers in suitable mounts was selected for this program. These transducers have a linear output over a range of ± 0.1 inch and a high sensitivity, typically three volts per inch. They also possess excellent long term stability properties and are very rugged.

A high compliance mounting for the moving cores of those transducers used for measuring wall motions was constructed. It consisted of 0.002 inch thick shim steel leaf springs which caused the core to float free of the transformer at all times. Careful polishing of the

leaf springs resulted in a contact force of less than two grams for a 0.025 inch displacement of the probe. A more conventional mounting was utilized for end shortening probes as contact forces were then not a problem. The particular mount used there was designed to position the probe beneath the upper end ring. The two types of transducer mounts are illustrated in Figures 16 and 17.

The device shown in Figure 18 permitted positioning of nine high compliance transducers along a generator of the shell. It was mounted on a releasing magnetic base, which in turn rested on the lower table of the test machine. A circumferential array was also constructed to simultaneously position the transducers at nine stringer locations around a sector of the shell. The vertical position of this mount was adjustable over the full length. This array is shown in position against the shell wall in Figure 19. The test specimen and all associated displacement instrumentation is shown in the test machine in Figure 20.

Strain Gage Installations

Hickson self-adhesive gages were used at various stages in the test program. These devices are rather unique because they may be removed from a structure and reused indefinitely as long as proper care is exercised in handling. The gages require no adhesive but utilize the natural cohesive properties of plate cured Poly-Vinyl-Cloride material from which the gage body is manufactured. The sensing element of the gages is a very thin gold strip formed by vacuum deposition. Operating characteristics are very much the same as the more conventional

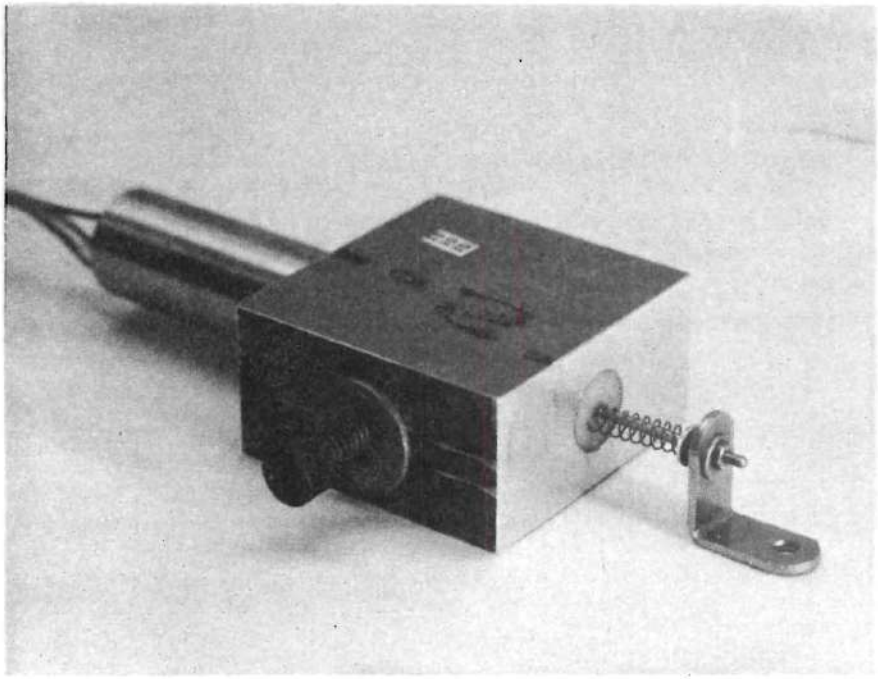

Figure 16. End Shortening Transducer Mount.

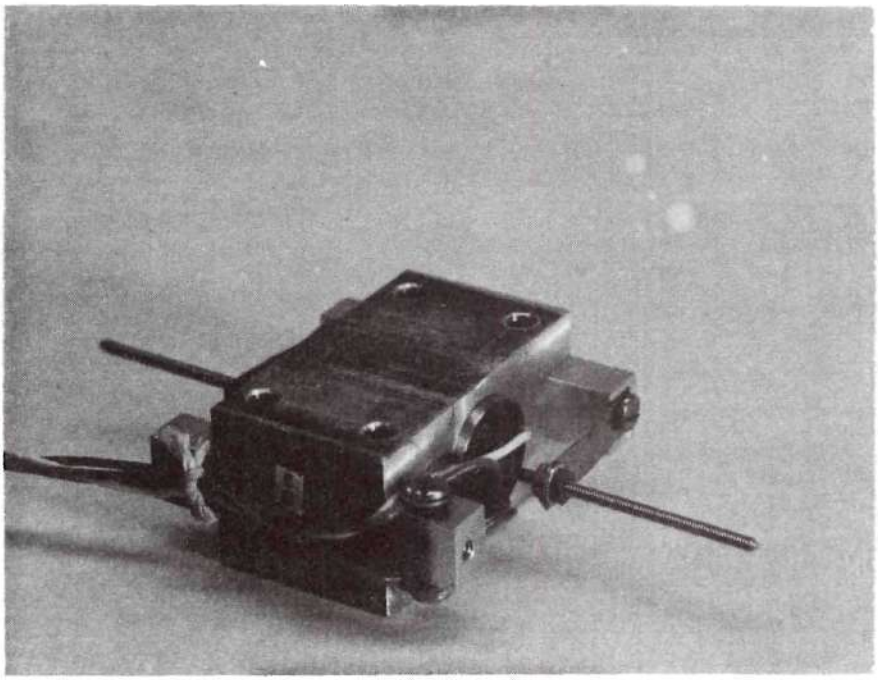

Figure 17. High Compliance Wall Motion Transducer Mount.

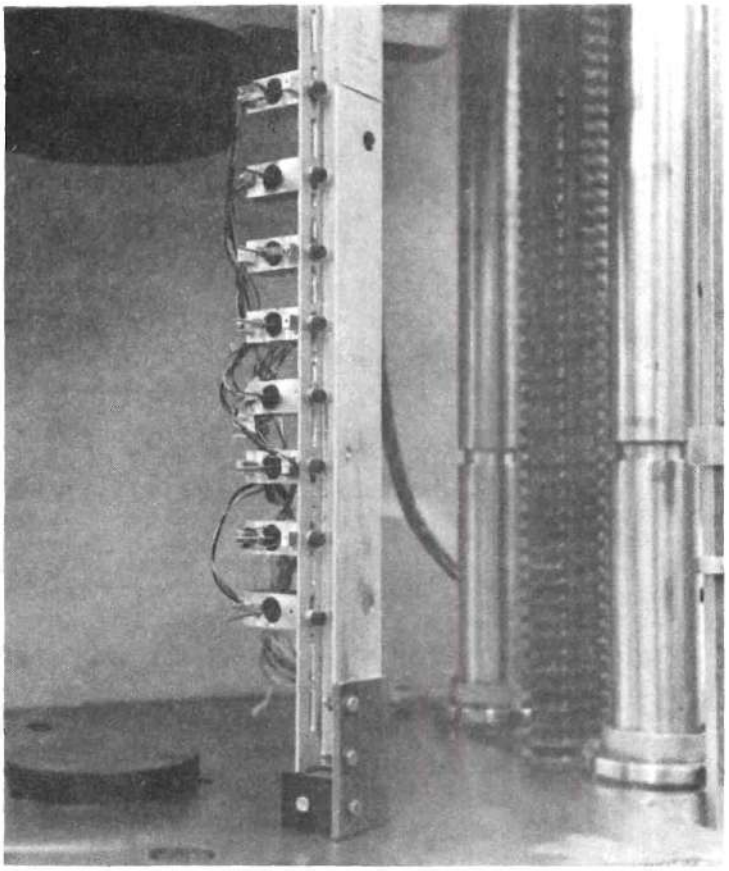

Figure 18. Vertical Transducer Array.

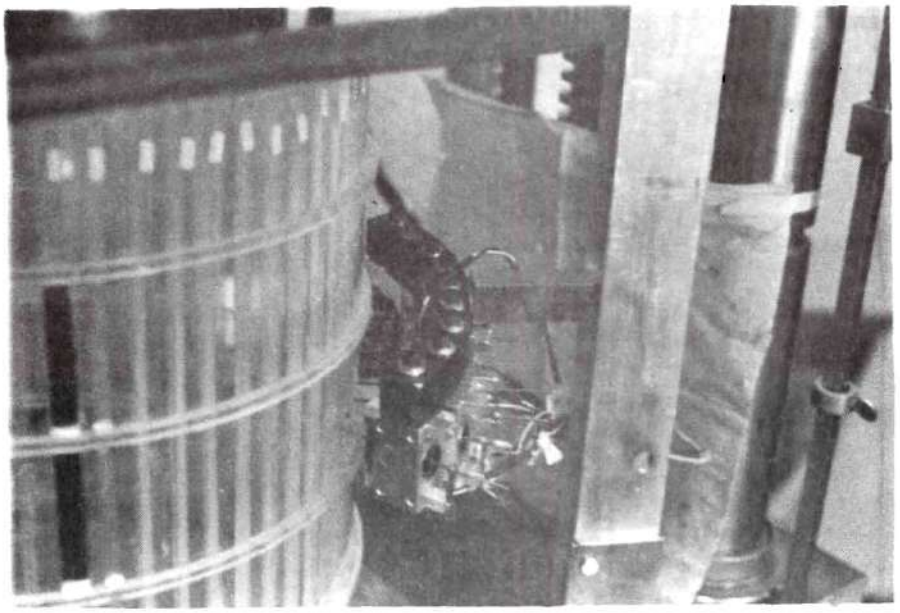

Figure 19. Circumferential Transducer Array.

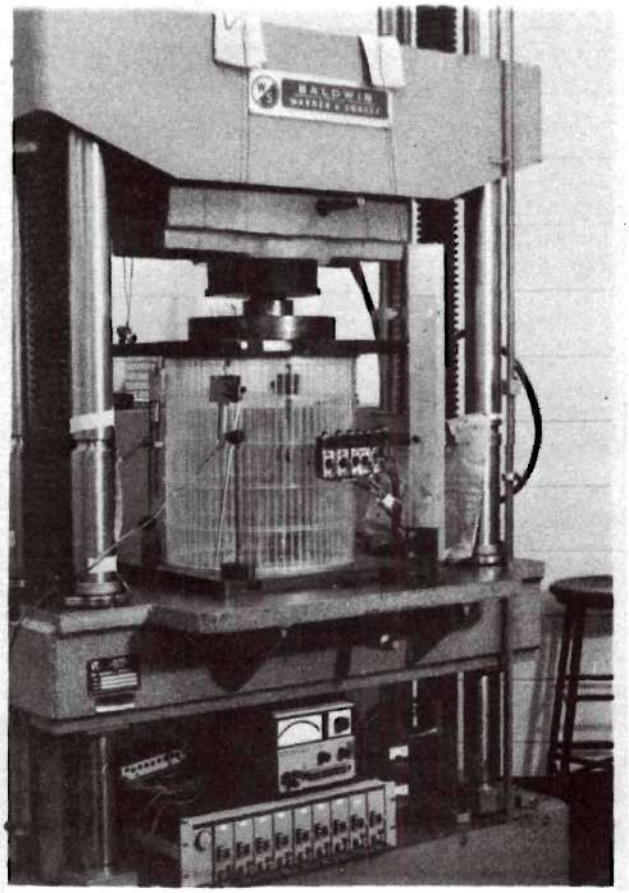

Figure 20. Test Specimen and Instrumentation Installed in Test Machine.

wire or foil gages with the exception of a gage current restriction of 30 ma. Application to a smooth surface consists of washing the gage and the shell surface with a dilute detergent solution, drying both surfaces with a clean tissue, and placing the gage into position with a rolling action. Figure 21 shows such a Hickson gage installed on a shell. Removal is accomplished by lifting a corner with a knife edge and peeling the gage from the surface.

The Hickson gages were arranged in a single active arm bridge using a system of signal conditioning modules. These modules provided individual excitation and balancing capability for ten strain gages. Output from the signal conditioning modules, representing bridge unbalance, was connected to a data acquisition system. Calibration of the gages was accomplished using the beam shown in Figure 22. Individual calibrations were required since it was observed that gage factors differed from those given by the manufacturer and also varied slightly with repeated applications. Insulating covers were used over each gage to reduce thermal drift, and a 30 minute warm-up was allowed after each installation for temperature stabilization. These precautions are necessary to obtain quantitative results since the temperature sensitivity of the gage is quite high. By using these insulating and "warm-up" techniques, the temperature drift was reduced to less than three micro-inches of indicated strain per minute.

Data Acquisition System

The development of high speed digital data processing equipment has made test programs involving large amounts of high precision

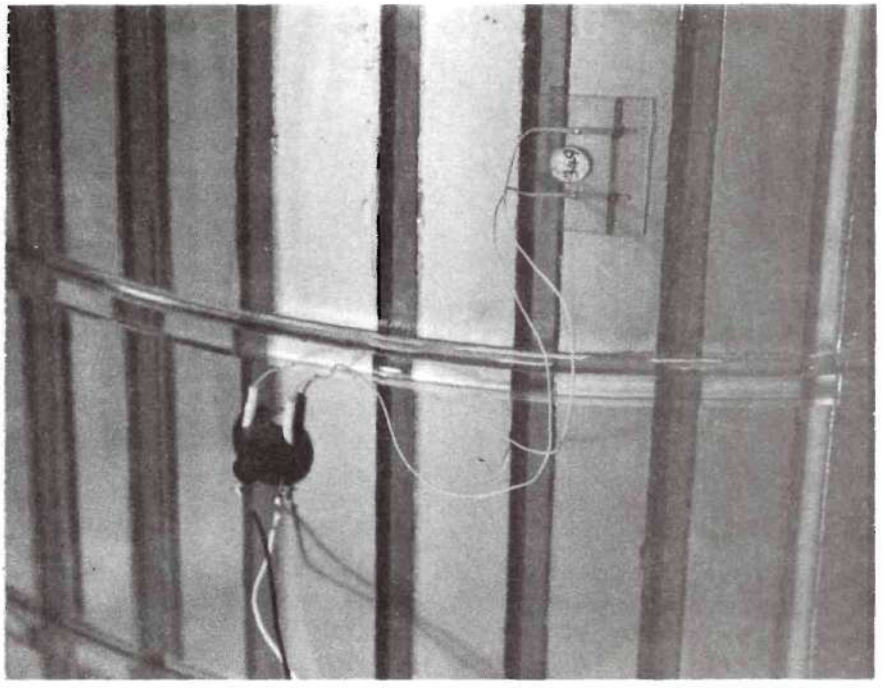

Figure 21. Hickson Self Adhesive Strain Gage Located on Shell.

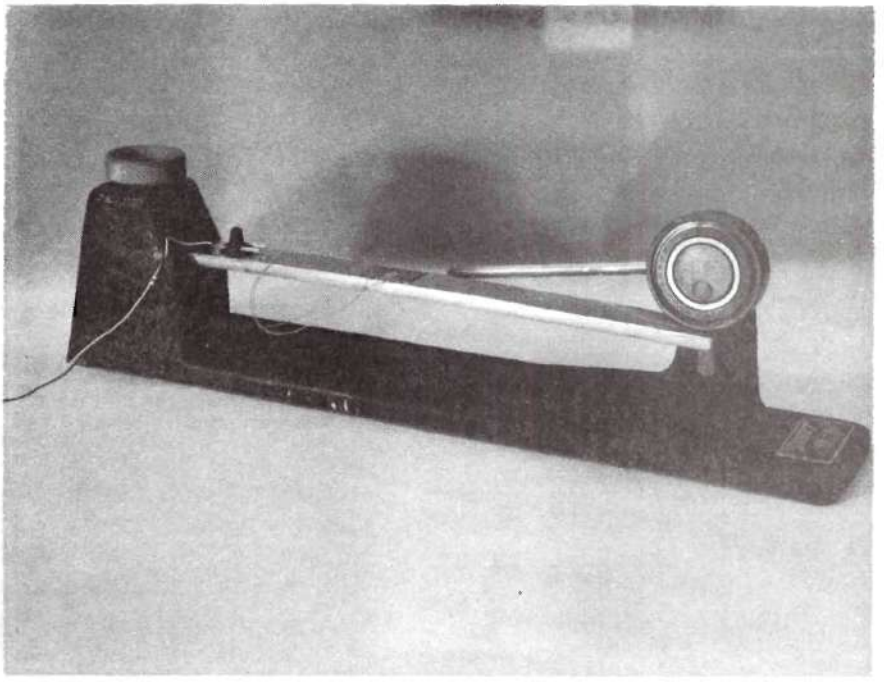

Figure 22. Calibration Beam for Hickson Strain Gages.

experimental data possible. The mapping of the wall motions of shells under a series of loadings represents an undertaking of this class. The actual data acquisition in such tests may not be in a digital form, nevertheless, the reduction and subsequent analysis of such information is impractical without conversion to a digital form at some stage in the process.

Three previously mentioned references (37, 42, 43), have dealt with experimental programs which involved extensive mapping of shell displacements. All these programs were concerned primarily with the study of initial imperfections. Nevertheless the data acquisition system requirements were similar in many respects to those of this program. It is of interest to discuss these systems in order to illustrate the advantages of the advanced data acquisition system adopted for this study.

Craig (37), utilized ten capacitive probes to investigate wall motions of unstiffened cylinders loaded principally in torsion. Analog data was recorded on an FM tape recorder. One channel of data was monitored on an X-Y recorder for immediate evaluation. Data from the FM tape recorder was subsequently fed into an analog to digital converter and re-recorded on a digital magnetic tape. The digital magnetic tape was later processed at a central computation center. Arbocz and Babcock (42) utilized a digital voltmeter to digitize the data generated by a single transducer as it was acquired. This data was transferred to punched cards for subsequent analysis at a central computational center. An X-Y plotter displayed the data as it was

acquired and provided the operator with an indication of system malfunctions. A distinct disadvantage of this system was the large volumn of punched cards which had to be sorted and maintained. The data acquisition system used by Tennyson et al (40) consisted primarily of an analog tape recorder and an X-Y recorder. Only a limited amount of data from these tests was digitized for subsequent analysis.

The system utilized in the present experimental program represents a more advanced concept in data acquisition and processing than was available to the previous investigators. Its principal feature is an on line, central digital computer, which maintains programmed control of all phases of the experiment. Data is acquired from the transducers, digitized, scaled, recorded, and displayed as required. The system is controlled by a program which is input through a teletype unit or punched tape. Real time analysis can be performed to the extent desired by the operator and within the program size limitations.

The data acquisition system consists of a Hewlett Packard model 2115 digital computer with a 8000 word memory. This computer was designed to interface with up to 20 separate functional systems and provide programmed control over their operation. Associated equipment consists of a crossbar scanner with 200 three wire guarded channels, a digital integrating voltmeter, a high speed paper tape photoreader, a high speed paper tape punch, a digital magnetic tape, a 16 channel analog to digital converter, and a teletype unit. All of the equipment in the system, with the exception of the analog to digital converter and the digital to analog converter, was utilized in this test program. A flow diagram of this system is shown in Figure 23. The system console

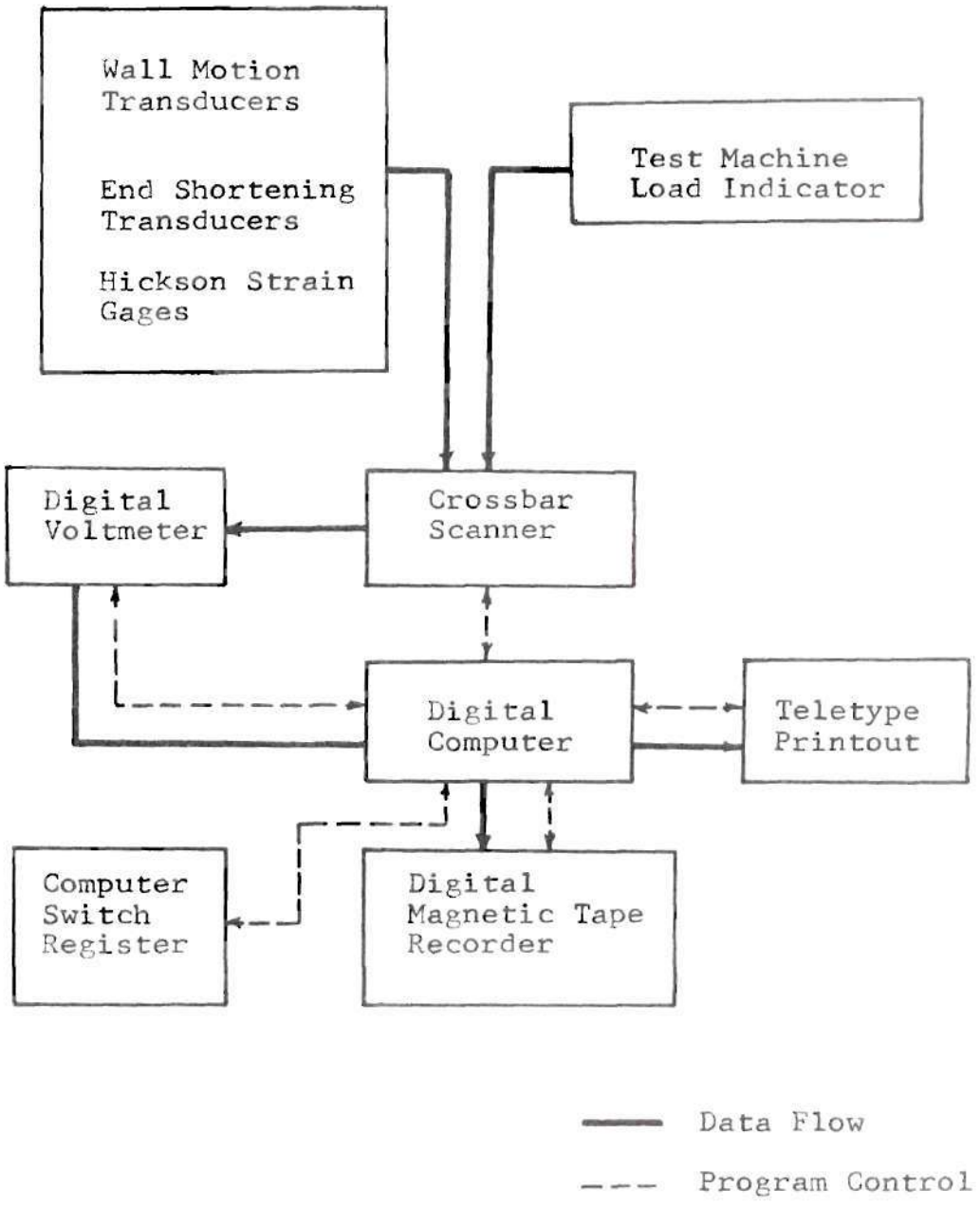

Figure 23. Data Acquisition System Flow Diagram.

is shown in Figure 24.

The system includes standard software compilers for programming in Assembly, Algol, Fortran II, and Basic Language. Basic Language, a highly interpretive algorithmetic language, was chosen for this test program. Since the compiler for Basic Language resides in the computer memory at all times during operation, a limitation is placed on the program length which can be utilized. By deleting that portion of the compiler which was not required, namely the matrix operations, additional space was made available in the computer memory for the programs needed in these tests.

The primary advantage provided by Basic Language over other programming modes for this computer is the ease of modifying the operating program. The real time features of an on line computer, which makes it possible to display results for immediate appraisal, can be utilized to the maximum in this way. An experimental program can thus be modified as testing is in progress through a simple input into the teletype keyboard. The data acquisition programs developed for this test series were modified many times in the course of the research. These program changes were primarily during early tests when an efficient measurement scheme was being sought. The system was capable of acquiring and processing data at a rate many times that used. However, an efficient acquisition of data, rather than the accumulation of a vast bulk of data was the goal of this program.

The central computer was utilized for off line data reduction in addition to data acquisition. In this mode the data was selectively

Figure 24. Digital Data Acquisition System.

read from the digital magnetic tape, processed by the computer, and results output to the teletype unit. Record format on the magnetic tape was established in such a way that random access of each test point could be accomplished.

CHAPTER IV

EXPERIMENTAL PROGRAM

Axial Load Distributions

A uniform load distribution was desired for the buckling tests. To obtain this a load alignment was accomplished on each shell. A series of loads was applied, and the position of the spherical bearing on the upper end plate was adjusted between loads until uniform end shortening was observed at three positions. This end shortening was determined with displacement probes. The probes were positioned such that the downward movement of the upper external end ring was measured. Verification that the uniform end shortening corresponded to nearly uniform loading was obtained by the use of the Hickson strain gages described in Chapter III. The gages were used in two ways. The stresses around the shell were checked with eight individual gages and then with one gage used sequentially at eight locations. The gages were placed two inches below the upper end ring with the sensing element over a skin/stringer junction. The first test resulted in a maximum deviation of 12 per cent in the indicated strain. In the second test the maximum deviation was 8 per cent. The decrease was attributed to an improved accuracy obtained through the use of a single gage. It is in such comparative strain evaluations that the Hickson gage is most valuable, since the result obtained is independent of the gage calibration factor.

Test Procedures

Systematic procedures for the evaluation of wall motions were developed during the course of these tests. Modifications were made as required to adapt to the particular test in progress. The flexibility of the data acquisition system, as explained in Chapter III, made such test optimization possible. Individual test procedures are discussed below.

Shells 0300 through 0500

Tests on these shells were conducted in axial compression with wall motion transducers arranged in a vertical array. Initial voltage readings from the transducers were taken at zero load to obtain a reference for displacement readings. Load was then applied to the shell in increments and corresponding displacement readings taken. These were printed in graphical form as they were acquired. Data was not recorded on the magnetic tape for these tests as the installation of the unit was not complete. The transducer array was positioned at various stringer locations around the shell circumference and the loading cycle repeated. In this way the load/deflection behavior was evaluated over a large part of the surface. Shells in this series were subsequently loaded to failure and the buckling loads so obtained were compared to theoretical predictions. Skin wrinkling was observed to precede general or panel instability.

Shells 0601 through 0608

Systematic scanning of the wall motions at each stringer location for a series of loads was performed on these shells. As in the previous tests a vertical array of nine transducers was used. Wall motions were

recorded on magnetic tape for subsequent analysis and selectively displayed. Eight uniform ring configurations were evaluated at load increments of 500 pounds. The loading range over which the readings were taken varied according to the predicted strength of the shells. Displacements were recorded for standardized load levels to insure that data could be portrayed in both circumferential and longitudinal plots.

Overall repeatability in these tests was important since the data acquired at different stringer locations were combined to map the displayed surface. To evaluate this issue, a series of five load cycles was accomplished at a single stringer location on Shell 0601. During these tests a residual load of 100 pounds was maintained at all times to preclude shifting of the load application system. The array of transducers was backed away from the surface and re-positioned after each load cycle. This simulated the movement of the array to a new stringer location. Displacement values were found to agree to within ± 0.0001 inch for all five load cycles. The possibility of a ± 0.0001 inch systematic error was accepted since it represented only a 1 per cent error in a typical wall displacement of 0.010 inch. Improvement might have been affected by increasing the integrating time for the voltmeter. This was not considered desirable, however, as error due to test machine load drift over the longer scanning period would then have become of the same order.

Wall displacements as large as .0003 inch were observed after removal of the loads during the above repeatability demonstration. These residual displacements were attributed to the viscoelastic behavior of the acrylic material. Typical radial wall displacements for the shells

at the maximum test load were from .010 inch to .015 inch. The viscoelastic part of the deformation therefore represented a small part of the total, typically less than 3 per cent. Residual displacements disappeared after the load had been removed for approximately ten minutes. As the time required for the repositioning of the transducer assembly and performing the other necessary pre-test operations exceeded this, consecutive tests were considered to be made on the same base line configuration. Small increases in the load maintained on the test machine between load cycles occurred as the residual deformations decayed. Particular care was taken to adjust the load to the standard value prior to obtaining zero position readings for a test.

Shells 0701 through 0913

A circumferential array of nine transducers was utilized for all tests in this series. The number of probes was dictated by the availability of transducers as well as the difficulty associated with positioning the array in the close confines of the test machine. Due to these limitations, multiple load cycles were required for each scan. The standard longitudinal position was at the midlength of the shell. This choice was made after a detailed study of wall motion data from nine circumferential positions along the length of shells 0601 through 0608. This data showed a definite decrease in the development of the circumferential wave form as a function of distance from the midlength of the shells. A deterioration in the quality of Southwell lines, as well as an increase in predicted instability loads was also observed for scan positions removed from the midlength.

The displacements were recorded on magnetic tape and selected values were displayed in graphical form. The latter information was particularly valuable in determining the range of loading required to produce significant circumferential wave motion. An example of such a display together with the Basic Language program for this data acquisition phase is included in Appendix B.

Shells 1000 through 1008

The test procedure for shells 1000 through 1008 differed from the previous in that an internal restraining mandrel was used. The mandrel was constructed in four segments as shown in Figure 25. It was positioned inside the shell such that a nominal 0.125 inch gap existed between it and the longitudinal stiffeners. Repeated load cycles were used to generate the wall motion data. Additionally, these shells were elastically buckled several times in each configuration. Figures 26 and 27 show shell 1006 buckled against the restraining mandrel. The diamond outlines were added after the shell had buckled.

A 12 to 14 hour interval was allowed between successive buckling tests to insure the decay of viscoelastic strains. Such strains were particularly significant due to the large wall motions which occurred when the shell buckled against the mandrel. A crack which occurred in one stringer web on the first buckling test was repaired. No further cracks occurred until the final test on shell 1008 when a ring failure caused catastrophic collapse. The basic shell body was buckled fourteen times and was held in the buckled state for as long as 20 minutes with no apparent degradation in subsequent loads.

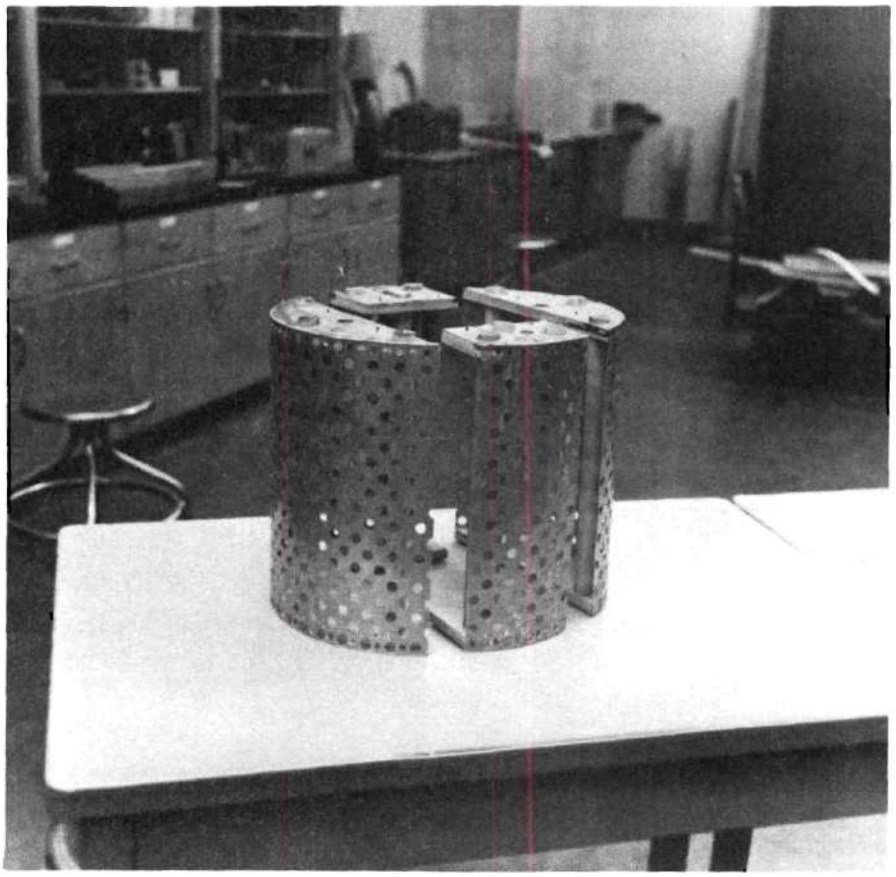

Figure 25. Disassembled Buckle Depth Restraining Mandrel.

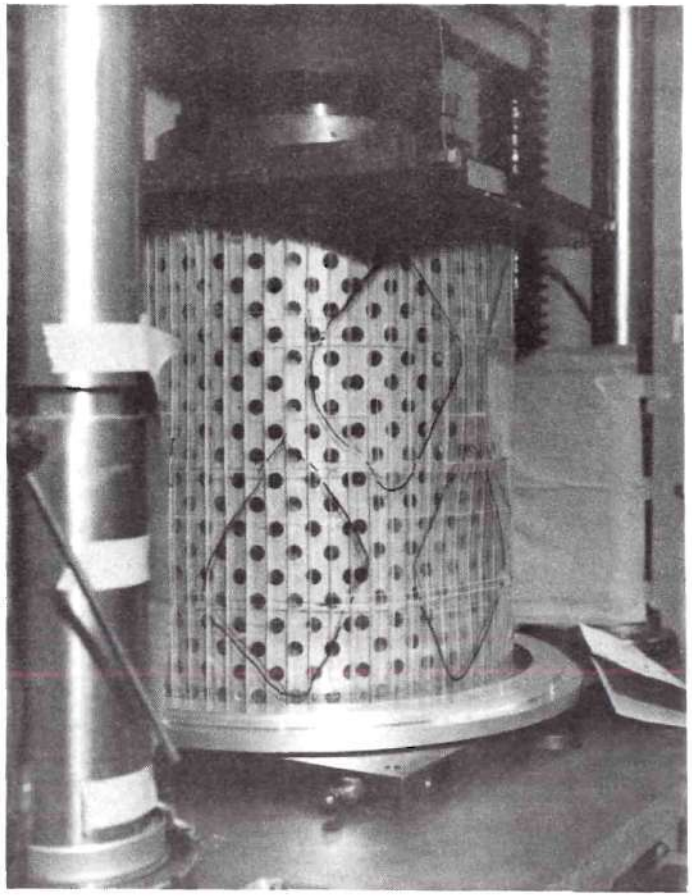

Figure 26. Highlighted Diamond Buckles on Shell 1006.

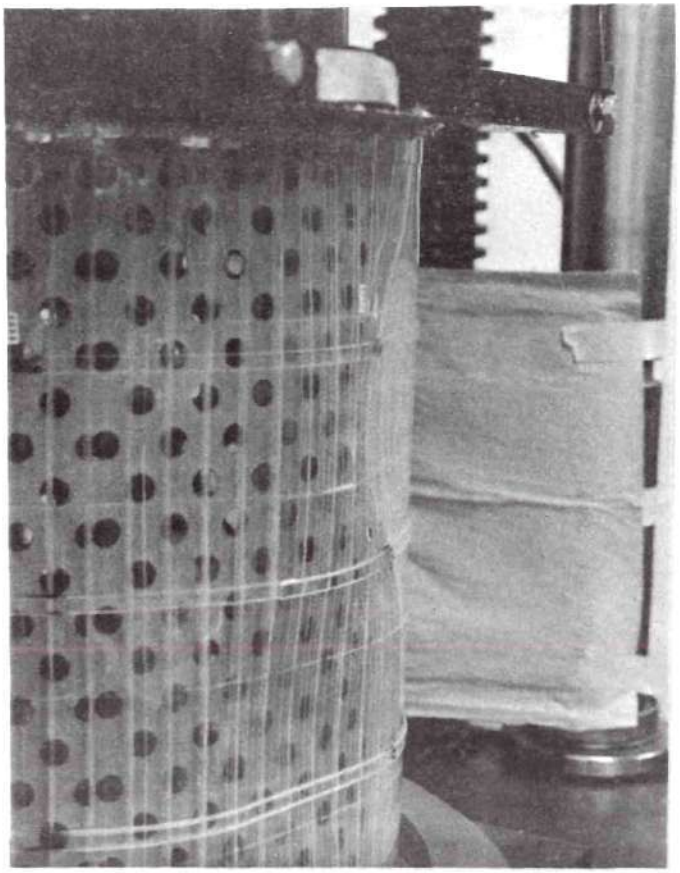

Figure 27. Buckles Covering Approximately 75% of the Surface of Shell 1006.

The initial shape of shell 1000 at the midlength circumference was determined using the accurately machined reference ring shown in Figure 28. A single transducer was used to determine the distance of each stringer from the ring. The largest excursions from circularity were observed in the seam area of the shell, most probably a result of the manufacturing technique.

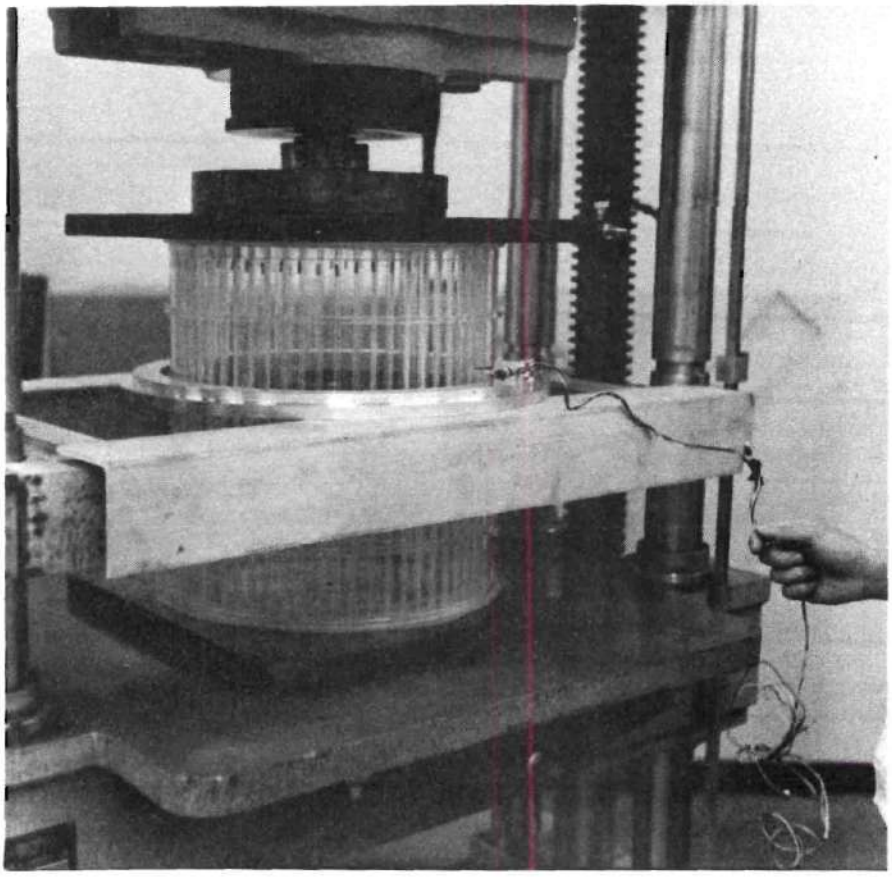

Figure 28. Scanning System for Determining the Initial Shape of Shell 1000.

CHAPTER V

DISCUSSION OF RESULTS

Tests under axial compression were performed on ring and stringer stiffened shell configurations as outlined in the previous chapter. These shells represented six stringer configurations and 41 different ring stiffenings. Two basic methods of wall motion measurements were used. For eight shell configurations the displacements were determined along generator lines. For the remaining bodies radial motions were determined in a plane normal to the generators. Actual buckling loads were obtained for nine of the shell systems. The remaining configurations were evaluated by means of the Southwell technique. Buckling test results and the various Southwell loads were compared to linear predictions using equations developed by Block (6). The computer program used for this comparison is contained in Appendix A.

Figure 29 shows the radial displacements of the midlength circumference of shell 1000 at several load levels. The initial shape is depicted by the heavy line on the figure. For the other shells in the program the initial shape was not determined. Figure 30 is a polar plot of the radial displacement at three loads for shell 1002. From these figures it is clear that as the load level increases a strong circumferential wave develops. This development takes place in a smooth fashion and the wave is well defined for load intensities substantially below critical.

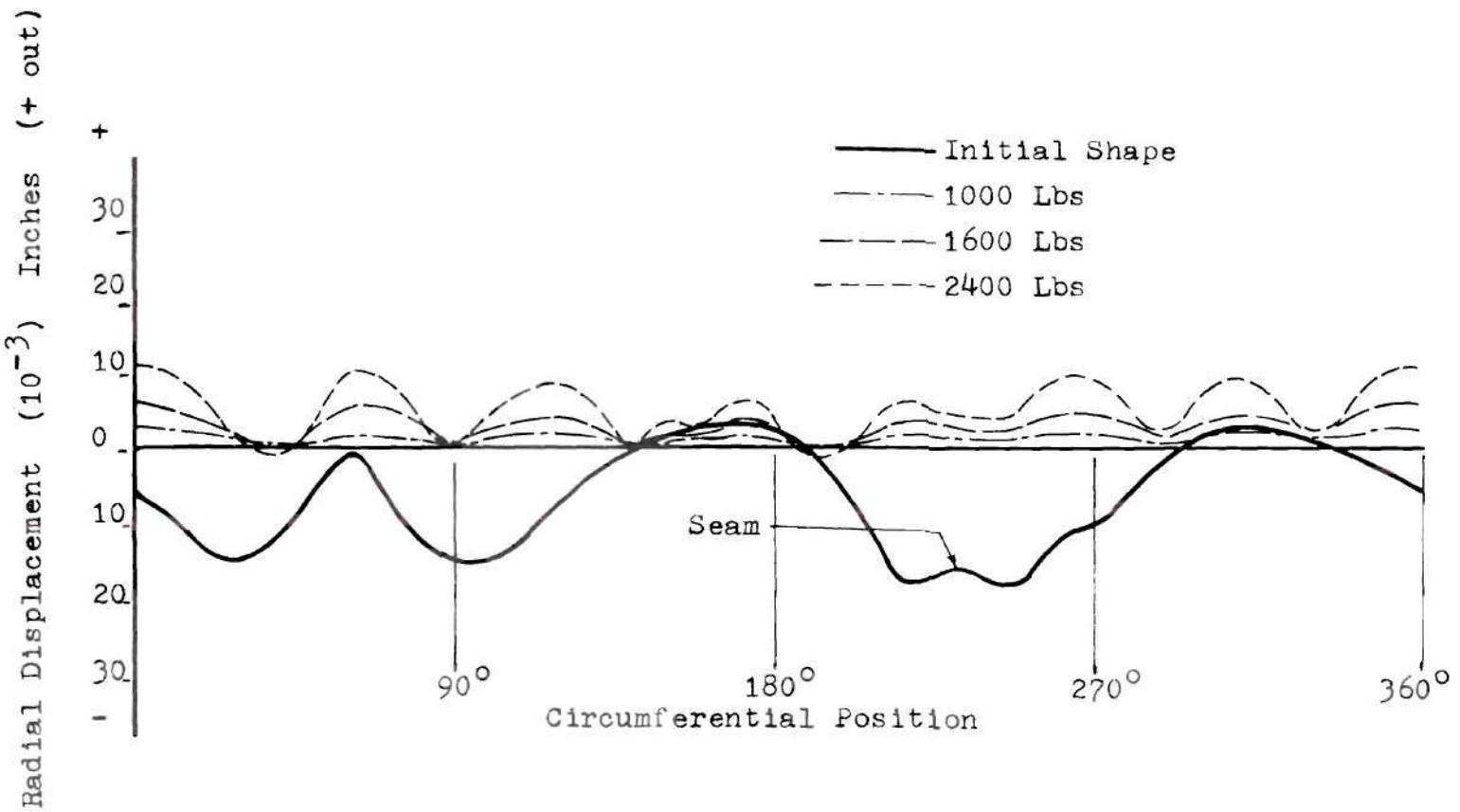

Figure 29. Initial Out-of Roundness, and Radial Displacement versus Circumferential Position for Three Loads - Shell 1000.

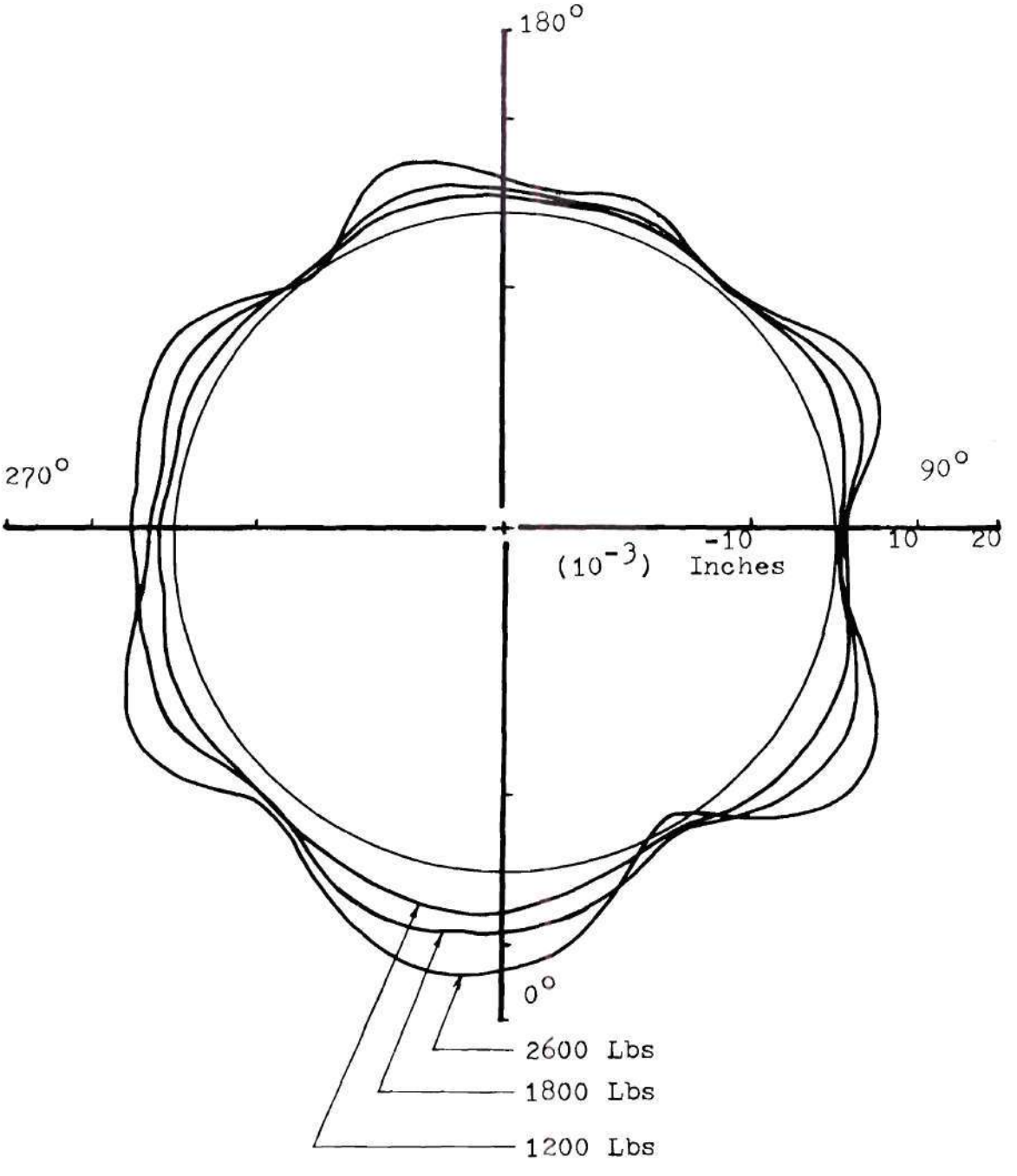

Figure 30. Radial Displacements versus Circumferential Position for Three Loads - Shell 1002

Displacement data along the full length was obtained on shell body 06XX. Graphs of radial wall displacements versus longitudinal position for a typical inward and outward displacement on shell 0601 are shown in Figures 31 and 32 respectively. These graphs give the displacement history for six axial loads, and reveal a well defined axial wave form. Figure 33 portrays the change in longitudinal wave form as a result of ring modification at a selected stringer location on shell 06XX.

The figures clearly demonstrate that the pre-buckle patterns tend to persist and increase in amplitude as the load increases. More significantly, the predominant wave length agrees well with that predicted by linear theory. The displacement histories also show the overall Poisson expansion of the shells under increasing load and a slight rigid body shift of the cross-sections.

The appearance of both longitudinal and circumferential waves in the pre-buckling deformations of axially compressed imperfect stiffened shells has been clearly demonstrated by Singer, Arbocz, and Babcock (16) and has been confirmed in the current program. These pre-buckle deformations are such as to validate the choice of the basic displacement function made in the simple linear theory development (6). Thus there are two distinct wave motions which can be investigated by means of a "Southwell type" analysis.

Since radial displacement measurements along shell generators were available earlier in the test program this form of the data received initial attention. The use of such a measurement scheme is also consistent with the usual convention for the Southwell

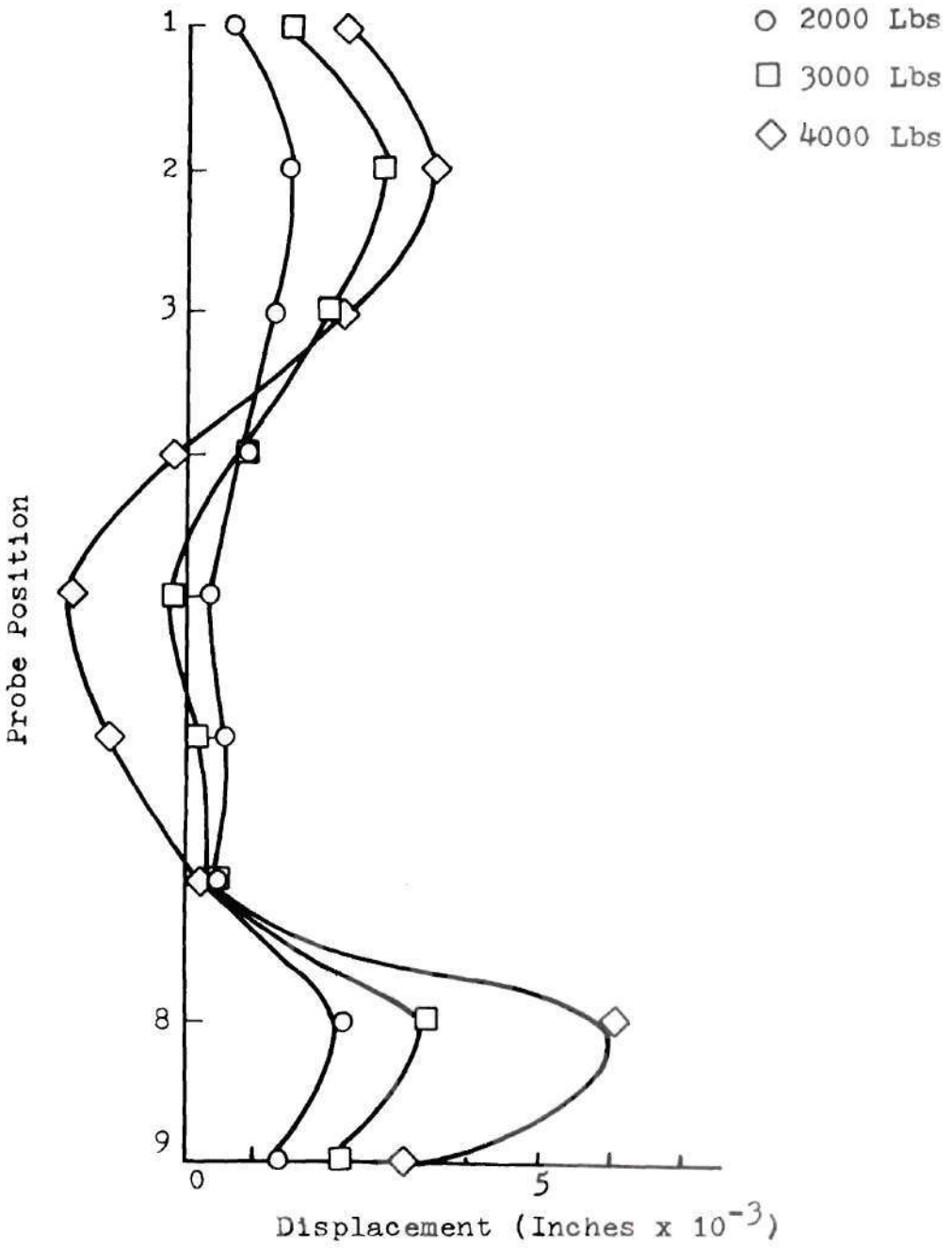

Figure 31. Wall Motion Along Longitudinal Generator for Three Loads at Station 36, Shell 0601.

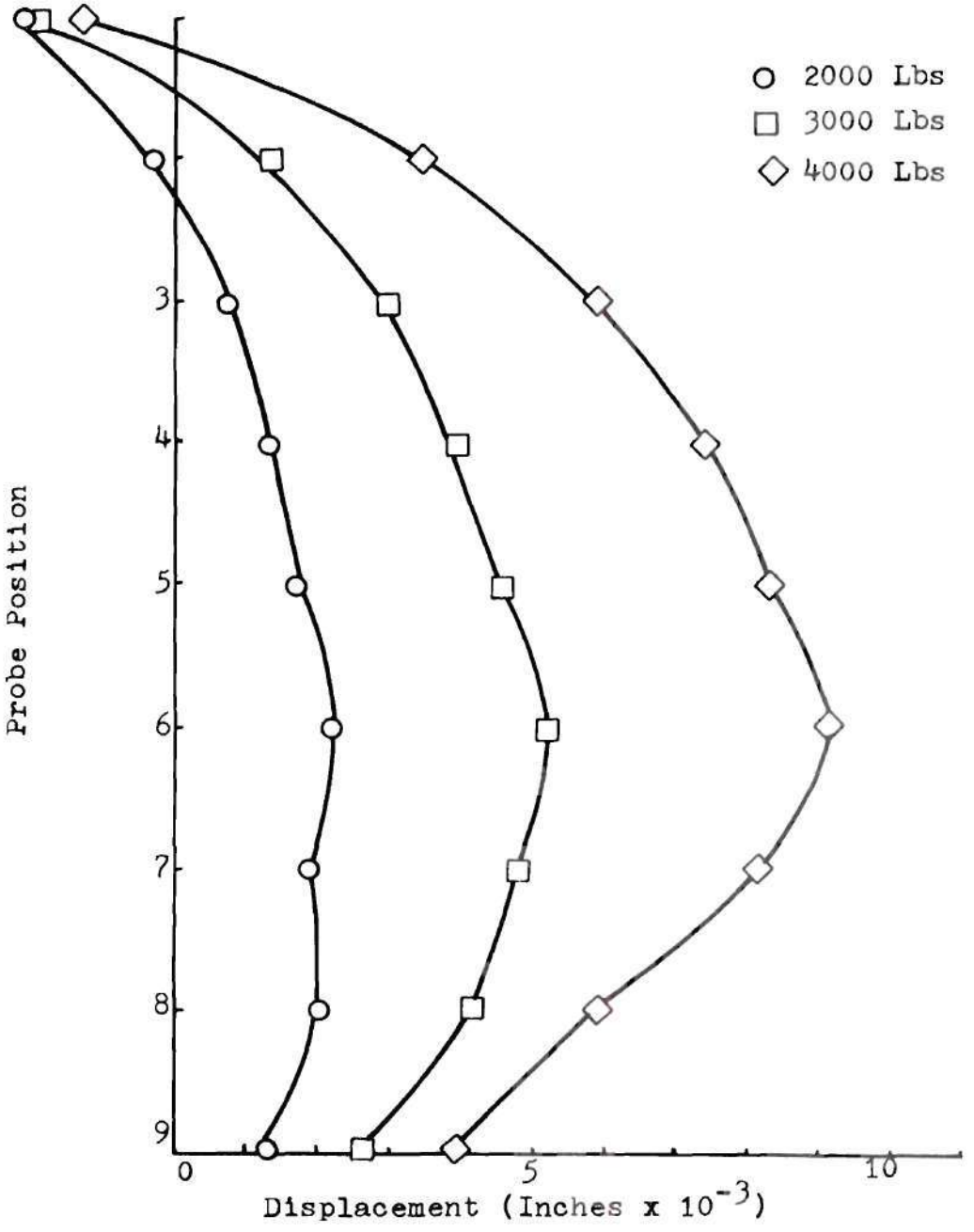

Figure 32. Wall Motion Along Longitudinal Generator for Three Loads at Station 44, Shell 0601.

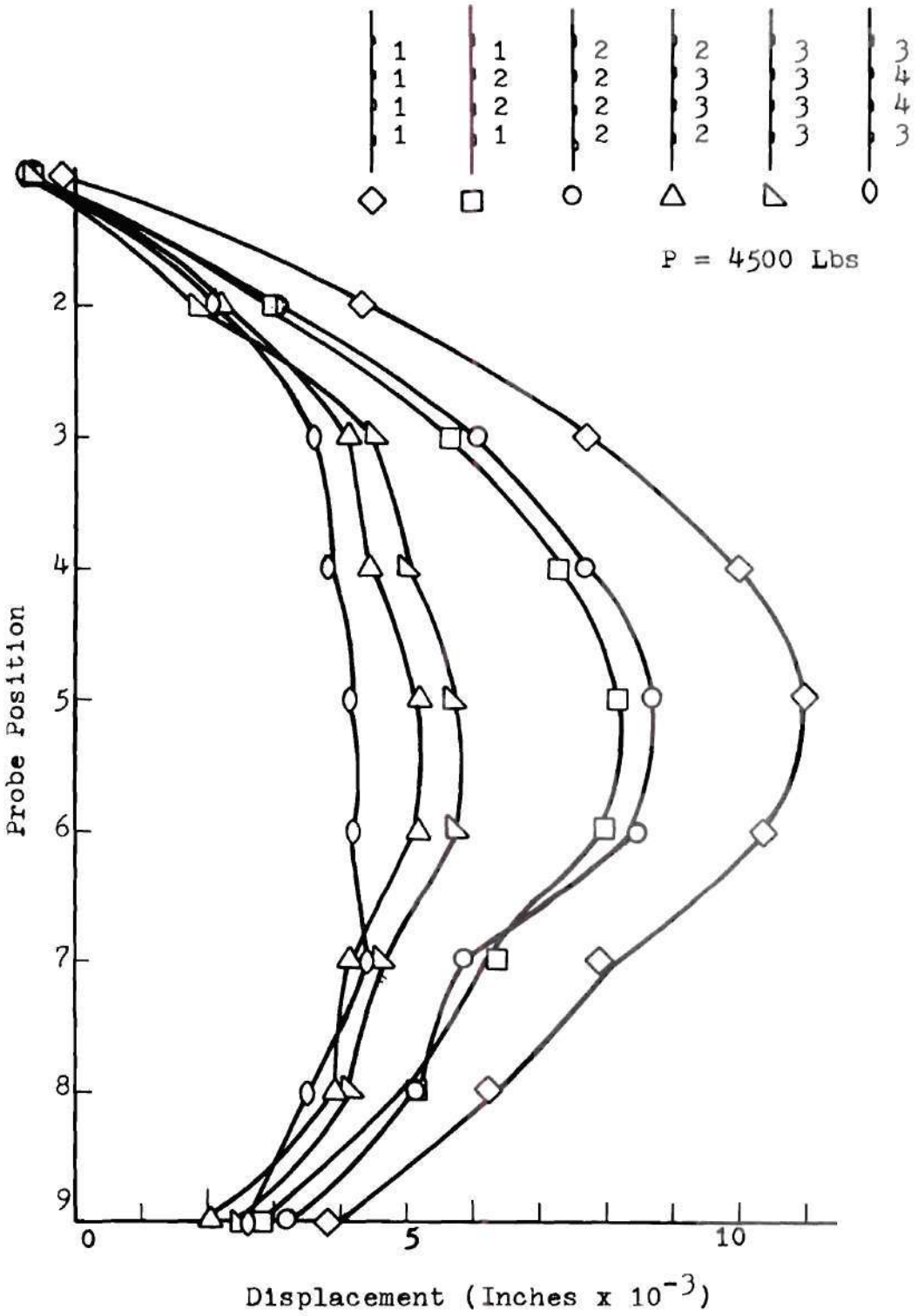

Figure 33. Wall Motion Along Longitudinal Generator for Six Ring Configurations at Station 56, Shell 06XX.

technique which utilizes lateral displacement data acquired at points along the line of action of the applied forces. Following this approach, a Southwell analysis of displacements along various stringers on shell 0601 was attempted. Although a well defined wave form was observed along the generators of this shell, the determination of a reference point from which to measure the displacements presented a problem. Previous investigators (11, 35) have shown that precise knowledge of such a reference point is essential. At those particular stringer locations which exhibited a strong inward motion under load, such as shown in Figure 31, the deflection for the Southwell attempt was taken as the difference between the maximum inward motion and the outer extremes of the curve. This resulted in Southwell plots of "fair" quality, the measure of quality being defined here as the degree of fit of the straight line to the data, and the number of load points for which the linear relation appeared to hold. The results of these calculations are listed in Table 6. Two examples of the Southwell lines obtained are shown in Figures 34 and 35. Additional plots of fair quality were obtained for certain stringer locations on shell 0608, which appeared to exhibit the panel type instability at higher loads (Figure 36). In these cases, the δ was taken as the difference between the center bay deflection and the average of the two adjacent ring deflections.

Loads obtained in these computations showed a wide variance, being both above and below the critical loads predicted by linear theory. It was clear at this point that an approximate Southwell relation could be obtained at a majority of the stringer locations.

Table 6. Southwell Data Obtained from Displacements along Generators on Shell 0601.

Stringer Number	P_{SW}
0	6550
2	8000
4	5340
6	7150
8	5760
10	6400
12	----
14	6100
16	----
18	6400
20	----
22	5000
24	5200
26	5000
28	5900
30	----
32	6500
34	5550
36	6200
38	5850
40	6000
42	7750
44	5900
46	6000
48	5720
50	5660
52	----
54	6750
56	5700
58	5310
60	5330

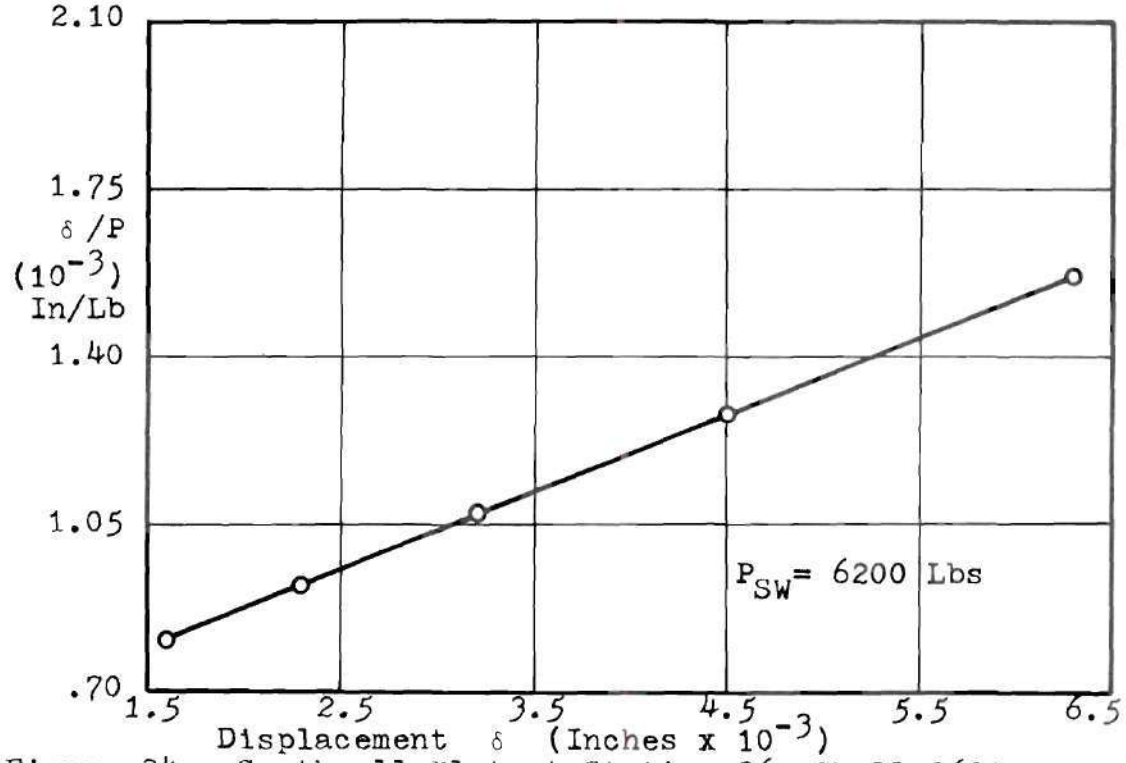

Figure 34. Southwell Plot at Station 36, Shell 0601.

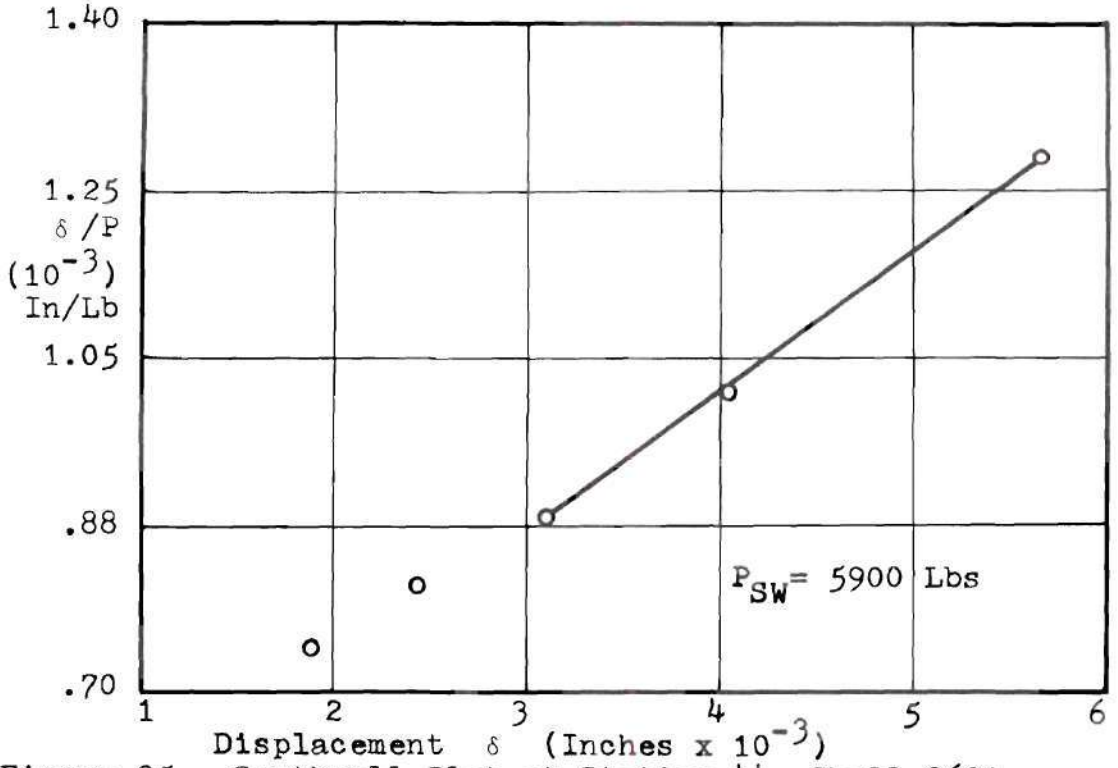

Figure 35. Southwell Plot at Station 44, Shell 0601.

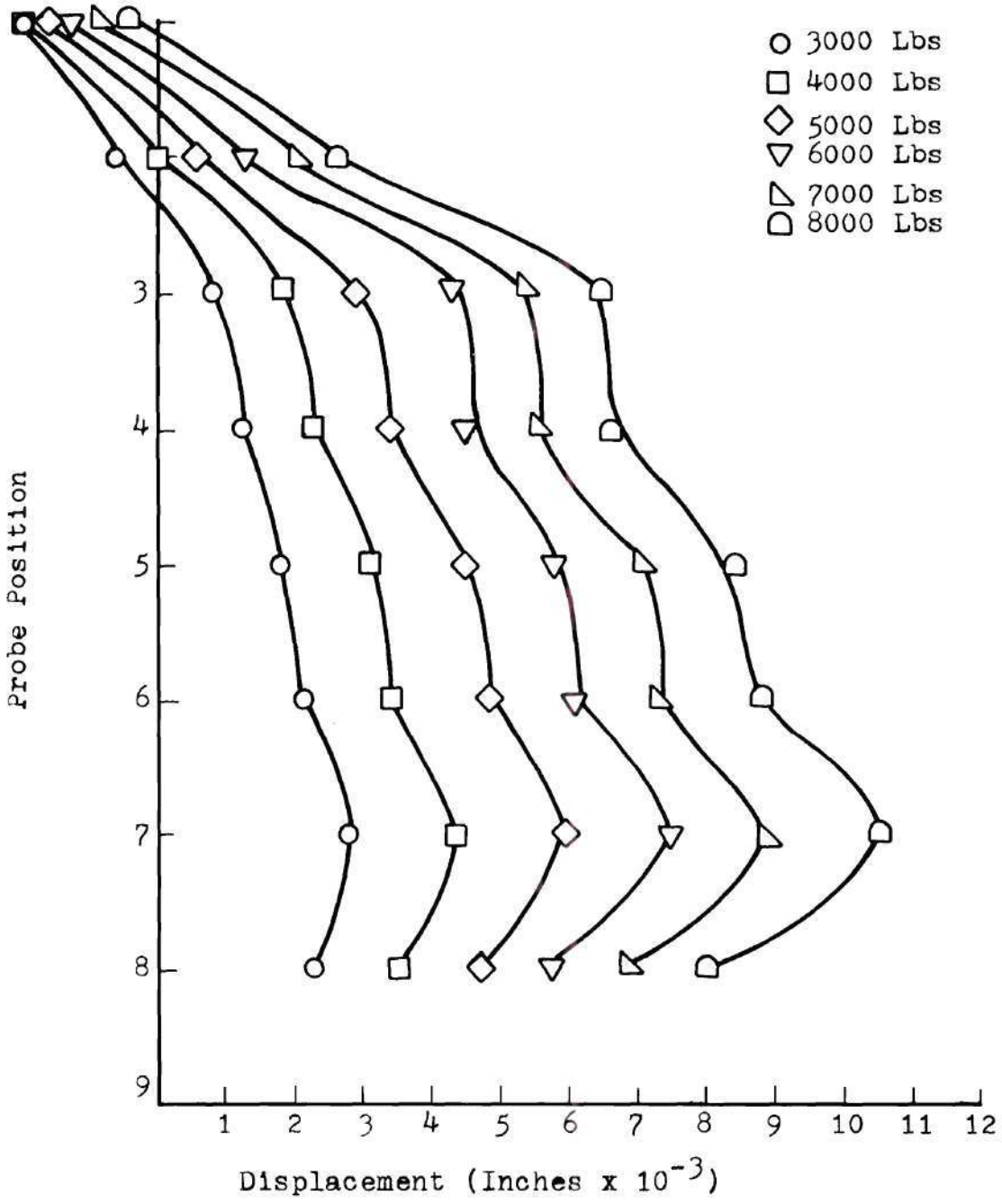

Figure 36. Wall Motion Along Longitudinal Generator for Six Loads at Station 44, Shell 0608.

However, the variation in the predicted buckling loads at different stringers and the fact that the results were highly dependent on the choice of reference point cast doubt on the usefulness of the method.

There seems to be little question that the problems encountered are due to several factors. First, the longitudinal wave form is highly influenced by boundary effects and ring discreteness. Second, it is sharply discontinuous at the shell boundaries. Finally, the Poisson expansion of the shell is included in the measurements of the imperfection growth. In view of these problems associated with the longitudinal wave form attention was directed to the radial displacement histories about a circumference. These displacements were of a complete periodic form. They contained a minimum of discreteness effects due to the closeness of the stringer spacing. Prior to attempting a Southwell analysis of this data a harmonic analysis was performed using the techniques described in Chapter II. The primary purpose of this analysis was to remove unwanted components of the deformation pattern, namely the zeroth and first modes. These components corresponded to overall Poisson expansion and the rigid body shift of the cross section respectively. The use of harmonic analysis also avoided the difficulty of searching for a single point at which to obtain a Southwell plot as the process automatically assesses the effects of all points over which it is applied.

The harmonic analysis of a periodic function, such as the circumferential distortions considered, results in a discrete spectrum. Such a spectrum is conventionally represented as a series of impulses at discrete wave lengths. Figures 37 through 39 show examples of such

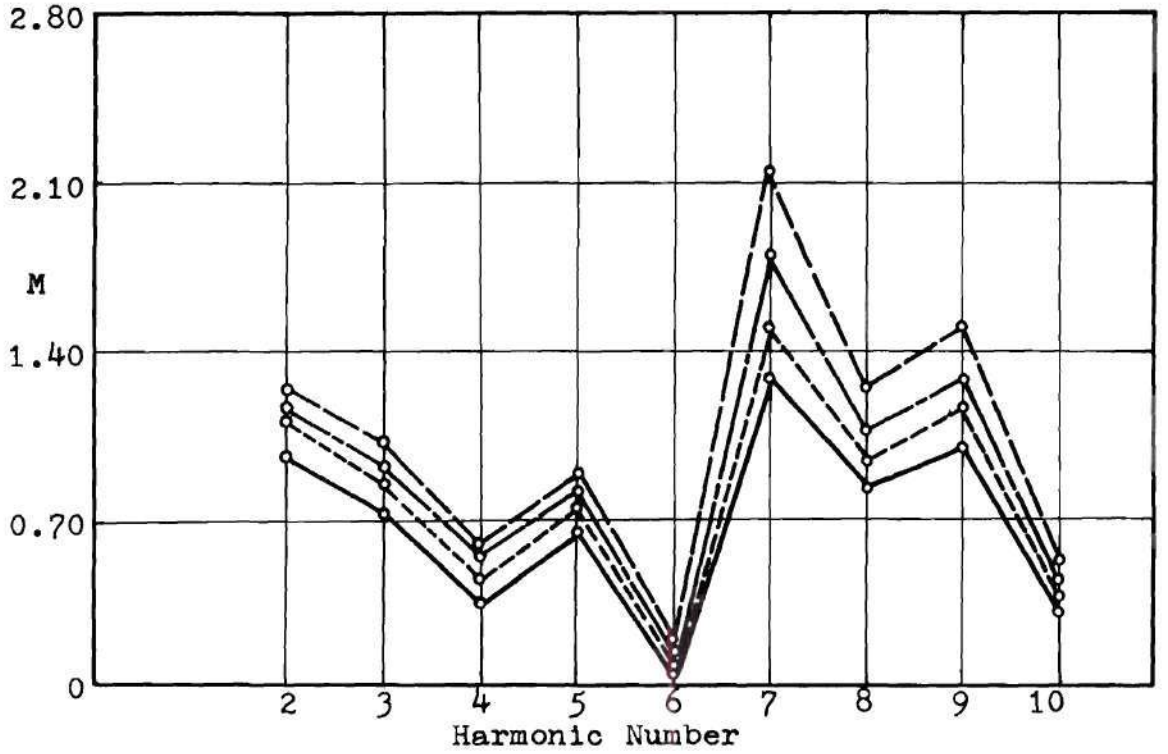

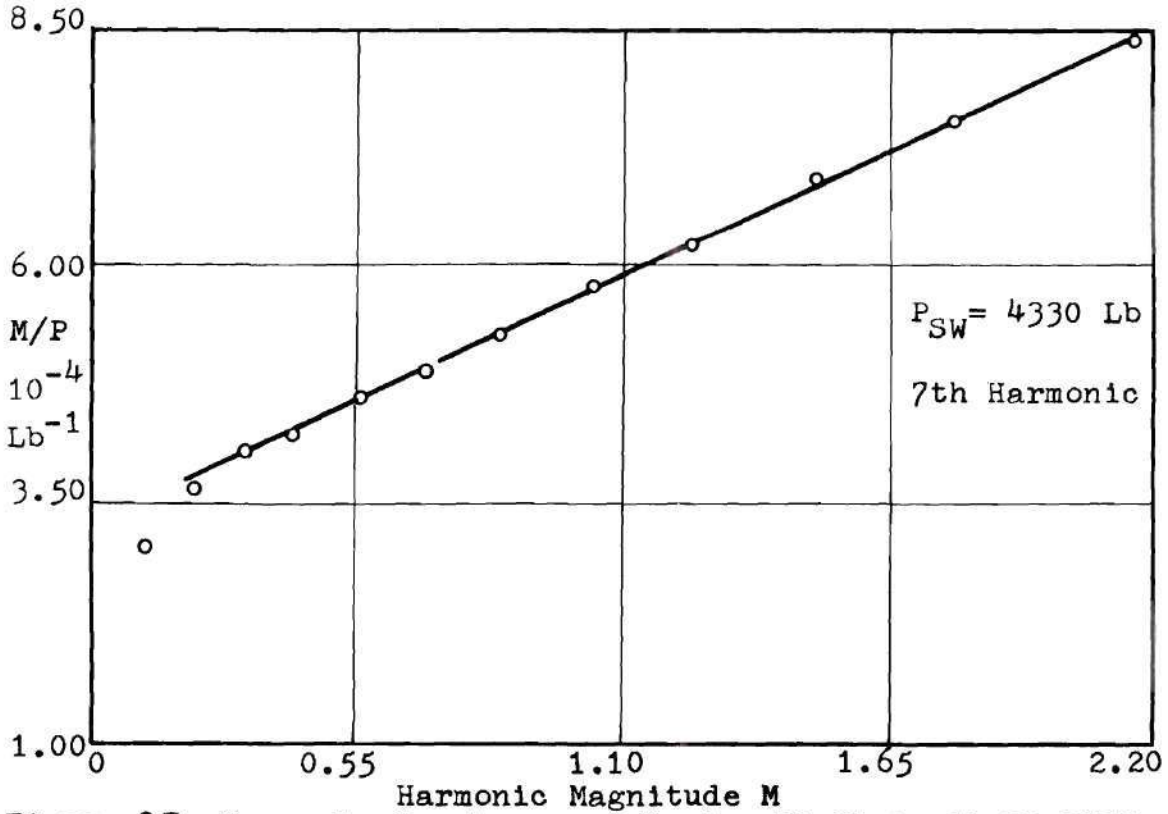

Figure 37. Harmonic Spectrum and Southwell Plot, Shell 0803.

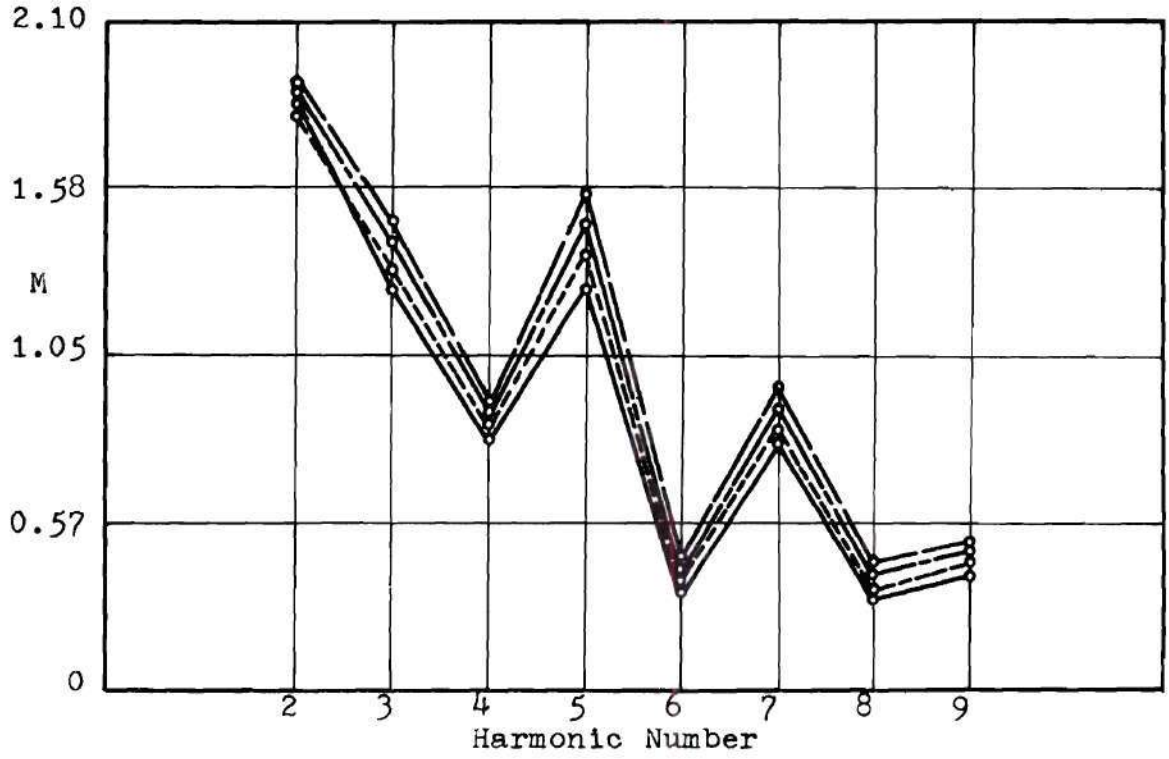

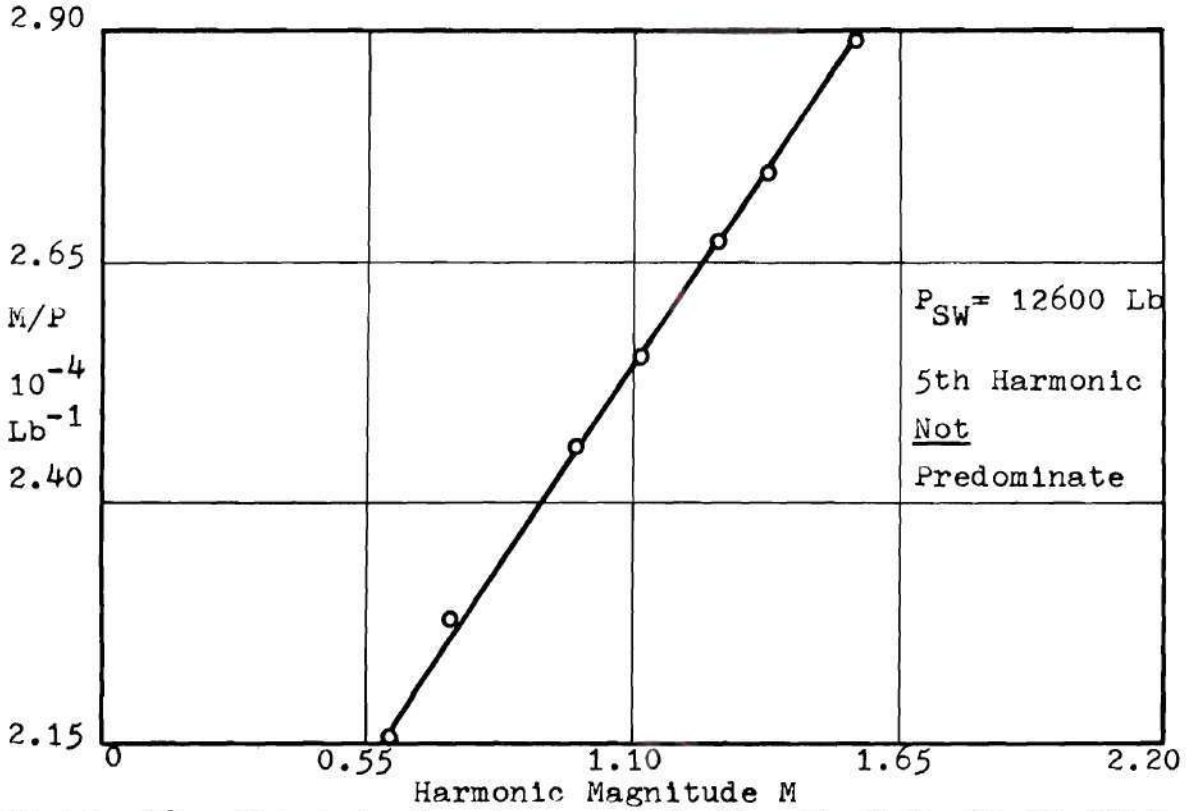

Figure 38, Harmonic Spectrum and Southwell Plot Shell 0813.

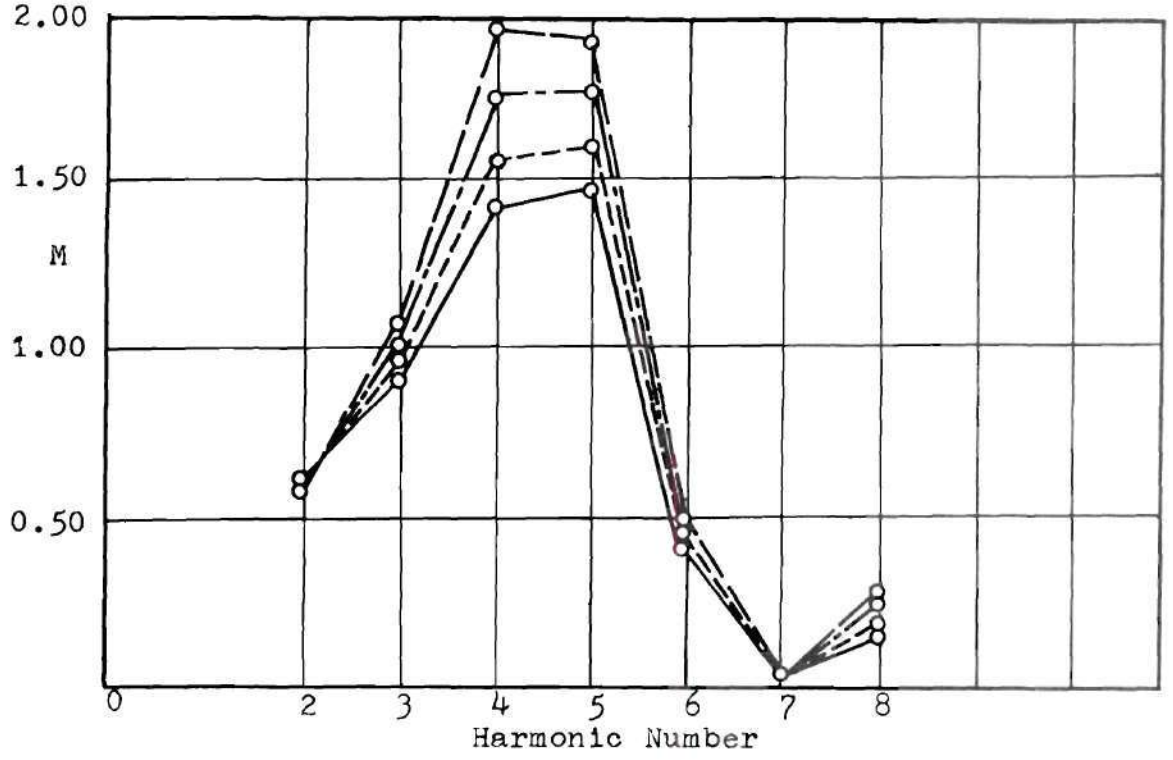

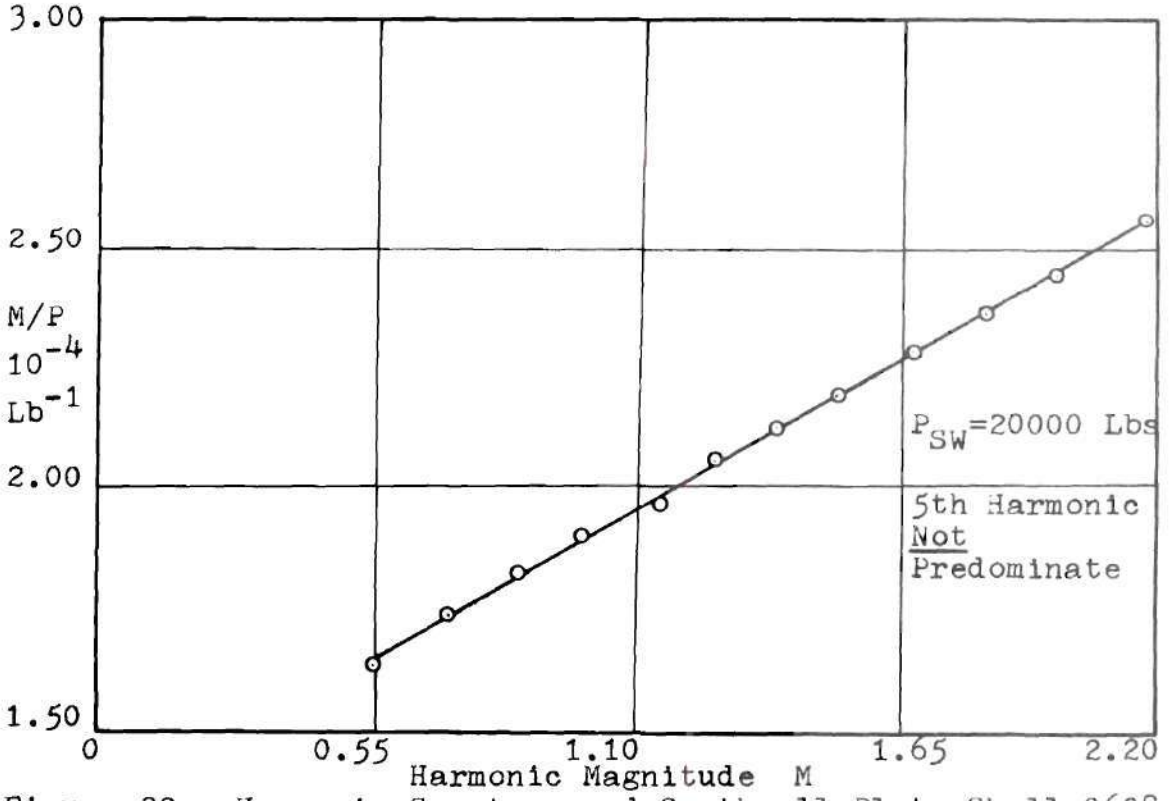

Figure 39. Harmonic Spectrum and Southwell Plot, Shell 0608

spectrums and the Southwell plots from this data. For clarity, the impulse peaks for the spectrum have been connected by straight lines to form an envelope.

With only a few exceptions, the Southwell results presented were obtained by treating the predominant harmonic as a displacement. Such a choice is equivalent to assuming the circumferential wave to closely resemble a sinusoid. The displacement histories of the shells, as shown in Figures 29 and 30, show that such an assumption is well justified. No displacement history was observed in which the shape deviated from a sinusoidal form to a large degree. Had such deviations been observed, a more complex form for the assumed displacement would have been required. Exception to the choice of the predominant harmonic was taken only when it was obvious that this wave was not representative of the shell buckle mode. An example is shown in Figure 38 where a second harmonic predominates as opposed to the expected 5th harmonic. One would suspect that this behavior may be related to the initial out-of-roundness of the shell in question. Unfortunately data was not available to confirm this hypothesis. In all, only three such cases were observed.

The use of the predominant harmonic was further substantiated by comparison to results obtained from a study of other components of the harmonic spectrum of selected shells. This analysis resulted in either the same predicted load as the predominant harmonic, a higher value, or no straight line relation. Such a Southwell plot is illustrated in Figure 39, showing a higher predicted load for the 5th harmonic

which represented the second highest value in the spectrum. The adequacy of the number of observations around the circumference is illustrated in Figure 40. This figure shows a Southwell load for shell 0608 obtained from data at 31 alternate spaced stringer locations. An analysis of the full set of 63 data points gave the same buckling load.

A problem in the determination of the Southwell load was the choice of position along the longitudinal axis of the shell at which to perform the circumferential scan. This was not a totally unexpected problem. Flügge (18) had similar difficulties with the compressed unstiffened shell and all subsequent experimenters have experienced the same trouble. Logically the choice of station must be such that the total motions most nearly represent sections through a fully developed buckle pattern. For the shell families tested the near central region of the shell surface fulfilled this requirement. The analysis of data from various scan locations to substantiate this choice is discussed in Chapter IV.

Figure 41 presents in graphical form a comparison of the Southwell loads for shells 0601 through 0608 to the corresponding linear theory values. The data is plotted against an artificial ring stiffness parameter S_R. This number represents the total number of 0.030 inch ring layers on the shell but does not provide an indication of distribution. The particular distribution of ring stiffness is indicated by the small diagram above each point. The lines connecting the discrete points are drawn to emphasize the trend of behavior and are not intended to infer that a continuous function is represented.

Close agreement between the Southwell loads and those predicted

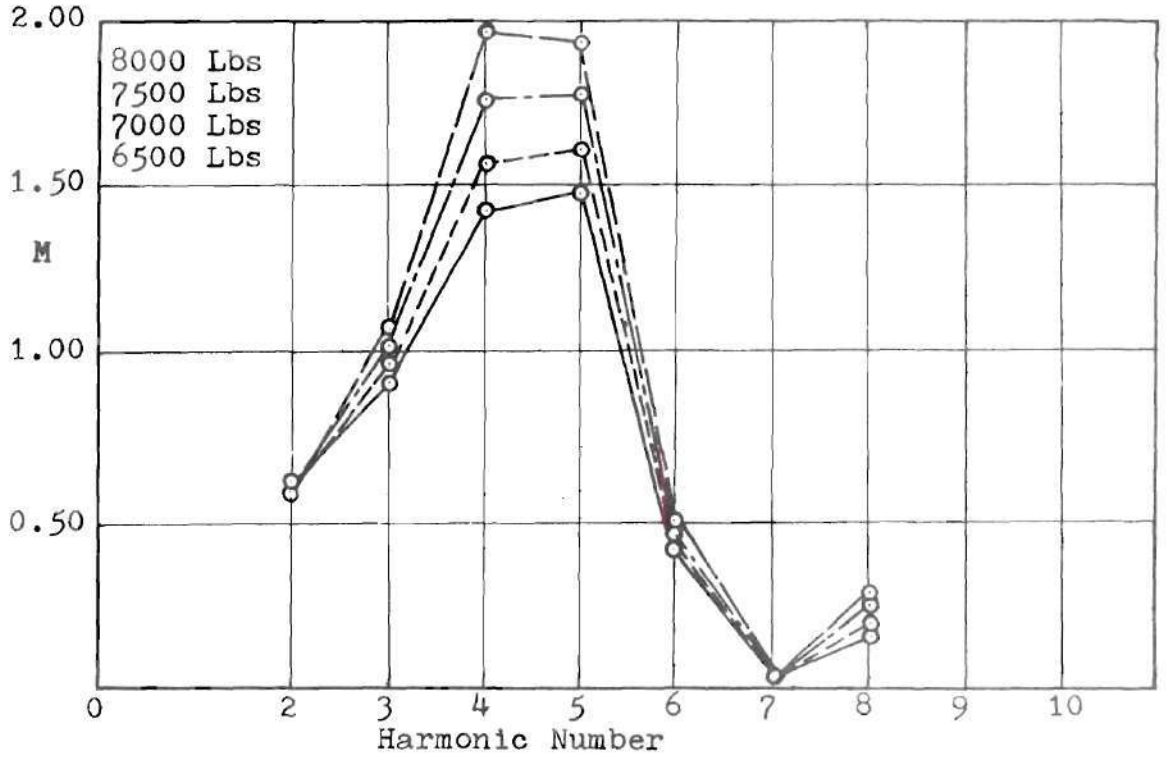

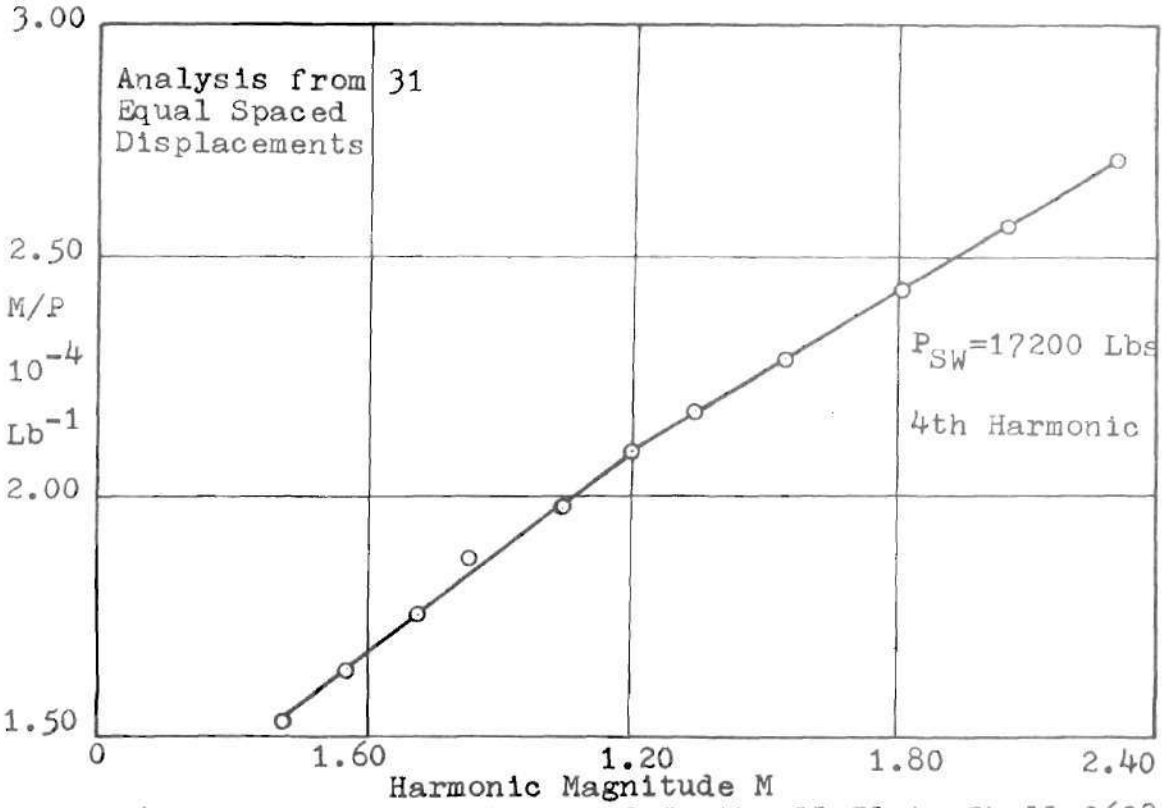

Figure 40. Harmonic Spectrum and Southwell Plot, Shell 0608.

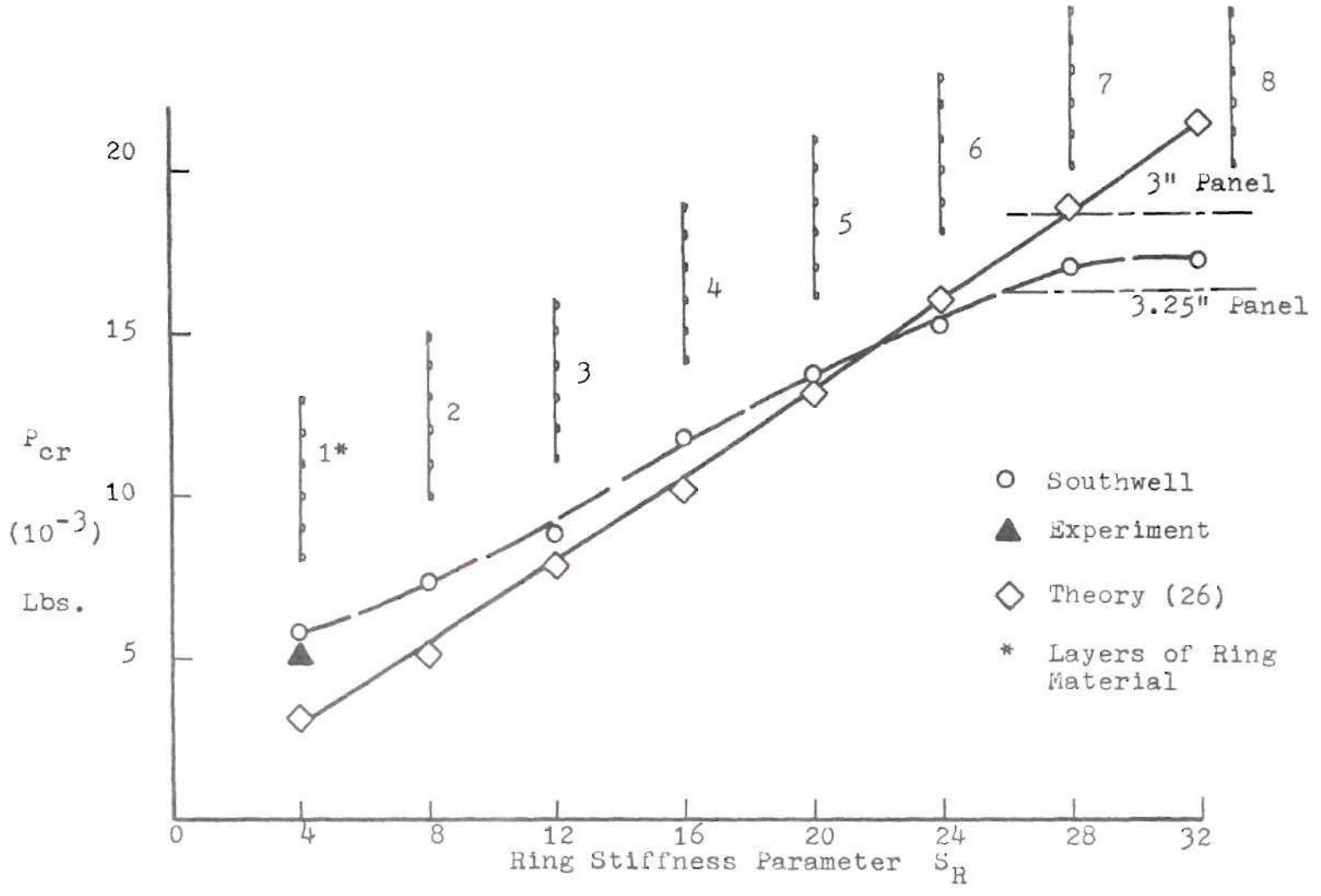

Figure 41. P_{sw} and P_{cr} versus Ring Stiffness - Shell06XX .

by linear theory is evident within the range of ring stiffening for which the linear theory is considered to be applicable, i.e., moderate to heavy rings. Load values for light ring configurations which approach the form of pure longitudinal stiffened shells are considerably higher than those predicted by linear theory. This result is not surprising since the conditions of simple support at the shell ends are not met. The effects of such end restraints, while not important for moderate to heavy ring stiffened shells, has been shown to be highly significant for longitudinally stiffened shells (27).

Additional features of Figure 41 are significant. The Southwell load corresponding to the lightest ring configuration, shell 0601, was considerably higher than that predicted by the linear theory, for the reason previously stated. The validity of this load was demonstrated by elastically buckling the shell. The instability load level is indicated by the solid triangle in the figure. The close agreement between actual load and Southwell load is obvious. It is possible that a theory incorporating effects of end restraints would predict this buckling load with the same accuracy as the Southwell technique. Such an analysis was not attempted since no measure of the end fixity was available. It is in such areas of unknown boundary restraint that experimental results often provide the only means to assess the actual behavior of a structure.

The determination of an effective length for panel instability is a particularly difficult problem as no method exists for accurately assessing the panel circumferential edge fixity. Hence, for the comparative analysis two simply supported effective bay lengths were used.

These were 3.00 inches and 3.25 inches respectively. The corresponding loads should represent a reasonable upper and lower bound to the critical panel instability load for this shell. It is clear from Figure 41 that the Southwell loads determined from the test data assymptotically approach a line which lies midway between these two. It is of interest to point out that there is no experimental evidence to suggest a sudden change in load carrying capability as the general instability gives way to panel instability. The transition is smooth, no jump in the predominant circumferential wave number being observed between general and panel instability.

Comparisons of Southwell and linear theory prediction data for shells 08XX and 09XX are shown in Figures 42 and 43. Except for the very light ring stiffener cases the correspondence is very close. Ring stiffnesses for these tests were not increased to the range of panel instability. The stresses which would have developed at the higher loads required for such testing in the panel instability region would have exceeded 50 per cent of the yield stress of the material. In light of the catastrophic failures which are characteristic of this plastic at high stresses such testing was not feasible. In order to reduce the stresses, and permit a buckling test, four rings were removed from shell 0813. The resulting three ring configuration was designated as shell 0814. The theoretical general instability load for this shell was calculated as 9463 pounds, and this compares favorably with the Southwell determined load of 9060 pounds. The shell actually buckled at 8100 pounds. This gave a predicted to actual load ratio of .86 when compared to the linear theory and .89 when compared to the

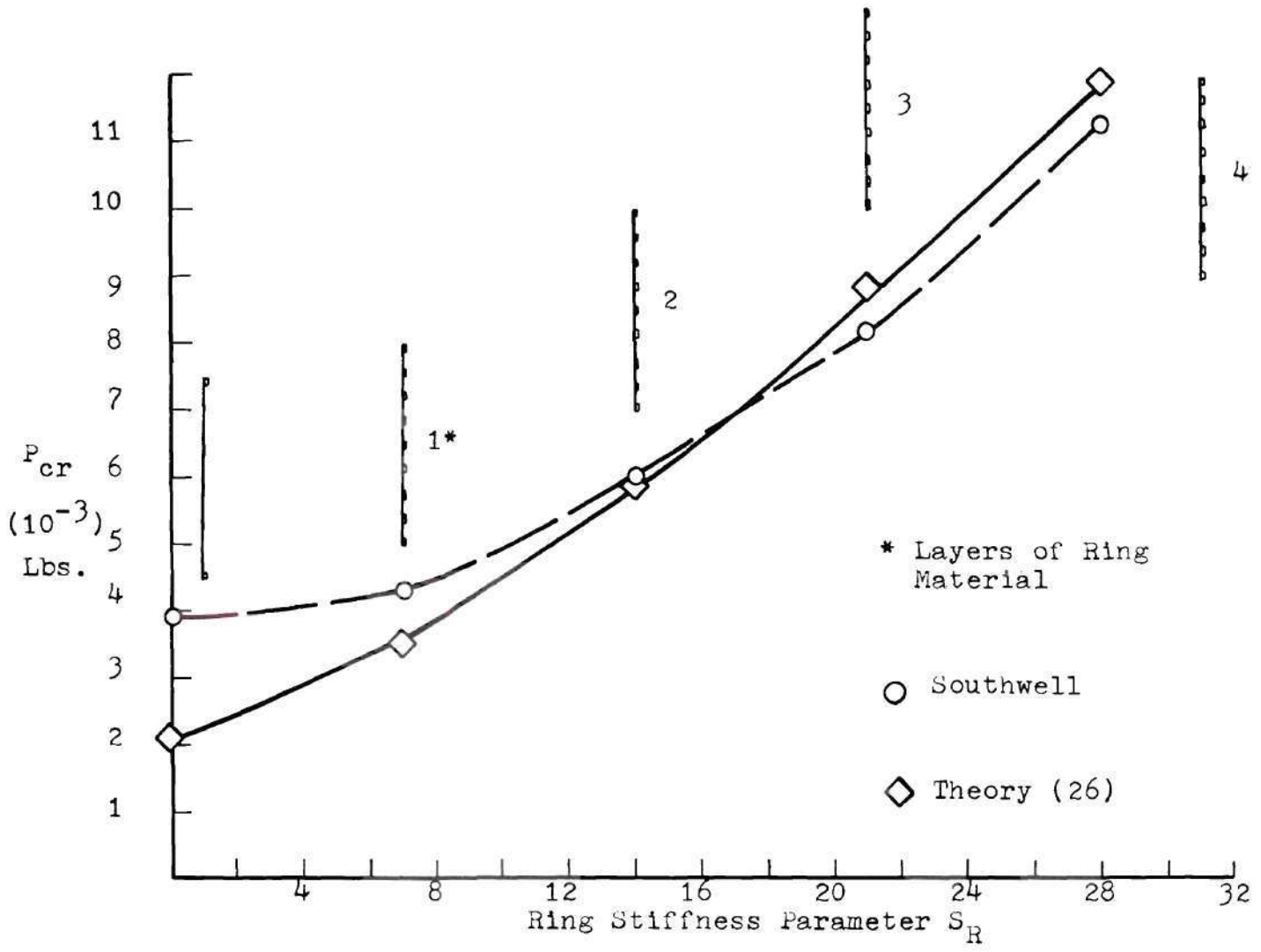

Figure 42. P_{cr} and P_{sw} versus S_R, Uniform Rings, Shell 08XX.

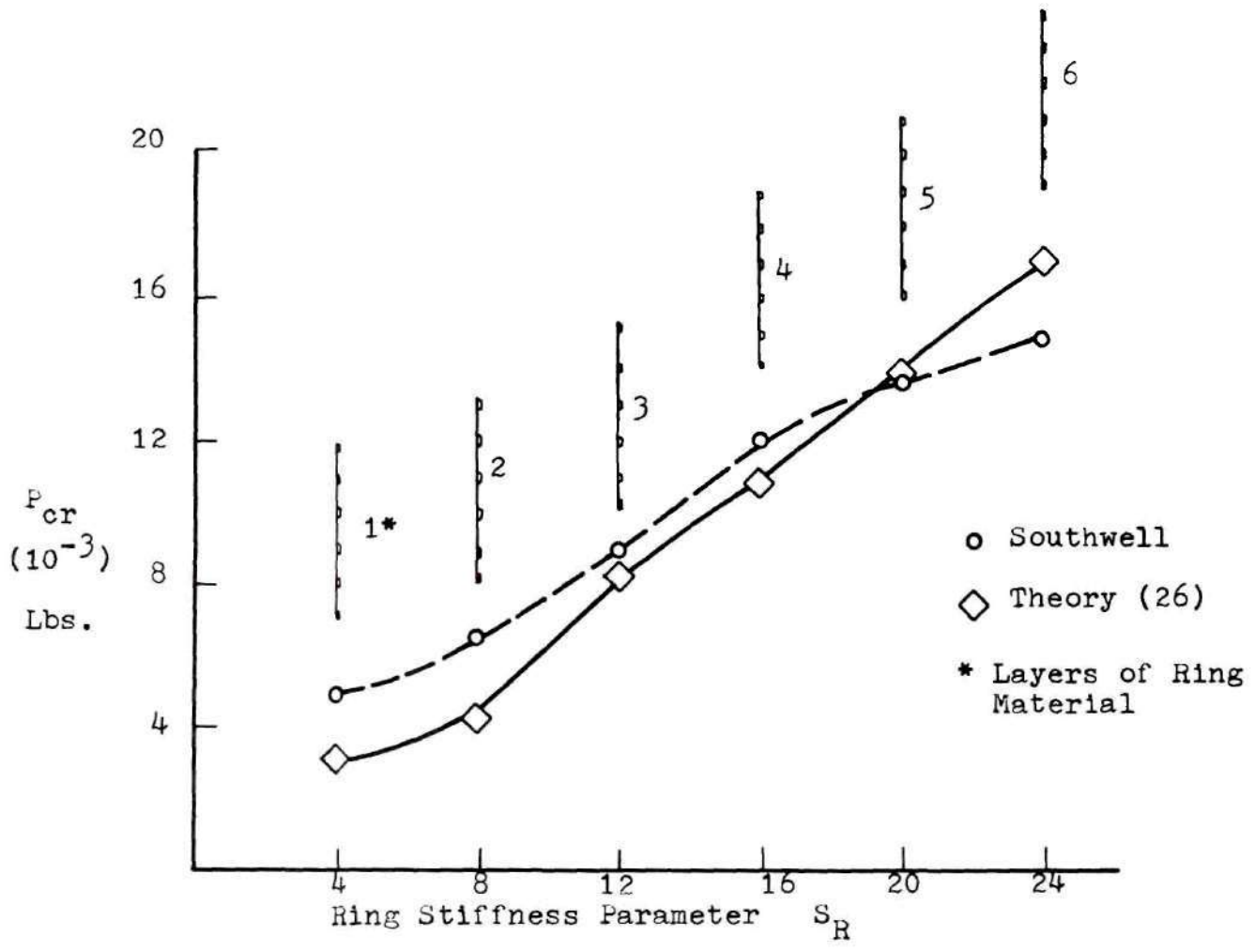

Figure 43. P_{cr} and P_{sw} versus S_R , Uniform Rings, Shell 09XX.

Southwell load. General instability was observed for an instant before destructive post-buckle behavior occurred.

Shell 0911, shown as the largest value of the ring stiffness parameter in Figure 43, was also buckled. Ring removal was not feasible on this shell because the bond between the skin and the lightweight stringers would have been damaged. Skin wrinkling was observed in the top bay of the shell and cracking of the material preceeded general instability. In view of the evidence of material failure as well as the onset of the skin wrinkling, the low load for this shell does not appear to be a contradiction of either the linear theory or the Southwell results.

Table 7 shows Southwell, theoretical, and experimental loads for the shells with uniform ring distributions. The ratios of buckling values indicate the degree of correspondence. Values of these ratios which exceed unity are for light ring configurations in which the effects of rotational end restraints are significant. The low value for the ratio P_{sw}/P_{cr} for shell 0608 is due to panel instability. Similarly, the low value for P_{exp}/P_{cr} on shell 0911 can be attributed to the skin wrinkling. All other values for the ratios shown are in good agreement with data obtained for stiffened shell tests by other investigators (7, 12, 19, 27). The values of n_{cr} and n_{exp} show relatively good agreement between circumferential wave number predicted by theory and the predominant harmonic obtained experimentally.

Results of elastic buckling, Southwell calculations, and linear theory predictions for shells 1000 through 1008 are plotted against the ring stiffness parameter, S_R, in Figure 44. Critical loads

Table 7. Uniform Ring Configurations

Shell Number	P_{cr*}	P_{SW}	P_{exp}	n_{cr}	n_{exp}	$\frac{P_{SW}}{P_{cr}}$	$\frac{P_{exp}}{P_{cr}}$	$\frac{P_{exp}}{P_{SW}}$
0300	16,049	-	14,650	-	-	-	0.91	-
0400	16,864	-	14,750	-	-	-	0.88	-
0500	16,792	-	15,200	-	-	-	0.92	-
0601	3,084	5,700	5,290	6	7	1.84	1.71	0.93
0602	5,183	7,500	-	5	6	1.45	-	-
0603	7,852	8,300	-	5	5	1.05	-	-
0604	10,000	11,650	-	5	5	1.16	-	-
0605	13,238	13,700	-	5	5	1.03	-	-
0606	15,857	15,200	-	5	4	0.96	-	-
0607	18,711	17,250	-	4	4	0.93	-	-
0608	21,212	17,200	-	4	3	0.80	-	-
0701	12,500	13,300	-	4	5	0.94	-	-
0800	2,151	3,900	-	6	7	1.82	-	-
0801	2,537	4,000	-	6	7	1.58	-	-
0802	2,902	4,100	-	6	7	1.41	-	-
0803	3,579	4,330	-	6	7	1.14	-	-
0807	5,943	6,000	-	6	7	1.01	-	-
0810	8,901	8,230	-	5	5	0.93	-	-
0813	11,999	11,300	-	5	5	0.95	-	-
0814	9,463	9,060	8,100	5	5	0.96	0.86	0.89
0901	3,188	4,870	-	6	6	1.53	-	-
0903	5,188	6,430	-	5	6	1.24	-	-
0905	8,204	8,850	-	4	6	1.08	-	-
0907	10,814	12,000	-	5	6	1.11	-	-
0909	14,009	13,700	-	5	6	0.97	-	-
0911	17,200	14,800	11,900	4	3	0.86	0.70	0.81
1000	1,863	4,100	3,720	7	7	2.20	2.00	0.91
1002	3,512	4,600	4,130	7	7	1.31	1.18	0.90
1006	4,452	5,430	5,160	7	7	1.22	1.16	0.95

* From General Instability Equation.

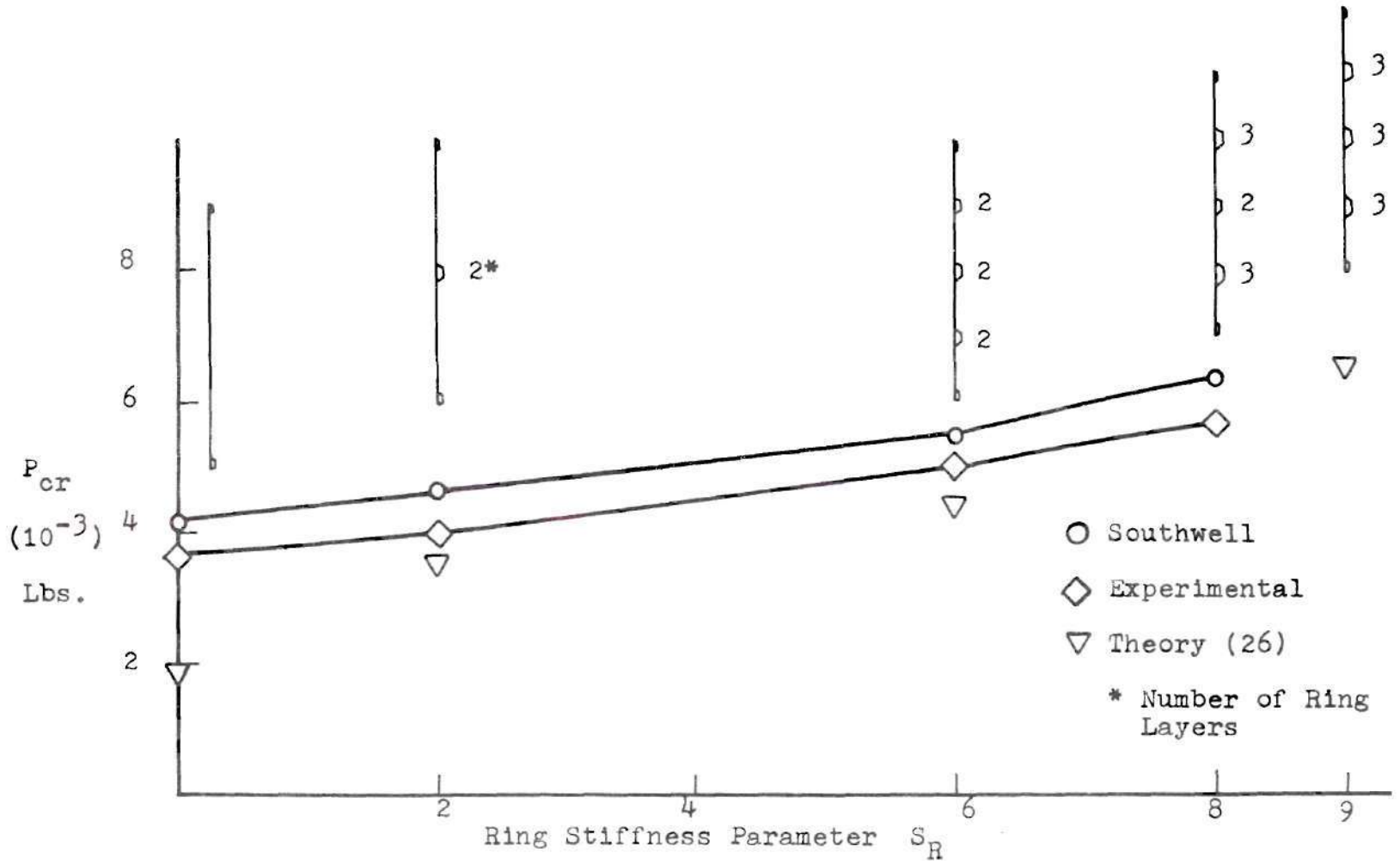

Figure 44. P_{cr} and P_{sw} Compared to Experimental Loads, Shell 10XX.

for repeated elastic buckling of these shells are given in Table 8. As can be seen from the table these show excellent repeatability, with the exception of the first instability load for shell 1006. This value was obtained only a few minutes after the shell had been subjected to a series of loadings which approached 80 per cent of the critical load for the shell. These loads were applied during the acquisition of displacement data. Viscoelastic effects in the material were apparently responsible for this low initial buckling load. Not only did the shell buckle at a higher value after an unloaded period of 12 hours but the higher load was repeated on four subsequent tests.

Photographs were obtained of buckles on shell 0300. These are given in Figures 45 and 46. Careful examination shows skin wrinkling in the area adjacent to the buckle. A definite buckle pattern was observed for all shells. However, photographs could not normally be obtained before explosive failure of the specimens occurred. High speed motion picture photography would have enabled recording of all the instability patterns but such instrumentation was not attempted. Figures 47 and 48 show second and third mode behavior on shells 1006 and 1007. The success of this photography was due to the use of a restraining mandrel and the relatively low stresses involved.

A number of tests were conducted on shells with non-uniform ring distributions along their length. The results are given in Table 9. Although such tests were not a primary part of this investigation, the opportunity to obtain data on such configurations resulted from the systematic build up the ring stiffeners. In all cases the non-uniform configurations tested were symmetric about the midlength of the shells.

Table 8. Repeated Buckling Tests for Shell 10XX.

Shell Number	Test Number	Load (Lbs.)
1000	1	3,720
	2	3,712
1002	1	4,120
	2	4,128
	3	4,124
	4	4,120
1006	1	4,720
	2	5,160
	3	5,150
	4	5,146
	5	5,158
1008	1	5,740
	2	5,737
	3	5,750

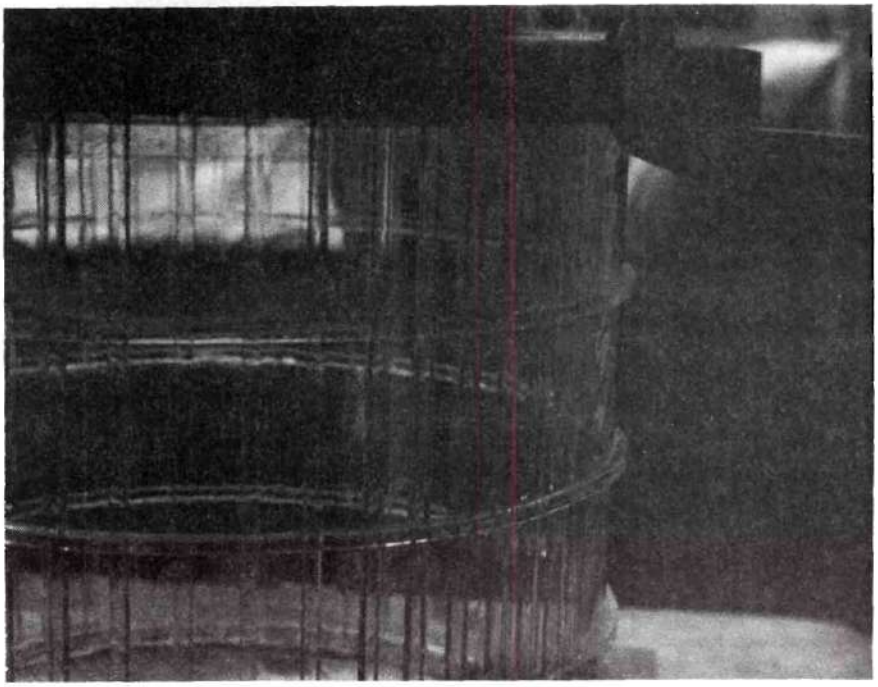

Figure 45. Skin Wrinkling on Shell 0300.

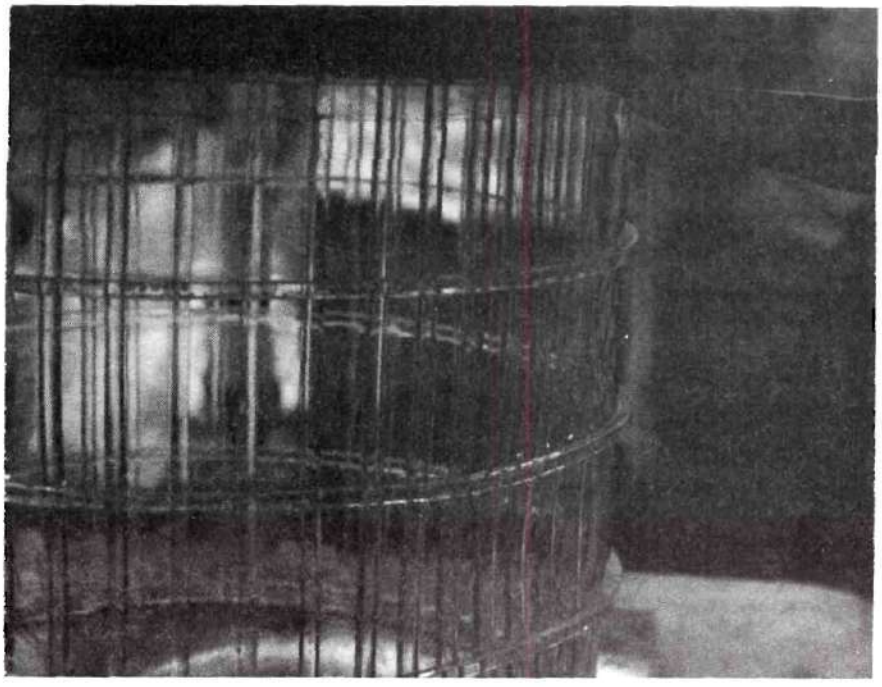

Figure 46. Panel Buckling on Shell 0300.

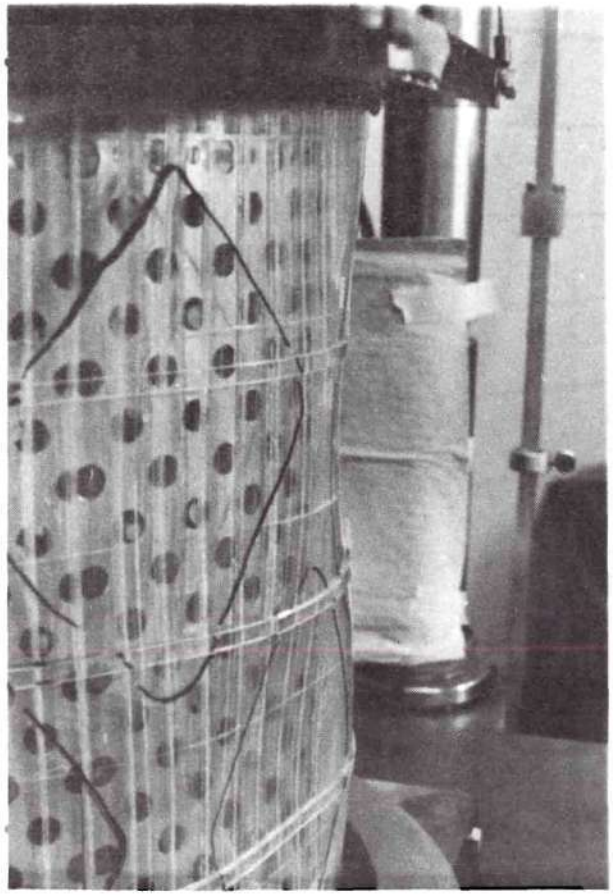

Figure 47. Buckling in Second Longitudinal Mode - Shell 1006.

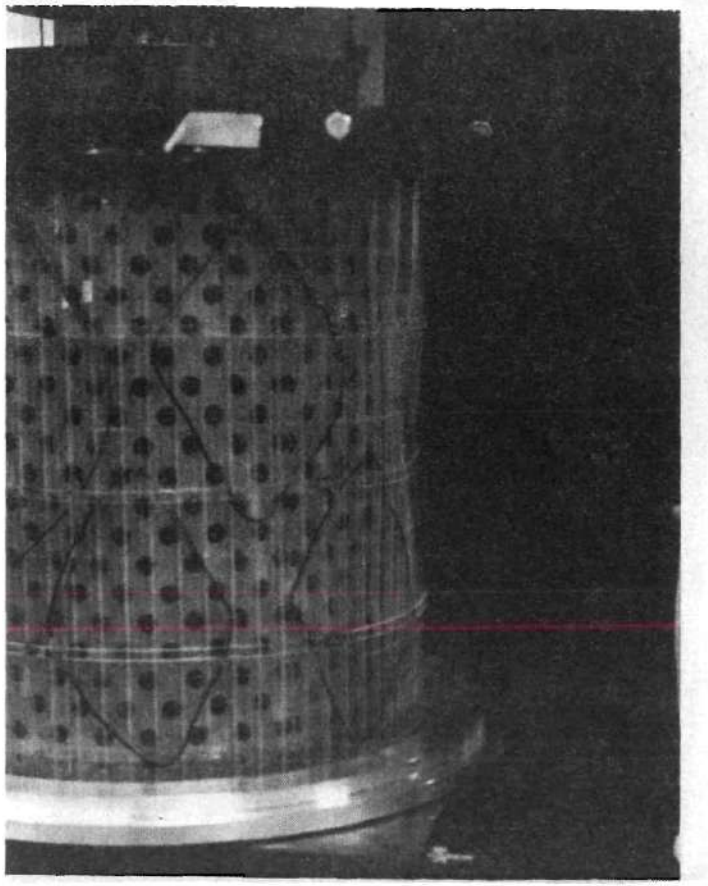

Figure 48. Buckling in Third Longitudinal Mode - Shell 1008. (Diamond Pattern is from Earlier Shell 1006.)

Table 9. Non-Uniform Ring Configurations

Shell Number	P_{SW} (Lbs.)	Ring Configuration (Figures 7 - 11)						
0804	5,230	1	1	1	2	1	1	1
0806	5,330	1	2	1	2	1	2	1
0808	7,900	2	2	2	3	2	2	2
0809	8,000	2	3	2	3	2	3	2
0811	9,150	3	3	3	4	3	3	3
0812	9,240	3	4	3	4	3	4	3
0902	6,440	1	2	2	1			
0904	7,000	3	2	2	3			
0906	10,200	3	4	4	3			
0908	11,400	5	4	4	5			
0910	13,600	6	5	5	6			
1008	6,360*	4	2	4				

* Shell 1008 Buckled at 5,750 Lbs.

An analysis of the general instability of cylindrical shells with non-uniform ring stiffness distributions involves a discrete theory. However, since a discrete type analysis was not a part of the program, the results of these tests are not compared with a theoretical value. The Southwell results are interesting when plotted along with the uniform ring cases against the parameter S_R. Such Southwell loads for tests conducted on shell 09XX are shown in Figure 49. The shells had four rings numbered consecutively from top to bottom. The cases in which the stiffnesses of rings two and three were greater than those of rings one and four (Shells 0902 and 0906) resulted in a significant increase in load. This behavior was expected from the results of earlier tests on shell 08XX shown in Figure 50 in which ring stiffness increases were accomplished in a similar fashion. However, the Southwell loads in the cases where the stiffness of rings one and four were increased over those of rings two and three did not show a similar effect. A very slight increase in load was indicated for shell 0904. Shell 0910 and shell 0908 actually indicated lower buckling loads.

The true significance of these results is a matter of conjecture at this point as an extensive study of the problem was not undertaken. However, the Southwell loads obtained by the identical procedure agree well with both linear theory and actual instability loads for uniform ring configurations. Additionally, Southwell lines obtained for these three configurations were some of the best "quality" in the entire program as can be seen in Figures 79, 83, and 85, Appendix C.

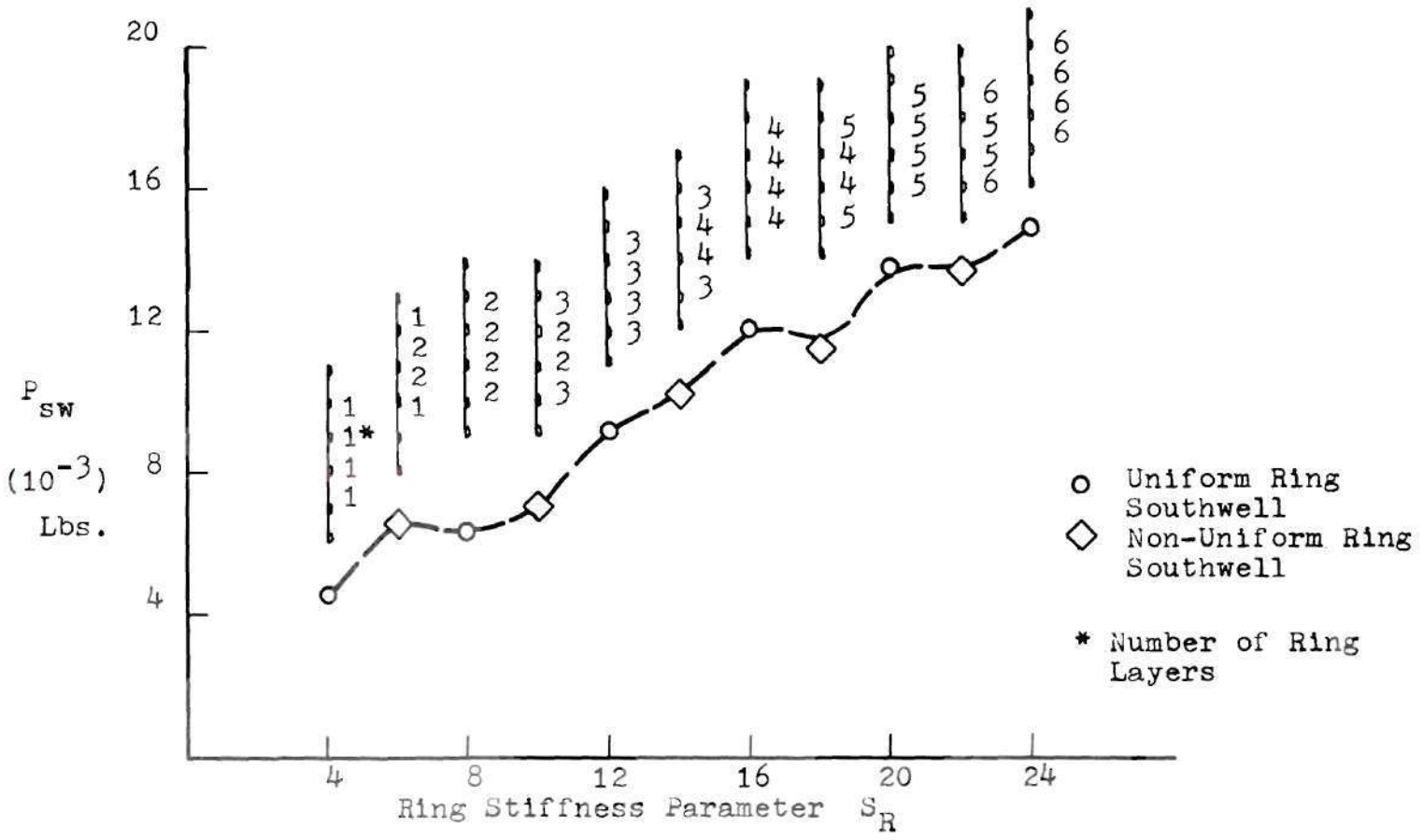

Figure 49. P_{sw} versus S_R, Non-Uniform Rings, Shell 09XX.

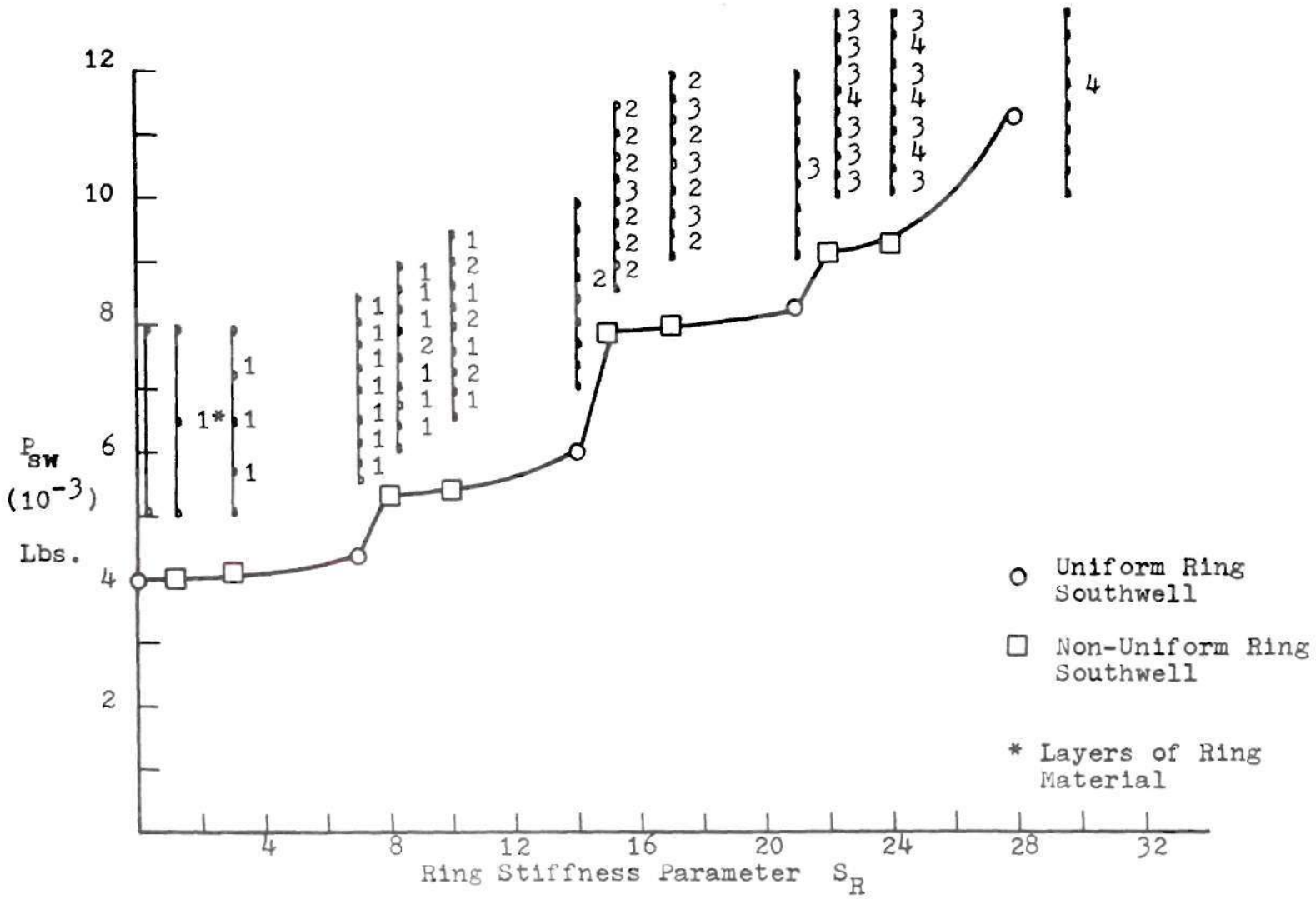

Figure 50. P_{sw} versus S_R , Non-Uniform Rings, Shell 08XX.

CHAPTER VI

CONCLUSIONS AND RECOMMENDATIONS

Acrylic materials are suitable for the manufacture of small scale ring and stringer stiffened shells used for instability studies. Tests on such shells under uniform axial compression give clear indication that the instability behavior is well described by a simple "smeared" linear theory. The tests give an indication of the range of ring stiffener parameters for which reasonable agreement with this theory can be expected. Data analysis by means of the Southwell method applied to normal motions along a circumferential path appears to be a powerful tool in parametric studies of stiffened shells. This method, along with other experimental techniques developed here seem appropriate for application to the testing of large scale ring and stringer stiffened shells.

As a result of the data obtained on shells with non-equal ring distribution a more detailed study of such configurations appears desirable. Experimental studies should be extended to shells with internal ring stiffeners as well as external stringers.

APPENDICES

APPENDIX A

BUCKLING EQUATIONS

A linear theory buckling equation for simply supported, stiffened, orthotropic cylinders under any combination of axial and circumferential loading can be written as

$$\left(\frac{m\pi}{a}\right)^2 \bar{N}_x + \left(\frac{n}{R}\right)^2 \bar{N}_y = A_{33} + \left(\frac{A_{12}A_{23} - A_{13}A_{22}}{A_{11}A_{22} - A_{12}^2}\right)A_{13} + \left(\frac{A_{12}A_{13} - A_{11}A_{23}}{A_{11}A_{22} - A_{12}^2}\right)A_{23} \tag{3}$$

in which

$$A_{11} = \left(\frac{E_x}{1 - \mu_x' \mu_y'} + \frac{E_s A_s}{d}\right)\left(\frac{m\pi}{a}\right)^2 + G_{xy}\left(\frac{n}{R}\right)^2$$

$$A_{12} = \left(\frac{\mu_y' E_x}{1 - \mu_x' \mu_y'} + G_{xy}\right)\left(\frac{m\pi}{a}\right)\left(\frac{n}{R}\right)$$

$$A_{13} = \frac{1}{R}\left(\frac{\mu_y' E_x}{1 - \mu_x' \mu_y'}\right)\left(\frac{m\pi}{a}\right) + \frac{E_s A_s}{d}\bar{z}_s\left(\frac{m\pi}{a}\right)^3$$

$$A_{22} = G_{xy}\left(\frac{m\pi}{a}\right)^2 + \left(\frac{E_y}{1 - \mu_x' \mu_y'} + \frac{E_r A_r}{\ell}\right)\left(\frac{n}{R}\right)^2$$

$$A_{23} = \frac{1}{R}\left(\frac{E_y}{1 - \mu_x' \mu_y'} + \frac{E_r A_r}{\ell}\right)\left(\frac{n}{R}\right) + \frac{E_r A_r}{\ell}\bar{z}_r\left(\frac{n}{R}\right)^3$$

$$A_{33} = \left(\frac{D_x}{1 - \mu_x\mu_y} + \frac{E_s I_{o_s}}{d}\right)\left(\frac{m\pi}{a}\right)^4 + \left(\frac{2\mu_y D_x}{1 - \mu_x\mu_y} + 2D_{xy} + \frac{G_s J_s}{d} + \frac{G_r J_r}{\ell}\right)\left(\frac{m\pi}{a}\right)^2\left(\frac{n}{R}\right)^2$$

$$+ \left(\frac{D_y}{1 - \mu_x\mu_y} + \frac{E_r I_{o_r}}{\ell}\right)\left(\frac{n}{R}\right)^4 + \frac{1}{R^2}\left(\frac{E_y}{1 - \mu_x'\mu_y'} + \frac{E_r A_r}{\ell}\right) + 2\frac{E_r A_r}{\ell}\frac{z_r}{R}\frac{n^2}{R^3}$$

This equation is taken from Block et al (26) and is used exclusively in this work for comparison of experimental results to theoretical prediction. To compute buckling loads from the equation, the specified loading must be minimized numerically for both m, the number of axial half waves in the buckle pattern, and n, the number of circumferential full waves in the buckle pattern. A computer program, written in Basic Language, which accomplishes this minimization for a particular shell geometry follows.

```
1   PRINT "GENERAL INSTABILITY OF PLEXIGLASS STIFFENED
     CYLINDER"
2   PRINT "PANEL THICKNESS =.030  DIAMETER=15.0"
3   PRINT "SHELL #";
4   INPUT B4
5   PRINT "SIZE OF M AND N ARE";
8   INPUT I,J
10   READ E,T,R,M1,L1
20   DATA 450000.,3.00000E-02,7.5,.33,.773
30   PRINT "SHELL LENGTH IS";
40   INPUT L
70   LET A1=3.20000E-02
80   LET I1=-.158↑2*3.20000E-02+(.25↑4-.17*.18↑3)/3
90   LET J1=(.43)*(7.50000E-02↑3)/3
100   LET Y1=.173
105   PRINT "NO. OF BAY        STRESS          LOAD
          M        N"
110   LET X=5
115   LET L2=L/X
120   LET A2=3.00000E-02*.25*B4/4
125   LET I2=(.25*(3.00000E-02*B4/4)↑3)/12
130   LET J2=((B4/4)*3.00000E-02)↑3*(.25/3)
```

```
135  LET Y2=-(1.50000E-02+(B4/4)*3.00000E-02)
140  LET M2=1+M1
150  LET M3=1-M1↑2
160  LET C1=A1/T/L1
170  LET C2=A2/T/L2
180  LET D=E*T↑3/(12*M3)
190  LET D1=E*I1/L1/D
200  LET D2=E*I2/L2/D
210  LET K1=3.14159
220  LET K2=6*(1-M1)/T↑3
230  LET K3=K1↑2/L↑2*D
233  LET K4=A1/L1+T
235  LET K5=2*K1*R
240  LET G1=K2*J1/L1
250  LET G2=K2*J2/L2
260  LET Z=L↑4*M3/R↑2/T↑2
270  LET Z1=-Y1/R
280  LET Z2=-Y2/R
290  LET V1=0
295  LET V2=0
300  LET W1=1.00000E+20
310  FOR M=1 TO I
320  FOR N=0 TO J
340  LET A=(M*K1*R/L)↑2
350  LET B=(N*L/M/K1/R)↑2
360  LET P=1+2*A*B*(1-B*M1)*Z2+A↑2*B↑2*(1+B)↑2*Z2↑2
370  LET Q=1+2*A*(B-M1)*Z1+A↑2*(1+B)↑2*Z1↑2
380  LET R1=M3+2*A*B*M3*(Z1+Z2)+A↑2*B↑2*(M3+2*B*M2)*Z2↑2
390  LET R2=2*A↑2*B↑2*M2↑2*Z1*Z2+A↑2*B*(2*M2+B*M3)*Z1↑2
400  LET V=R1+R2
410  LET S=(1+B)↑2+2*B*M2*(C1+C2)+M3*(C1+2*B*C1*C2*M2+B↑2*C
     2)
420  LET U=(1+C1*Q+C2*P+C1*C2*V)/S
430  LET F=M↑2*((1+B)↑2+D1+D2*B↑2+(G1+G2)*B)
440  LET H=12*Z*U/(M↑2*K1↑4)+F
450  IF H<W1 THEN 500
455  GOTO 530
460  LET K4=A1/L1+T
500  LET W1=H
510  LET V1=M
520  LET V2=N
530  NEXT N
535  NEXT M
560  PRINT X,W1*K3/K4,W1*K3*K5,V1;V2
565  PRINT
999  END
```

APPENDIX B

DATA ACQUISITION AND REDUCTION PROGRAMS

The programs for data acquisition and reduction were changed frequently during the course of the tests. These changes were made to fit the procedure to a particular testing situation. However, the flow diagrams for the programs as shown in Figures 51 and 52 remained for the most part unchanged. A typical data acquisition program and the associated teletype display follows.

```
1   REM THIS TAPE USES THE HP MAG TAPE DRIVER DTD
     11,5,70
2   REM THIS IS TAPE NO 28  LVDT ON CHN 30- LOAD
     CHN130
5   FOR I=1 TO 10
6   CALL (10,2,S)
7   IF S#0 THEN 980
8   NEXT I
10   DIM U[20],C[8],W[8],S[20],P[1],K[29],L[20]
11   DIM M[20],G[20]
20   READ D,P,R,N,N1,N2,C0
25   FOR I=9 TO 20
26   READ U[I]
27   NEXT I
35   LET R=512*D+64*P+R+32
40   PRINT "STIFFENED SHELL DATA ACQ."
45   PRINT "SHELL ID #",
50   INPUT I1
55   PRINT "LOAD INCREMENT",
60   INPUT L1
61   PRINT "START LOAD INCREMENT AT";
62   INPUT L2
63   PRINT "RECORD OPTION";
64   INPUT A
67   PRINT "STARTING RECORD WILL BE";
68   INPUT K[28]
69   GOTO 982
75   PRINT "ENTER DAY,MO,YR";
```

```
76  INPUT K[23],K[24],K[25]
77  LET K[28]=(R1-1)
78  PRINT "RUN #,LOCATION";
79  INPUT K[26],K[27]
80  LET Q=INT(L2/L1)
140  PRINT "NO CONTACT READ"
142  CALL (3,X)
144  IF X#1 THEN 142
145  CALL (1,G[9],31,R,N2)
146  PRINT "POSITION PROBE"
148  CALL (3,X)
149  IF X#1 THEN 148
150  CALL (1,K[9],31,R,N2)
151  CALL (1,P[1],130,R,1)
152  FOR I=9 TO 20
154  LET M[I]=(G[I]-K[I])/U[I]
156  PRINT INT(-M[I]*10000)/10;
157  LET S[I]=K[I]
158  NEXT I
159  PRINT
171  PRINT "INIT LOAD";INT((P[1]/C0)*1000+.5)
200  CALL (3,X)
203  IF X=8 THEN 240
205  IF X=0 THEN 200
210  IF X=1 THEN 240
215  IF X=2 THEN 230
225  IF X=4 THEN 620
230  CALL (1,P[1],130,R,1)
235  IF 1000*P[1]/C0<L1*Q THEN 230
240  CALL (1,P[1],130,R,1)
242  CALL (1,K[9],31,R,N2)
244  FOR I=9 TO 20
246  LET K[I]=1000*(K[I]-S[I])/U[I]
248  LET K[I]=INT(K[I]*10+.5)/10
250  LET L[I]=K[I]+20
252  NEXT I
254  IF X=8 THEN 320
270  IF A=1 THEN 550
272  IF A=2 THEN 320
320  PRINT
400  PRINT "LAT DISP"
405  PRINT "LVDT";TAB(20);"I"
410  FOR I=9 TO 17
446  PRINT (I-8);TAB(L[I]);"*";K[I]
450  PRINT
452  NEXT I
458  PRINT TAB(20);"I"
500  PRINT "END SHORT"
517  FOR I=18 TO 20
```

```
520  PRINT INT(K[I]),
522  NEXT I
524  PRINT
550  PRINT "LOAD";
551  LET P[1]=1000*P[1]
552  LET K[29]=P[1]/C0
555  PRINT INT(K[29]);
556  IF X=8 THEN 620
560  IF A=1 THEN 900
600  LET Q=Q+1
605  GOTO 200
620  PRINT "RUN TERM  RECORD COUNT ";K[28]
621  PRINT
622  PRINT "DATE";K[23];K[24];K[25]
630  GOTO 78
700  DATA 2,1,0
710  DATA 8,9,12,1
720  DATA 26.8
721  DATA 34.2
722  DATA 31
723  DATA 33.9
724  DATA 21.5
725  DATA 35.2
726  DATA 24.55
727  DATA 24.7
728  DATA 19.8
729  DATA 28.3
730  DATA 28.5
731  DATA 25.7
900  LET K[28]=K[28]+1
905  LET K[22]=I1
910  CALL (11,K[1],S,29)
911  IF S#0 THEN 980
920  PRINT "DATA REC";K[28]
930  GOTO 600
980  PRINT "ERROR CODE IS S=";S
981  GOTO 40
982  LET R1=K[28]
983  CALL (12,K[1],S,29)
984  IF S#0 THEN 980
985  IF K[28] >= R1 THEN 991
986  FOR I=1 TO (R1-K[28]-1)
987  CALL (10,1,S)
988  IF S#0 THEN 980
989  NEXT I
990  GOTO 75
991  FOR I=1 TO (K[28]-R1+1)
992  CALL (10,2,S)
993  IF S#0 THEN 980
994  NEXT I
995  GOTO 75
999  END
```

TYPICAL TELETYPE DISPLAY FOR DATA ACQUISITION

```
LATERAL DISPLACEMENT
LVDT #                  I

 1                *-2.8

 2                *-2.2

 3                        *4.9

 4                                      *13.7

 5                                       *14.3

 6                           *6.5

 7                     *0

 8              *-3.9

 9                *-1.2

END SHORT

 24                23                24

LOAD  2409      RUN TERMINATED  RECORD COUNT 2961
```

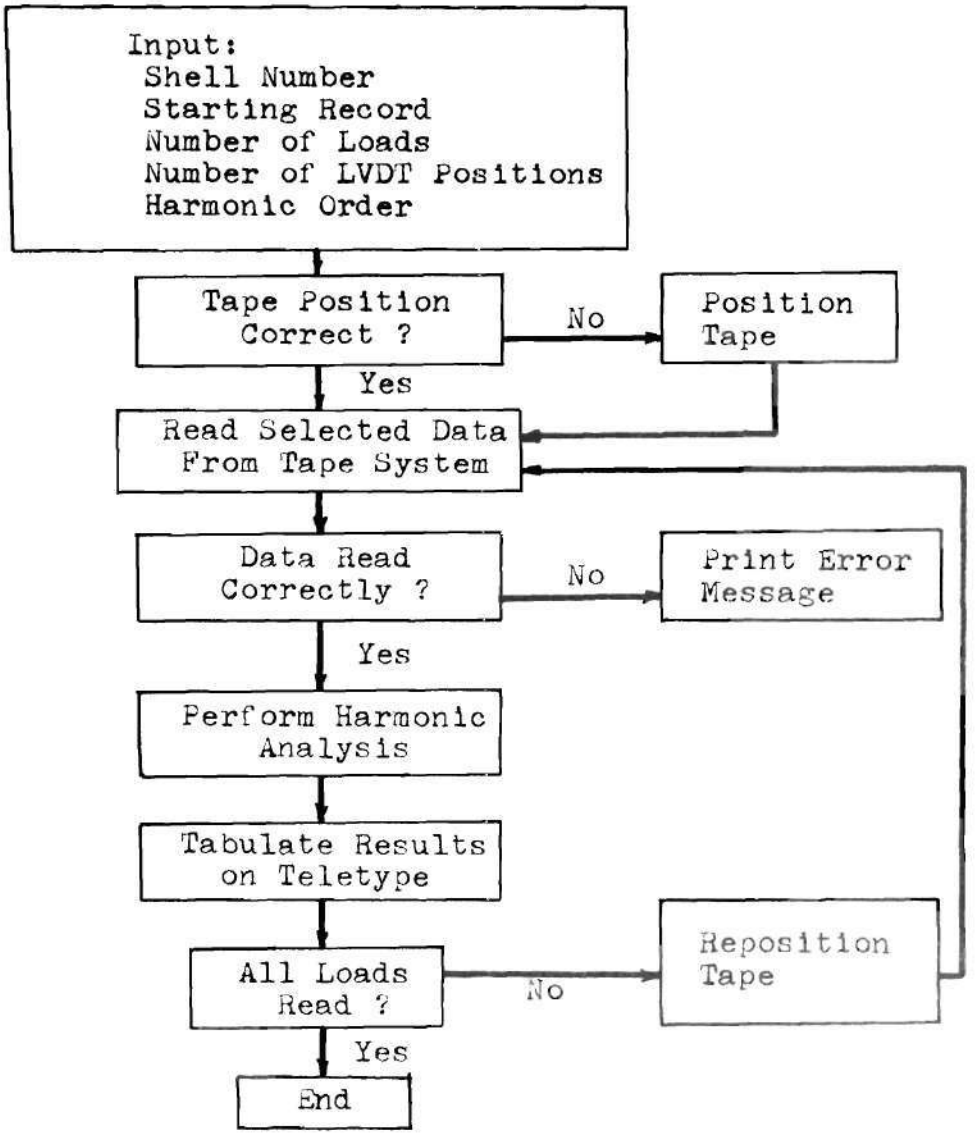

Figure 51. Harmonic Analysis Program Flow Diagram

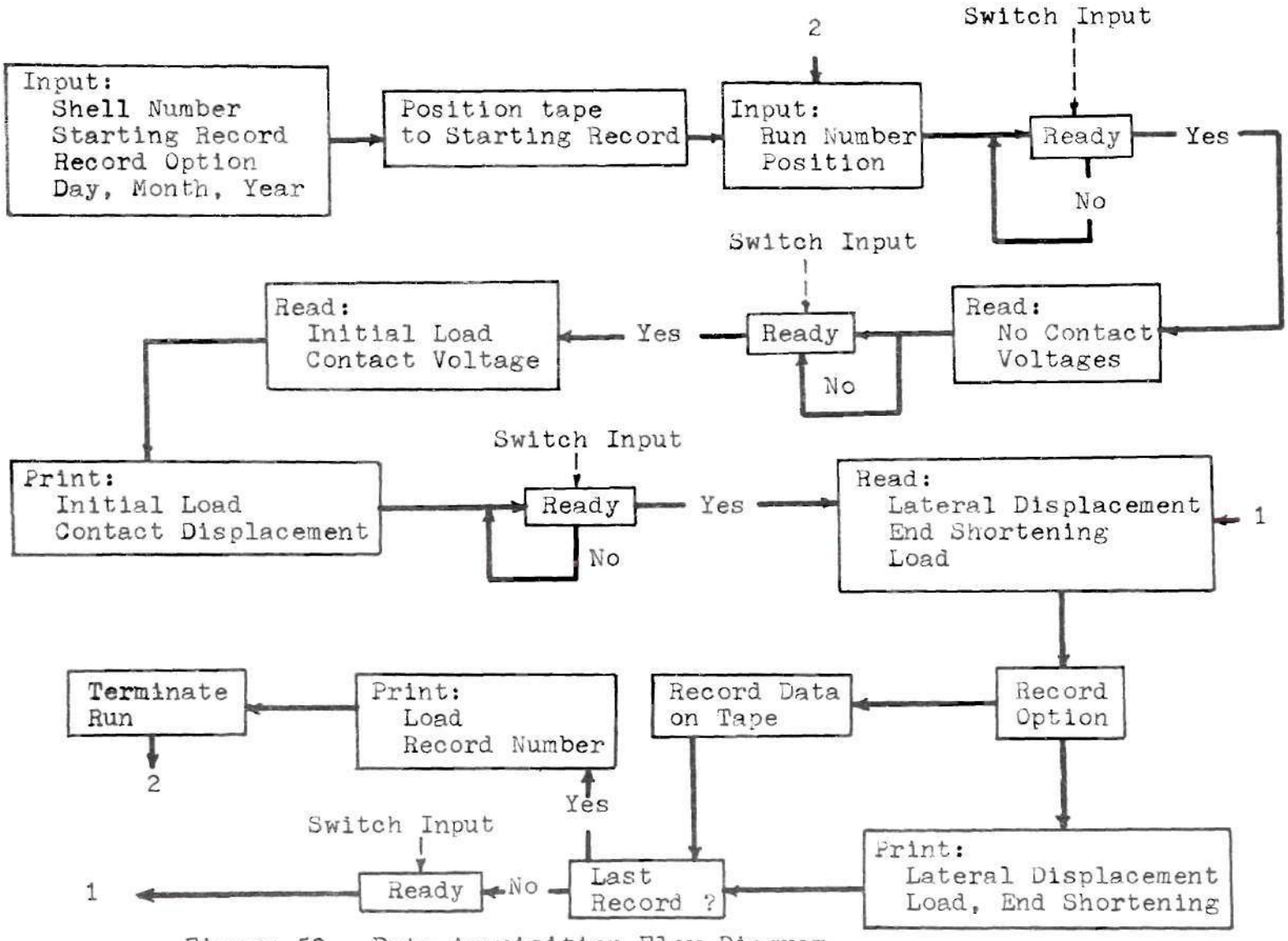

Figure 52. Data Acquisition Flow Diagram

APPENDIX C

TEST DATA

Figures 53 through 89 show the harmonic spectrum and Southwell plot for the shell configurations tested in this program.

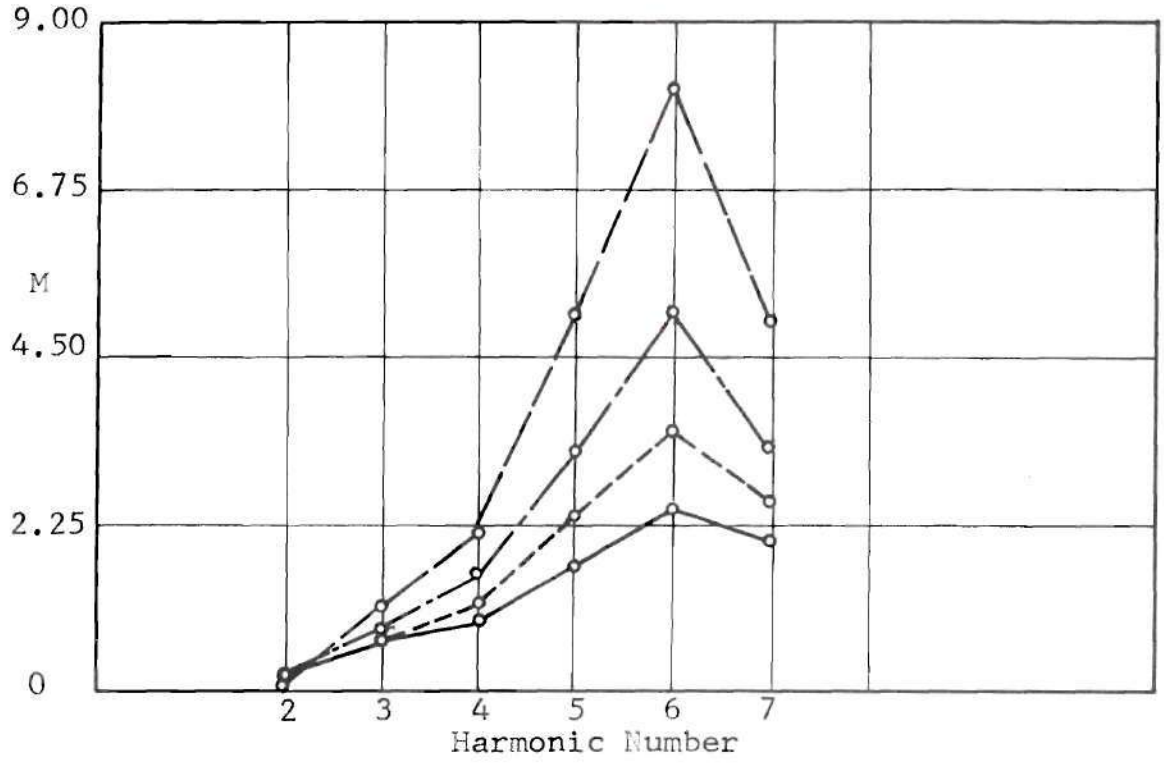

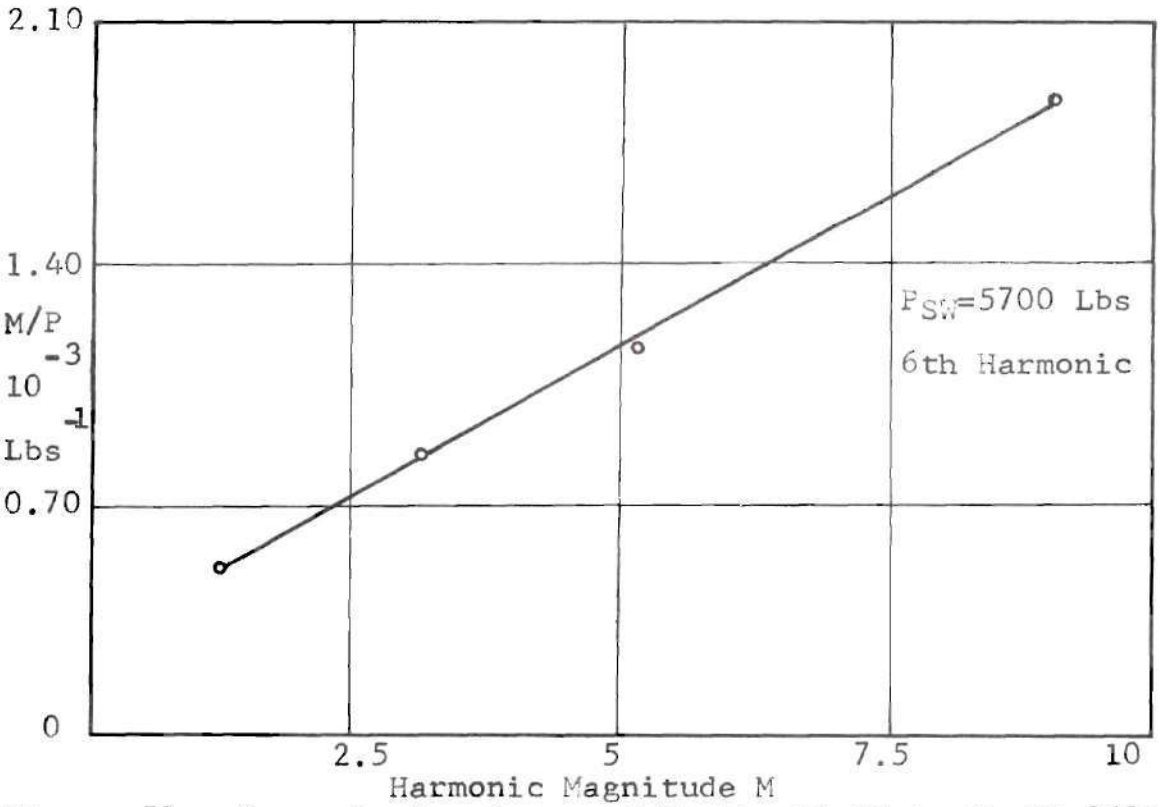

Figure 53. Harmonic Spectrum and Southwell Plot, Shell 0601.

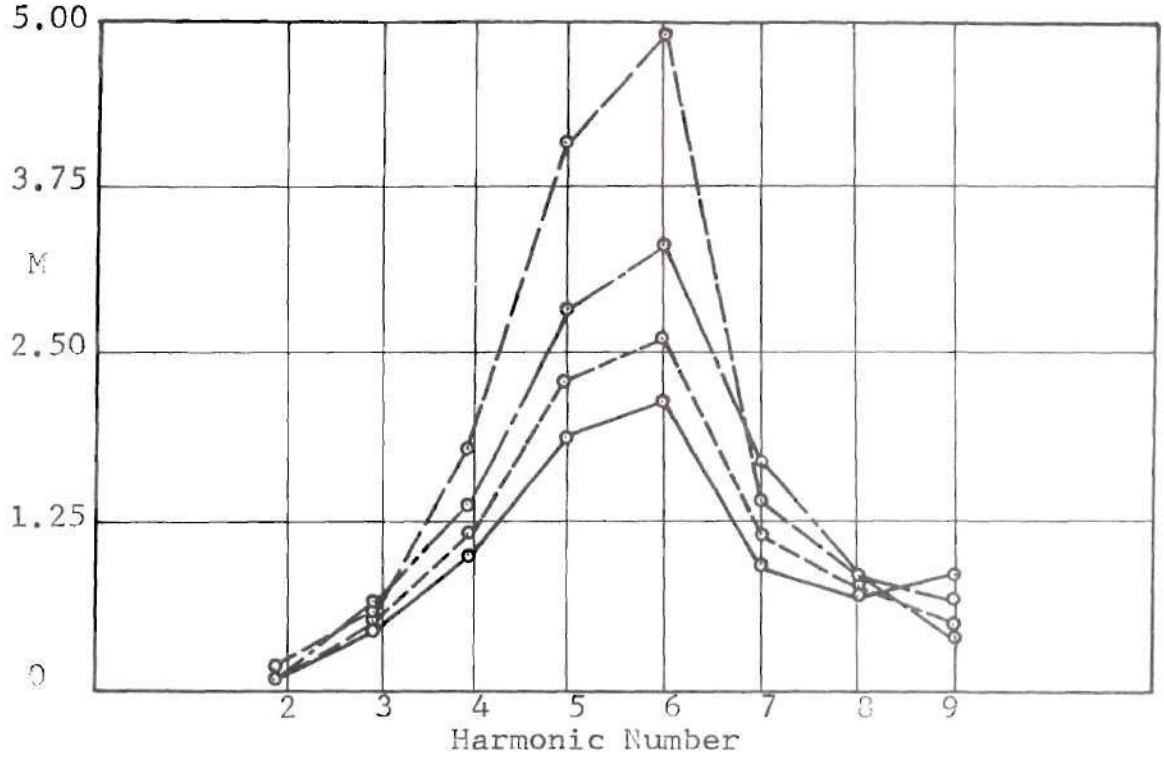

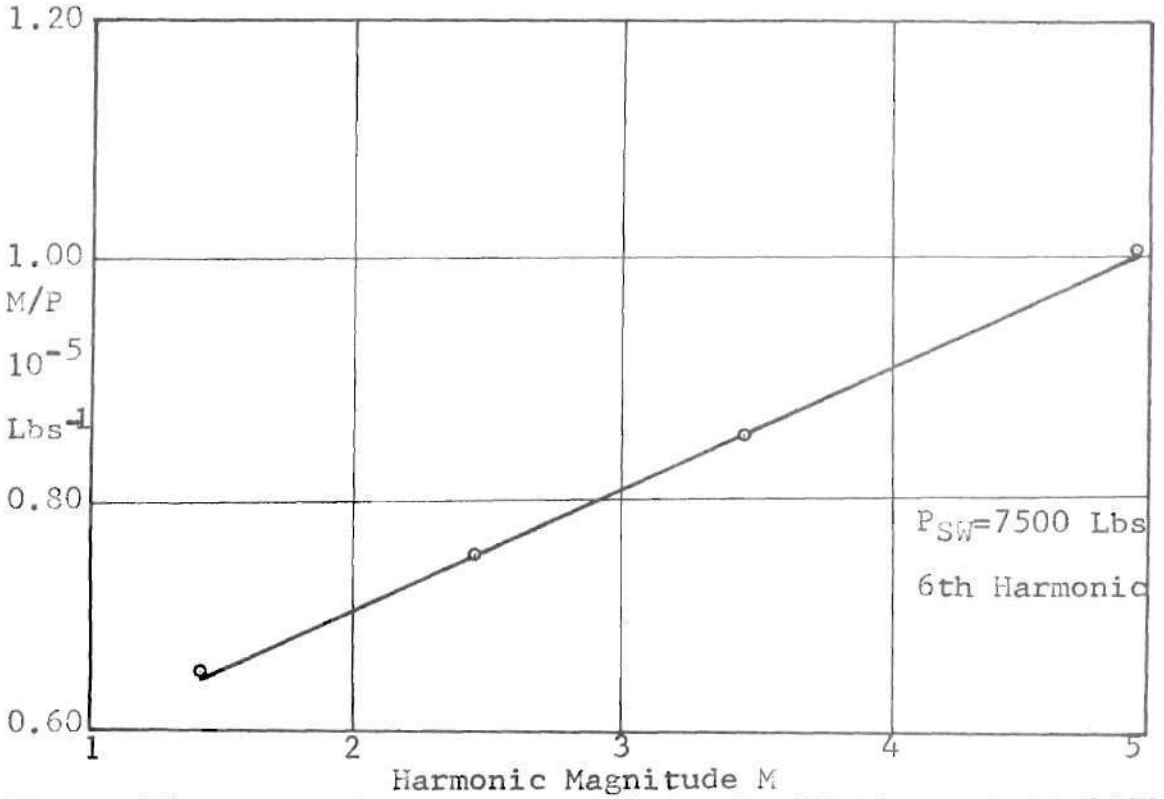

Figure 54. Harmonic Spectrum and Southwell Plot, Shell 0602.

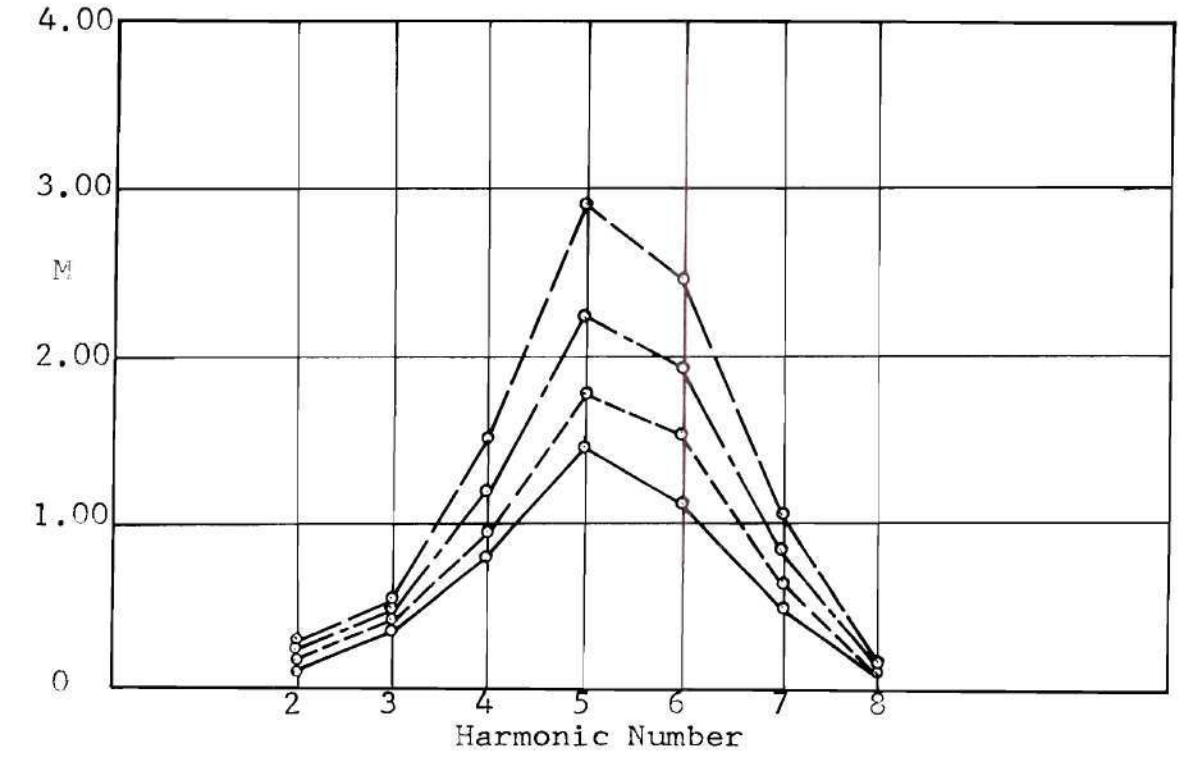

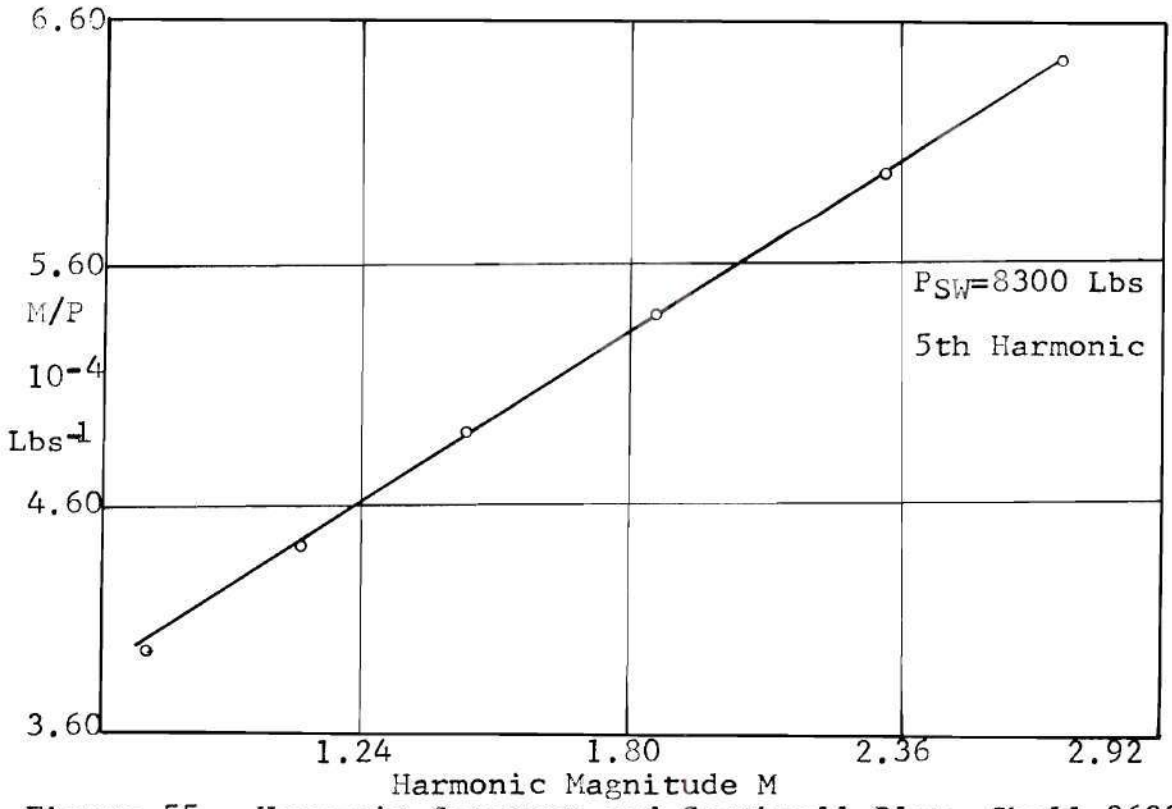

Figure 55. Harmonic Spectrum and Southwell Plot, Shell 0603.

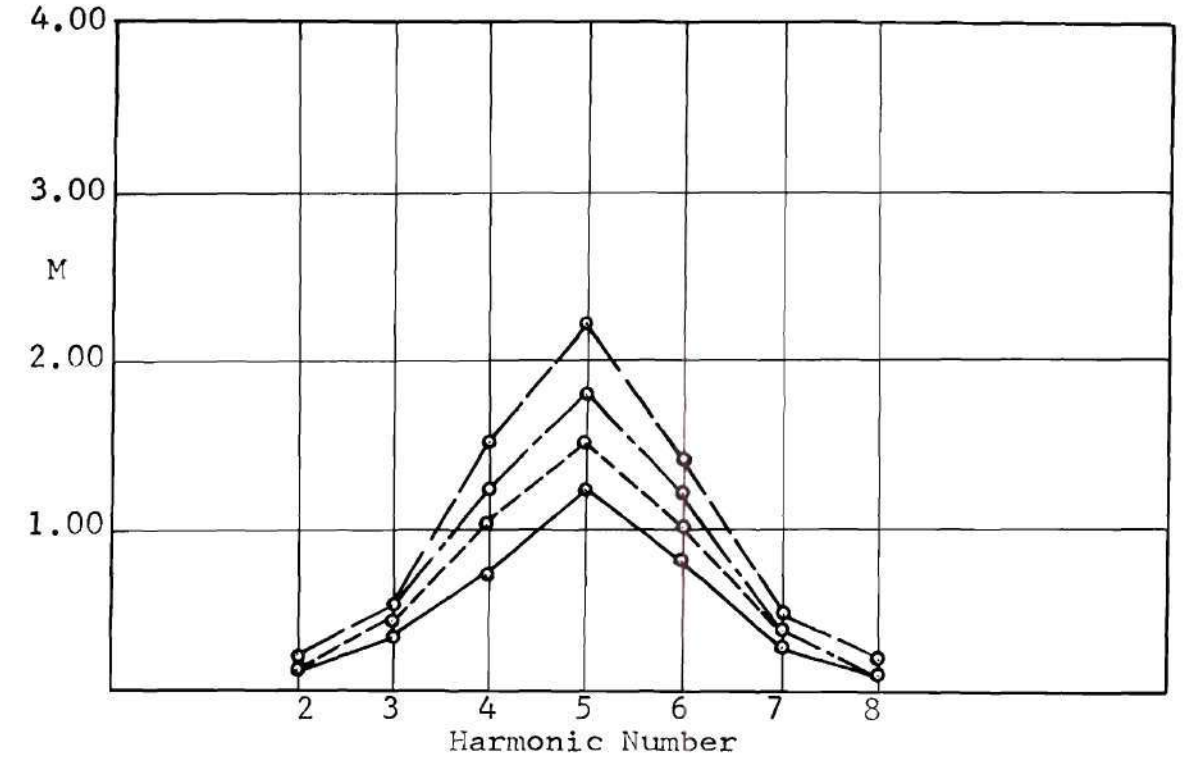

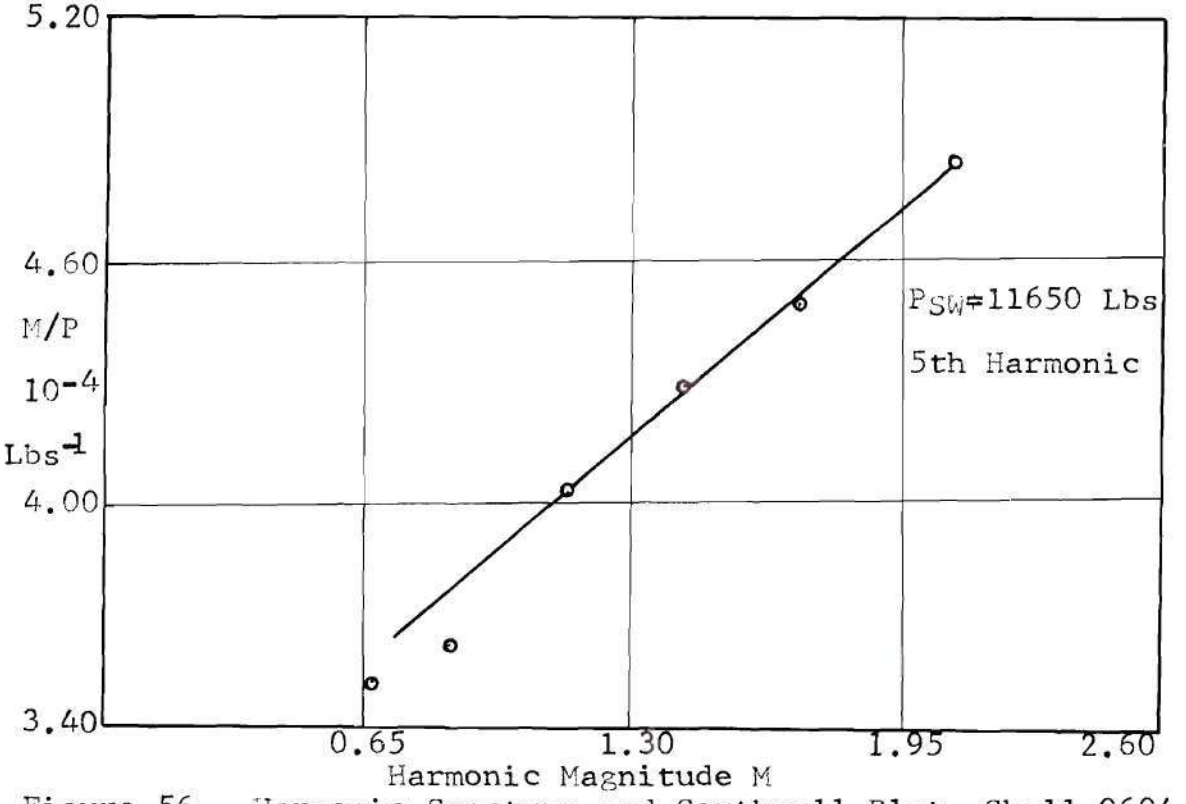

Figure 56. Harmonic Spectrum and Southwell Plot, Shell 0604.

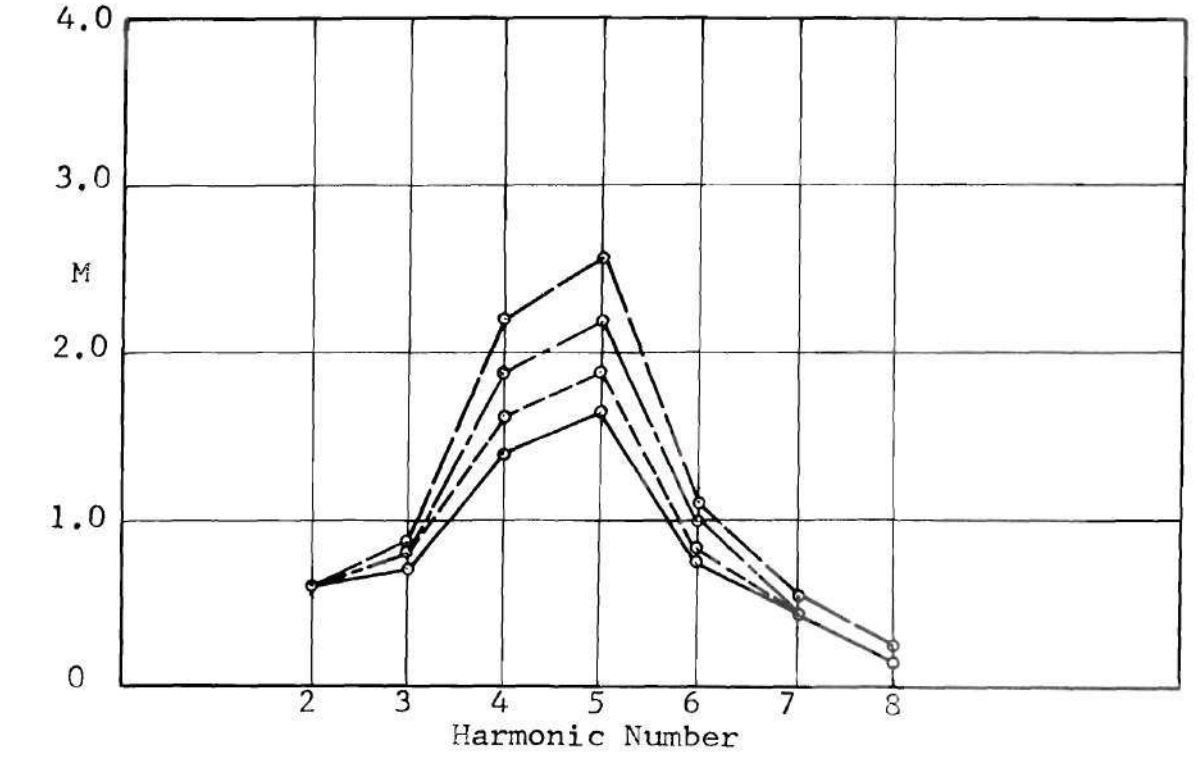

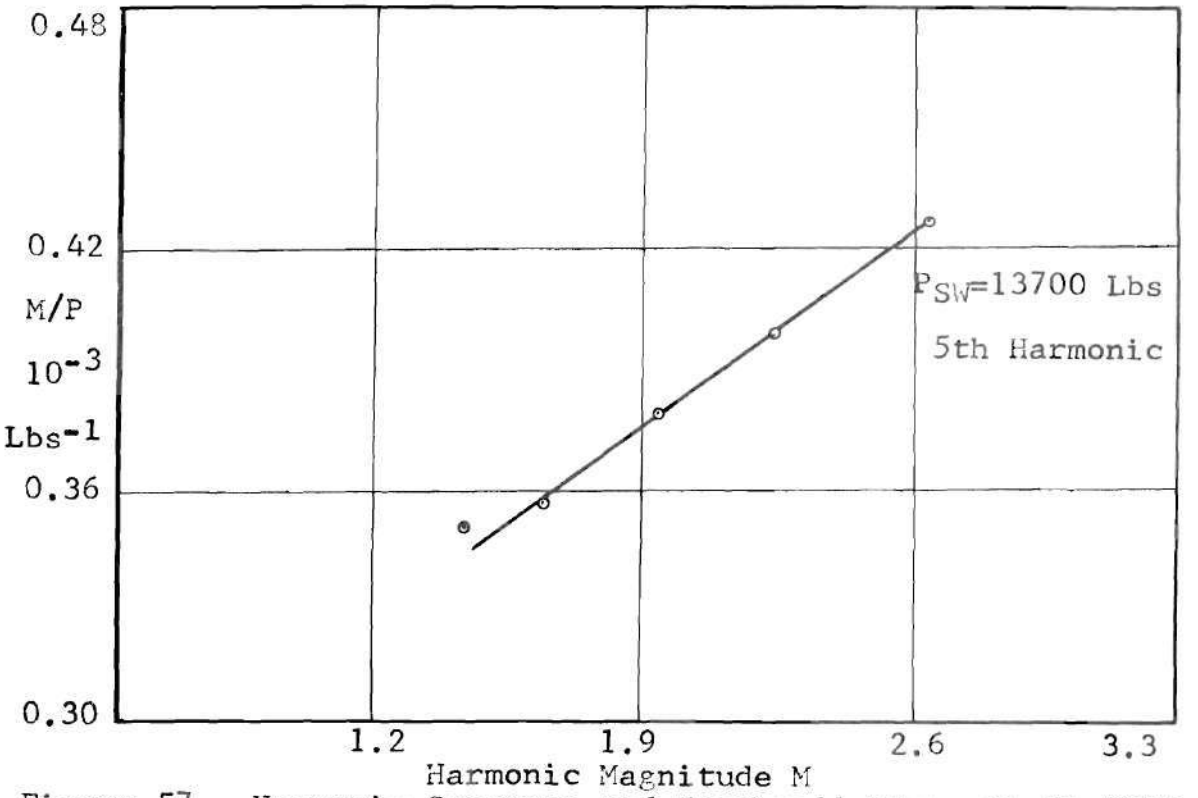

Figure 57. Harmonic Spectrum and Southwell Plot, Shell 0605.

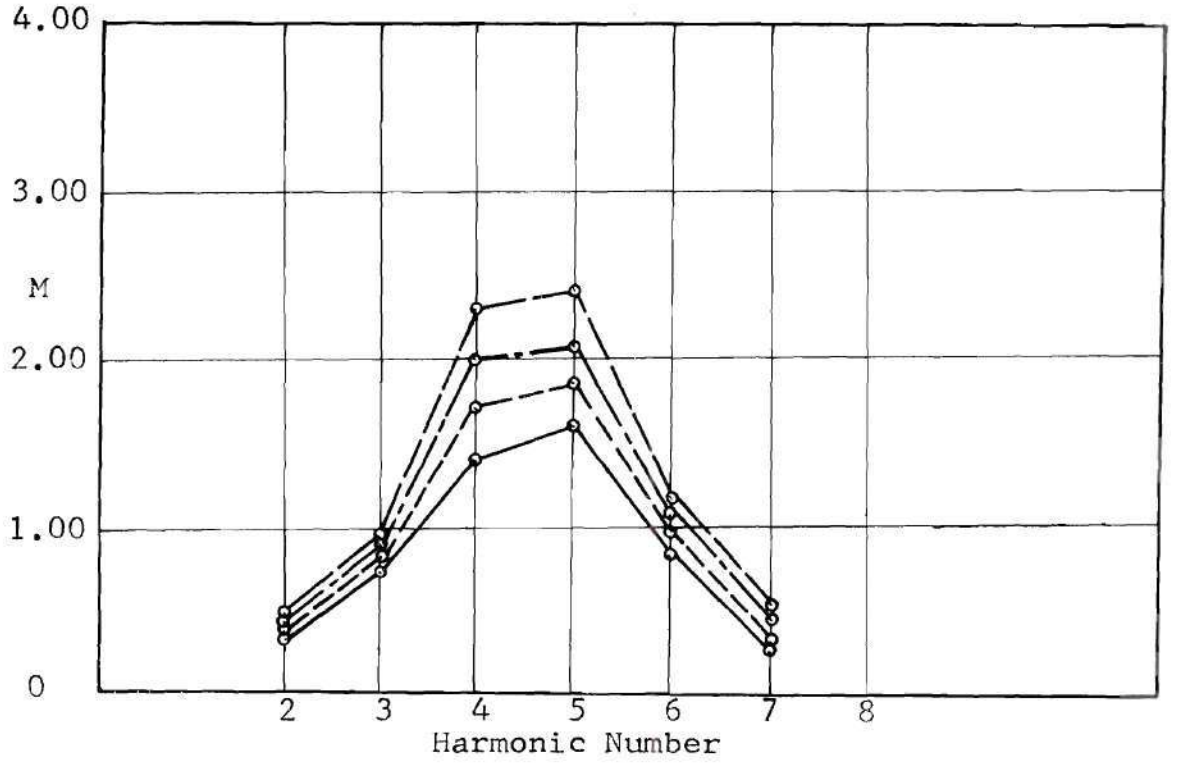

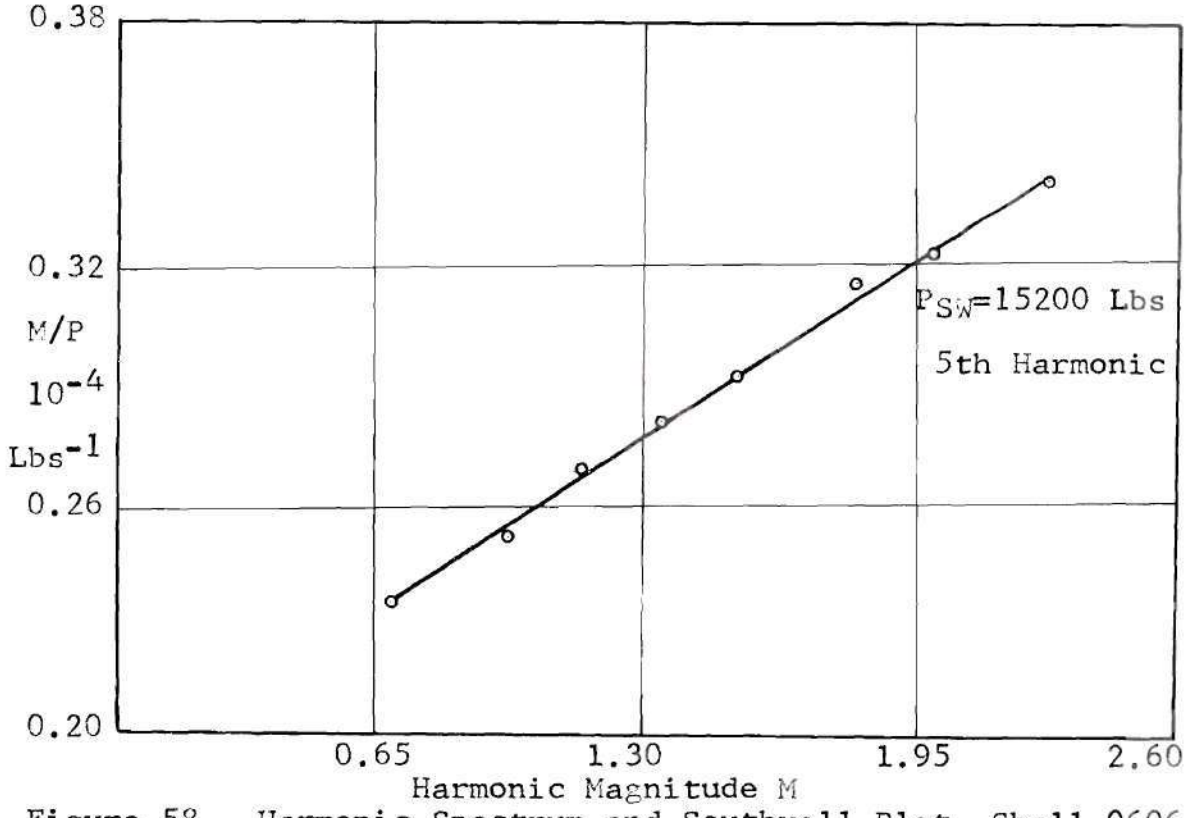

Figure 58. Harmonic Spectrum and Southwell Plot, Shell 0606.

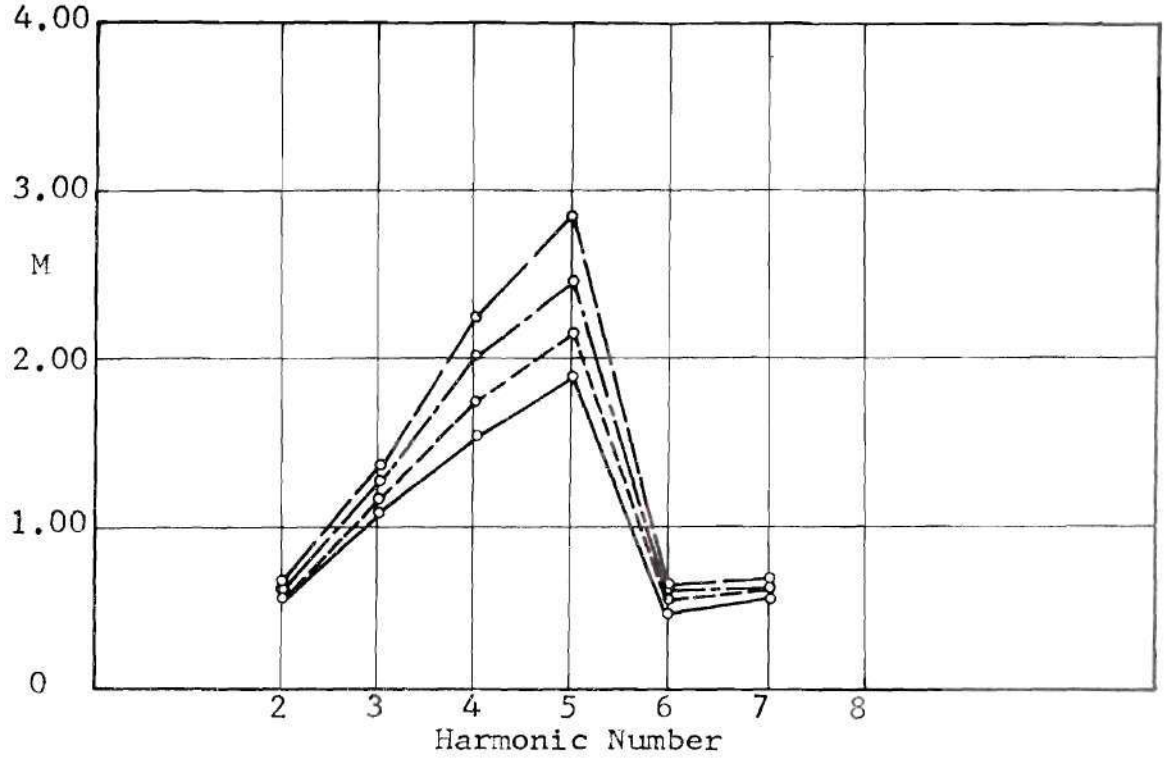

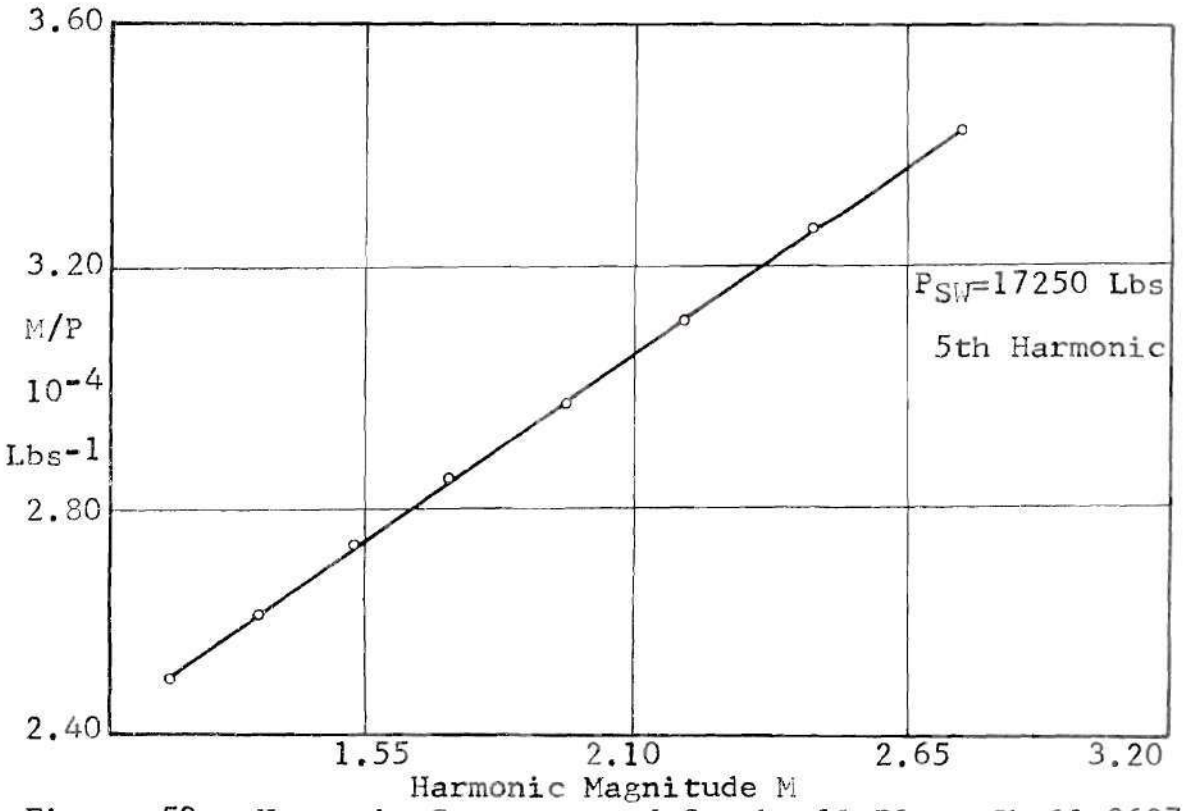

Figure 59. Harmonic Spectrum and Southwell Plot, Shell 0607.

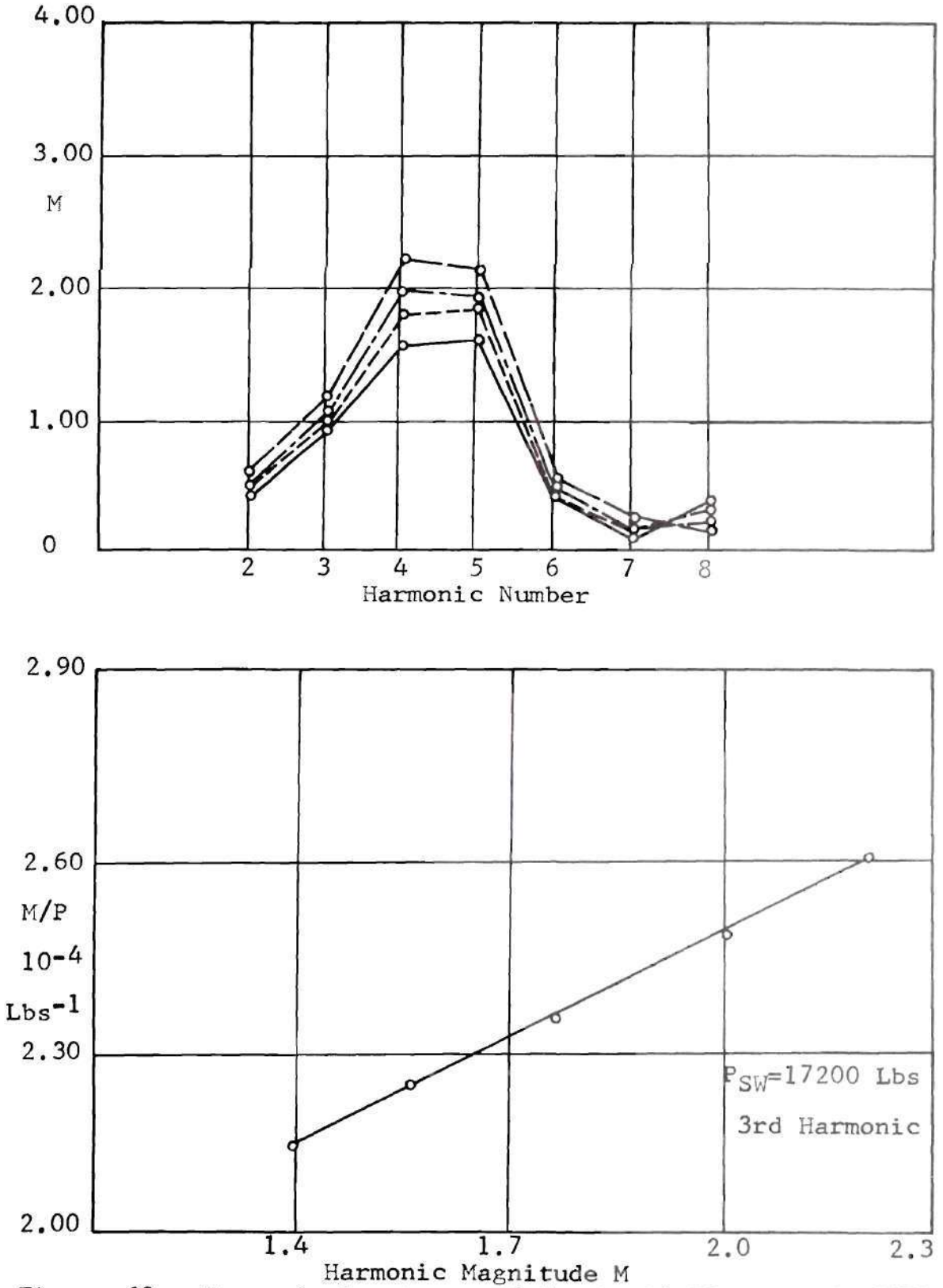

Figure 60. Harmonic Spectrum and Southwell Plot, Shell 0608.

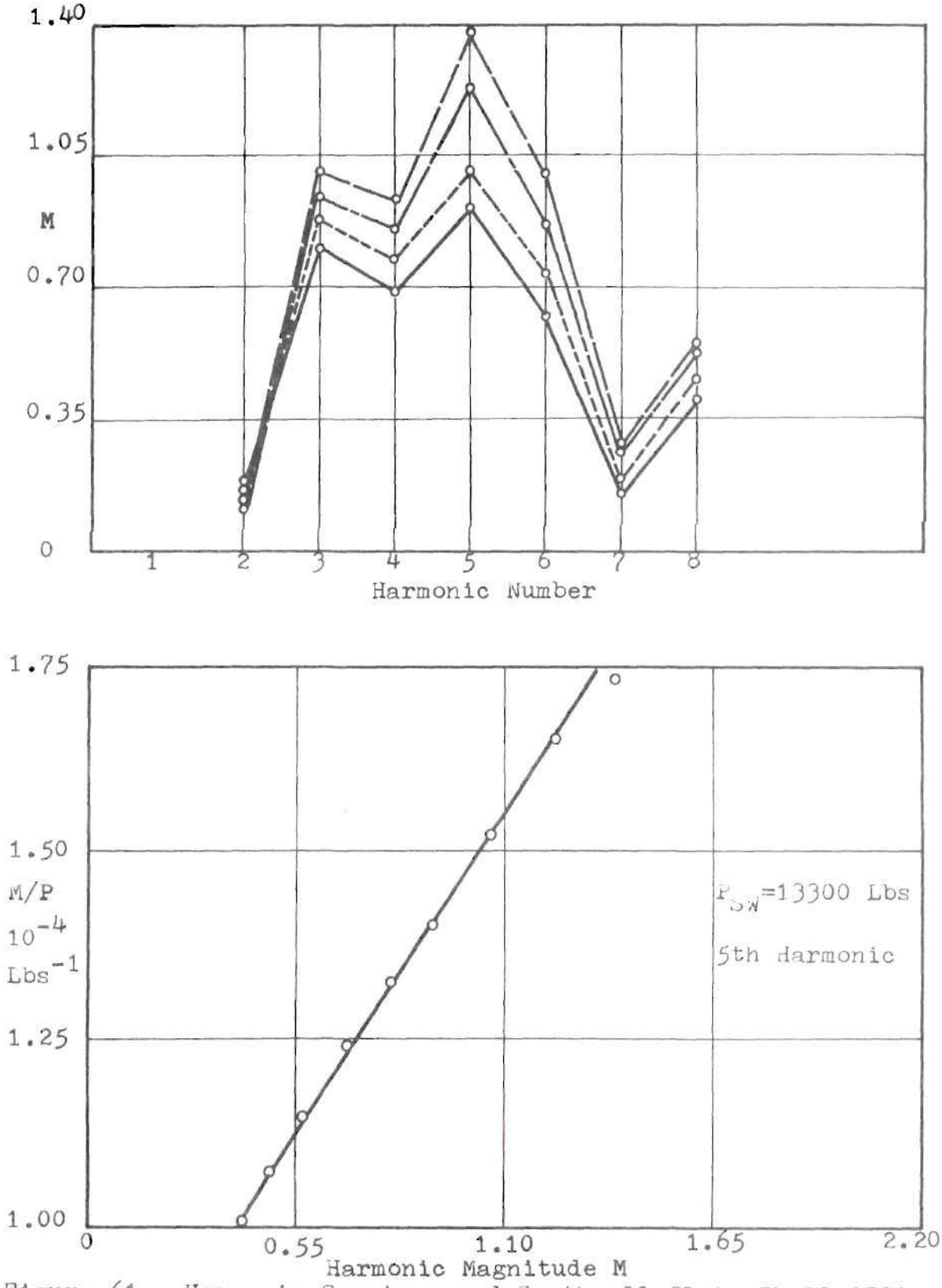

Figure 61. Harmonic Spectrum and Southwell Plot, Shell 0701.

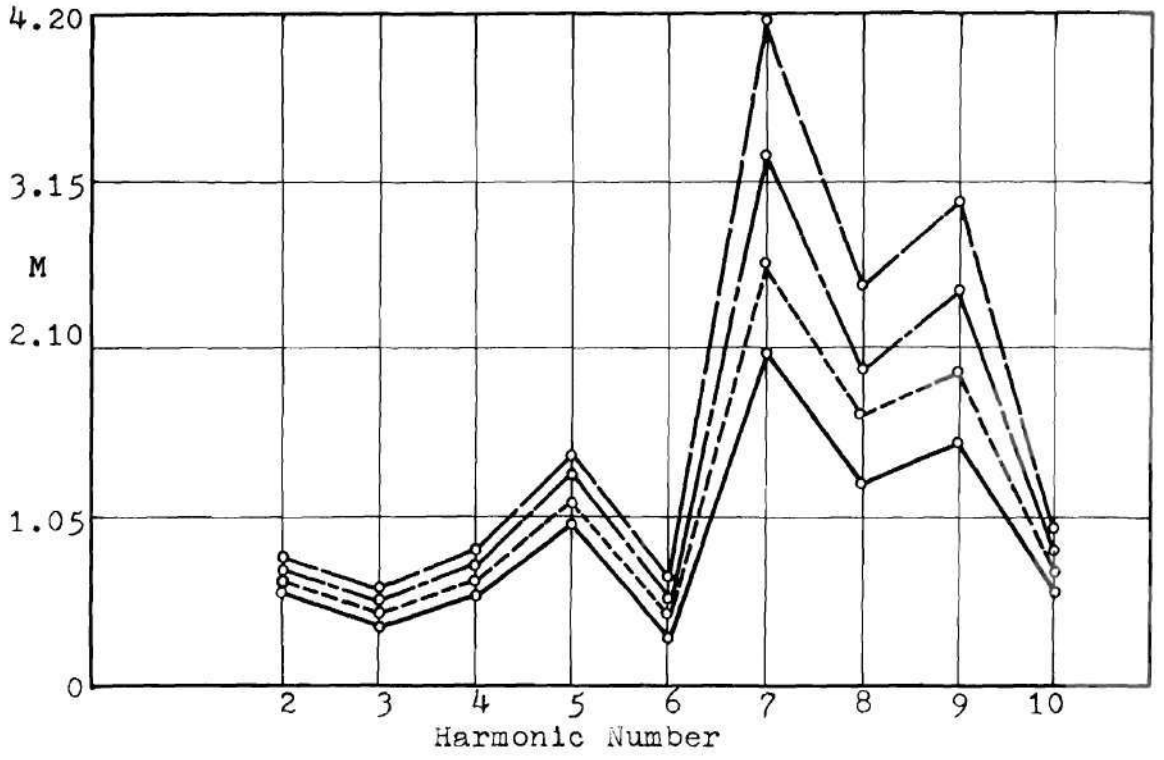

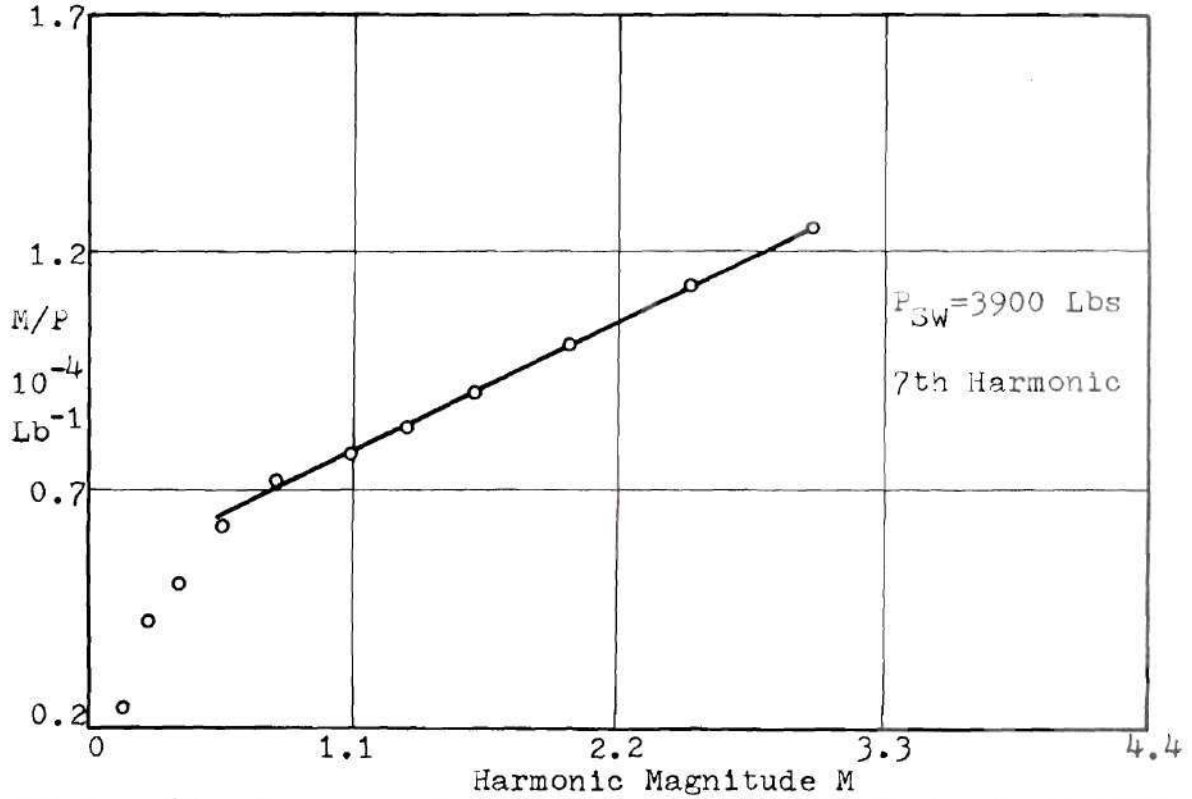

Figure 62. Harmonic Spectrum and Southwell Plot, Shell 0800.

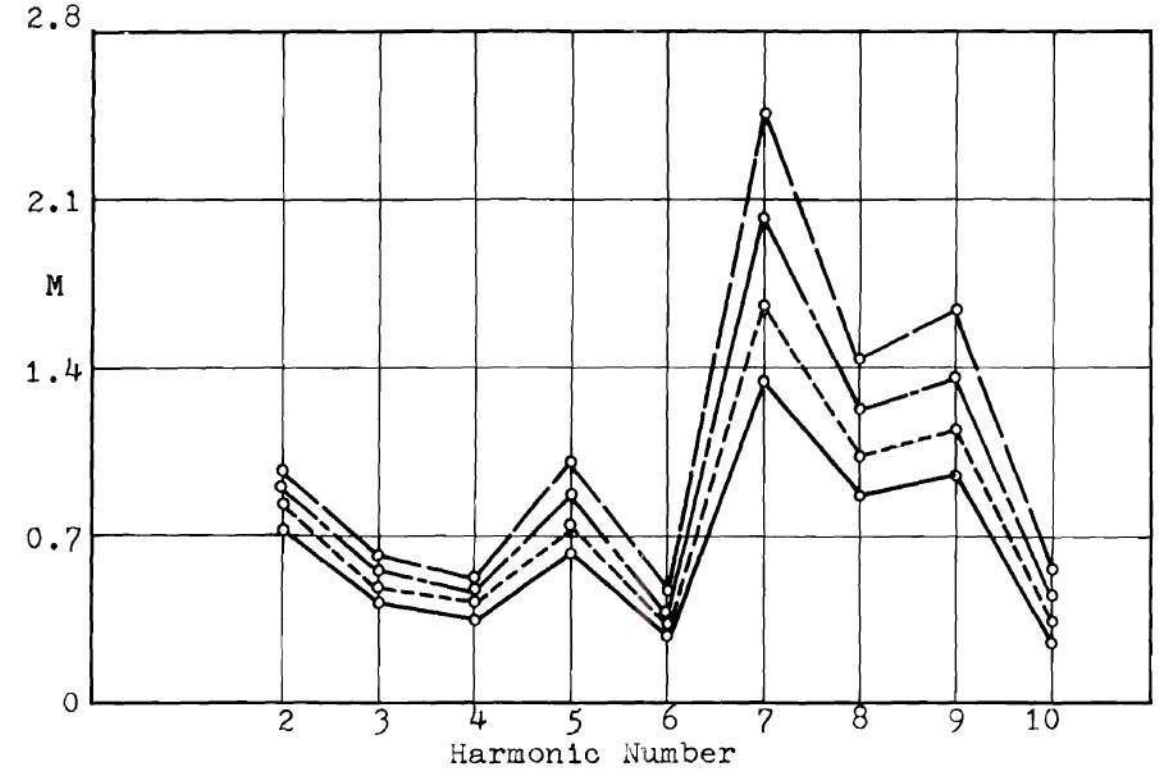

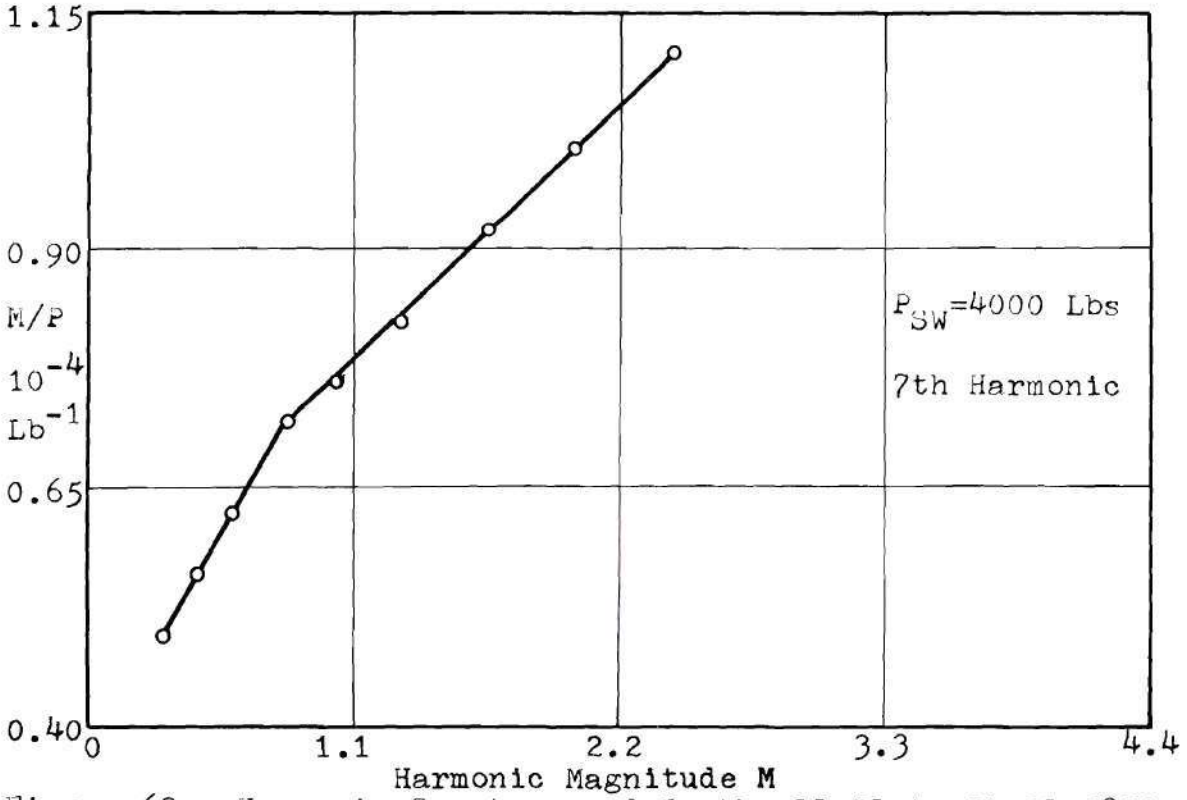

Figure 63. Harmonic Spectrum and Southwell Plot, Shell 0801.

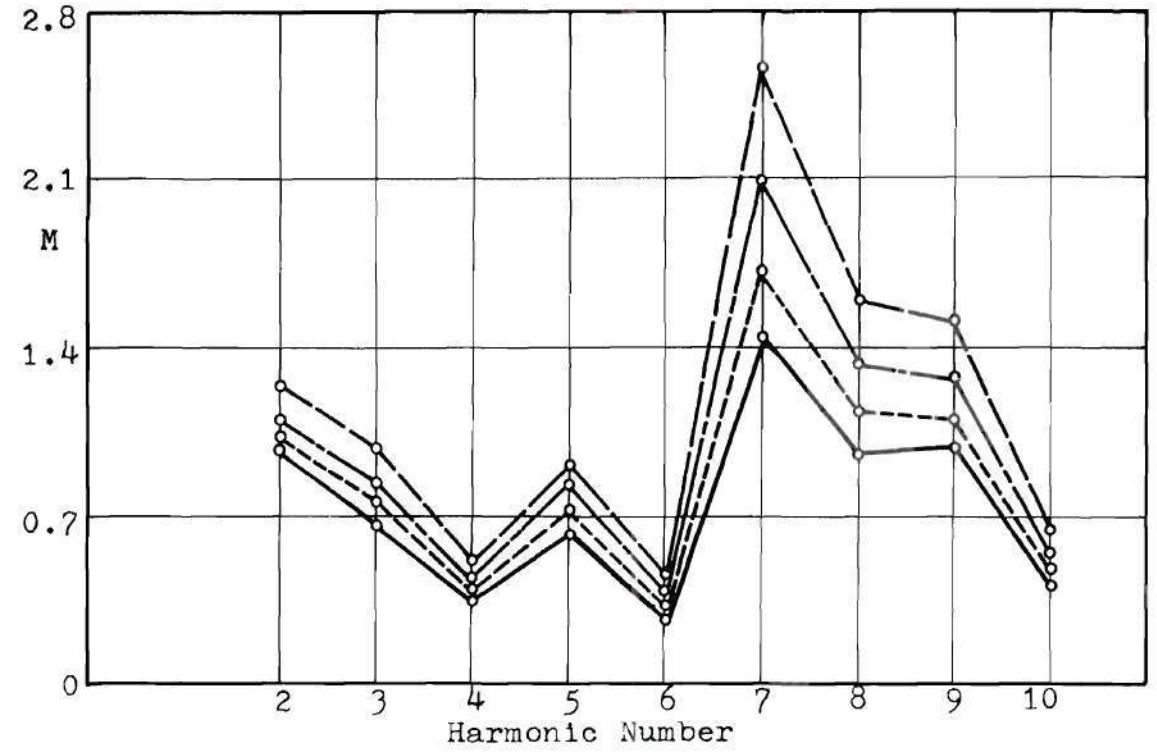

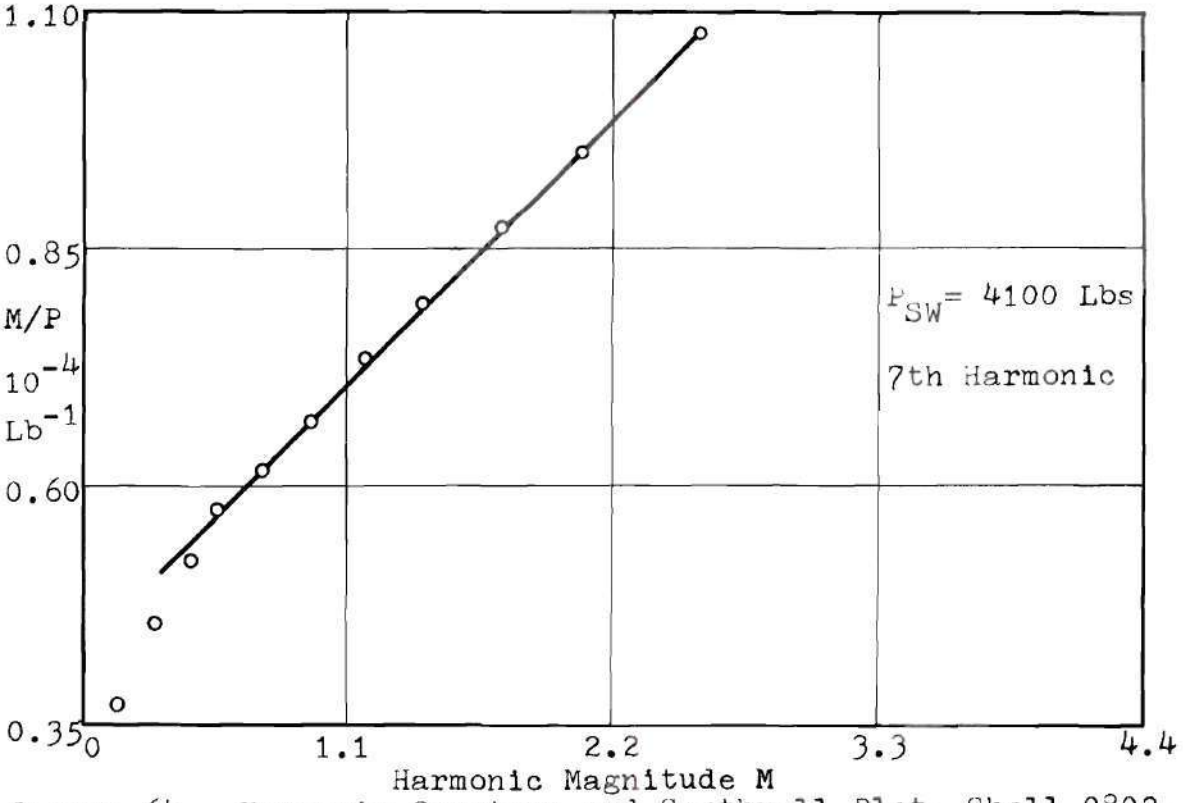

Figure 64. Harmonic Spectrum and Southwell Plot, Shell 0802.

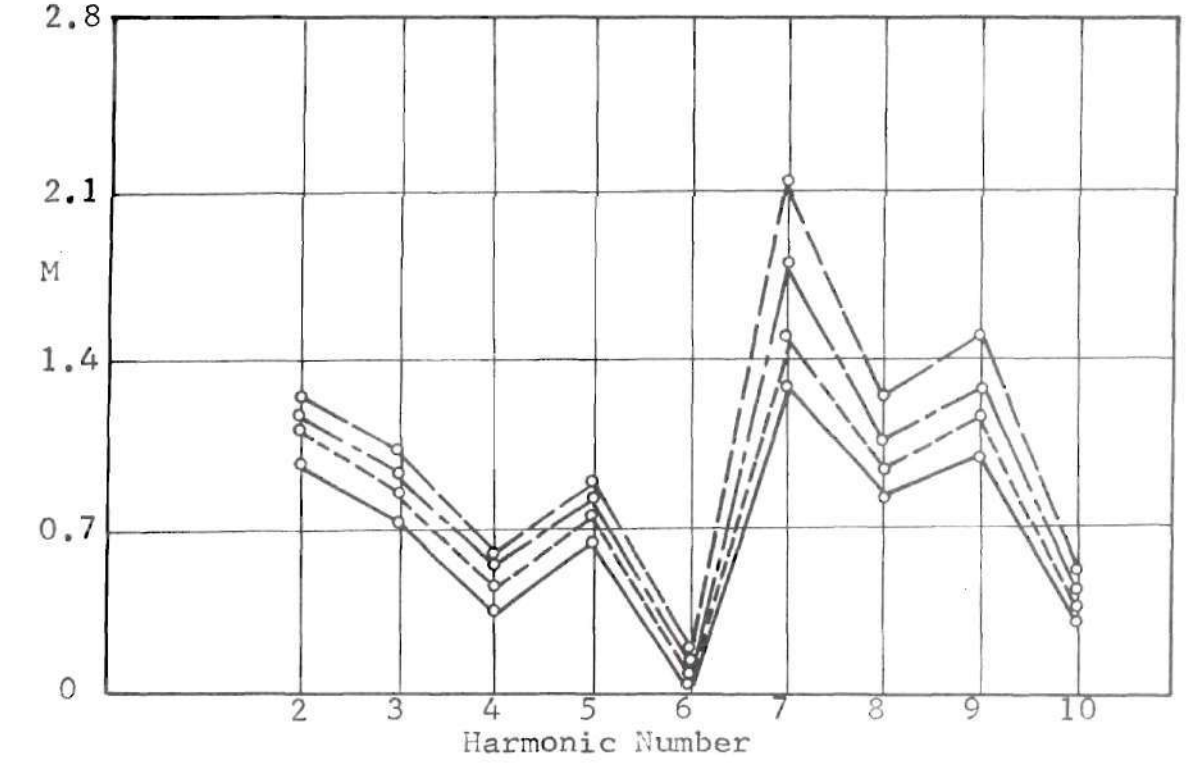

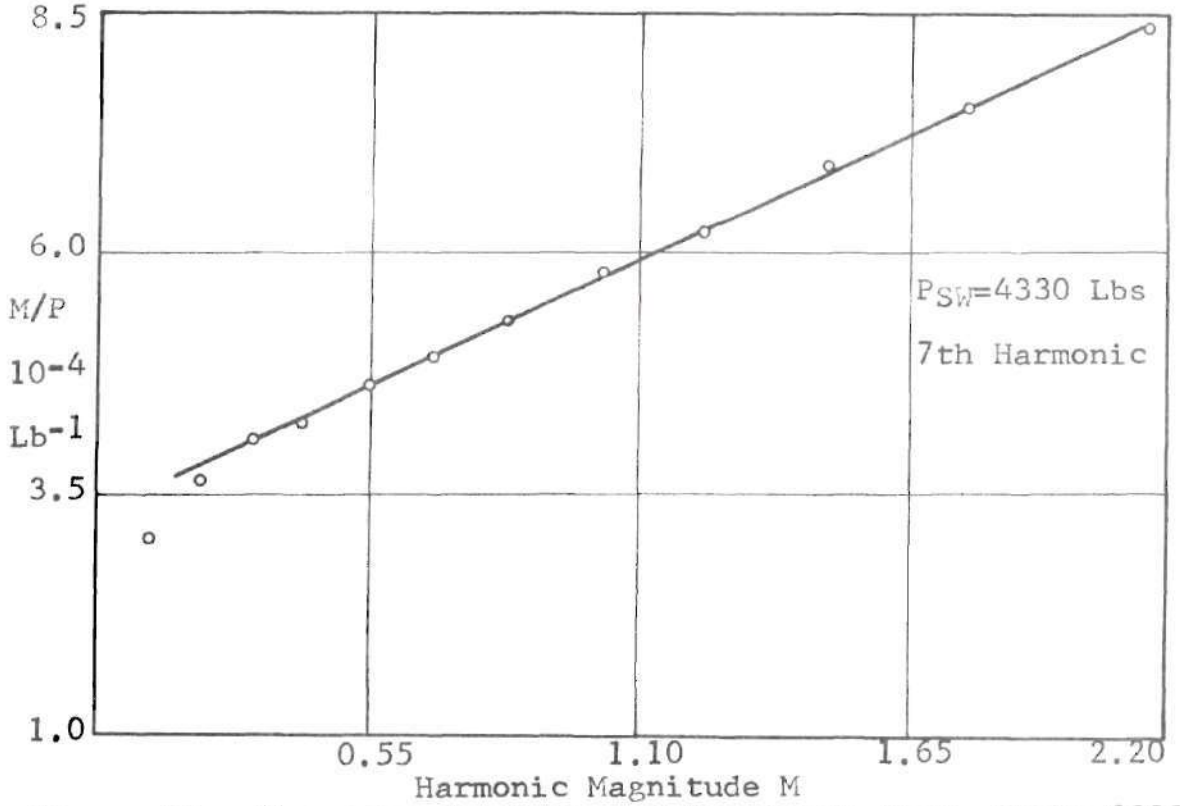

Figure 65. Harmonic Spectrum and Southwell Plot, Shell 0803.

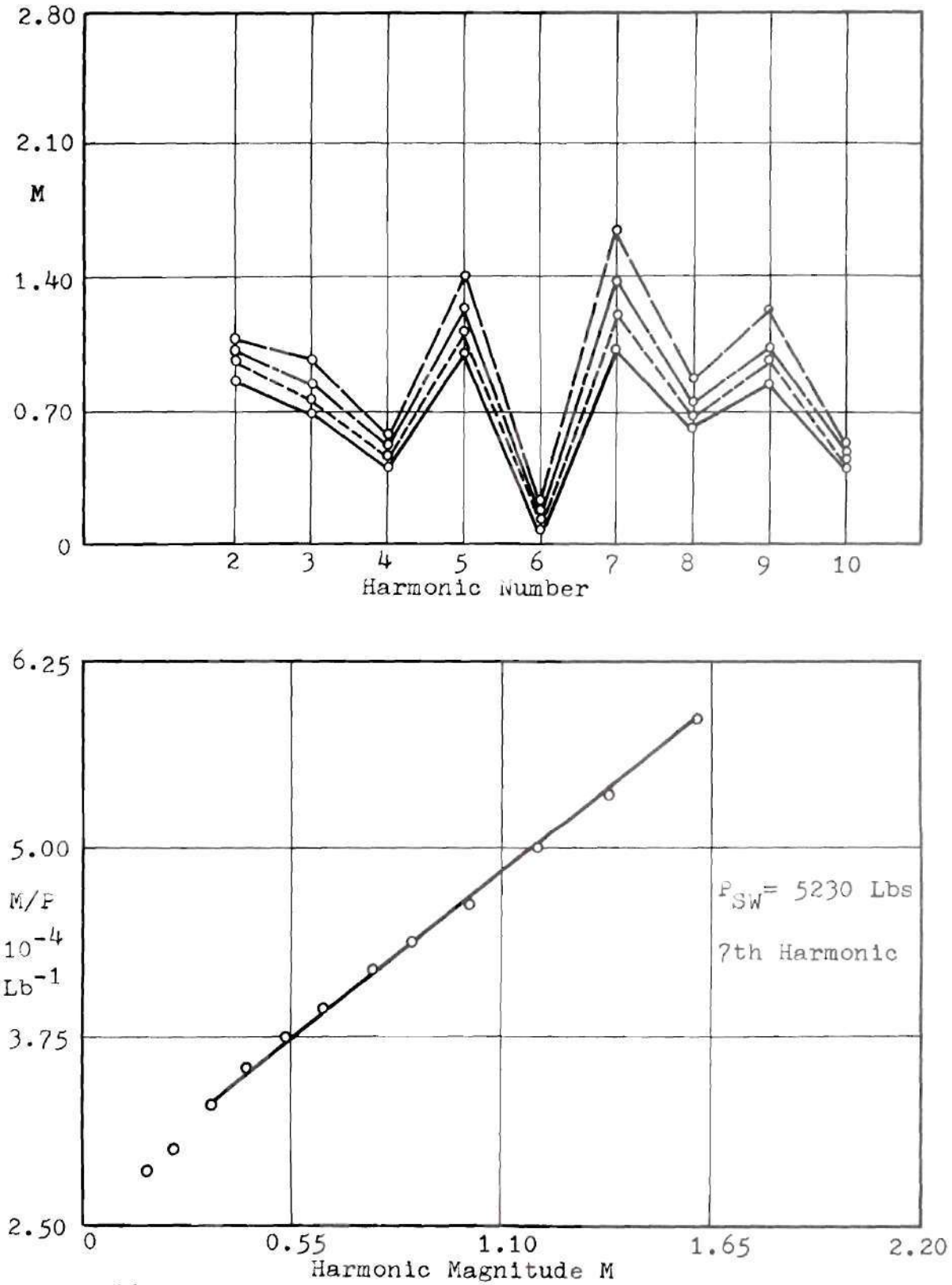

Figure 66. Harmonic Spectrum and Southwell Plot, Shell 0804.

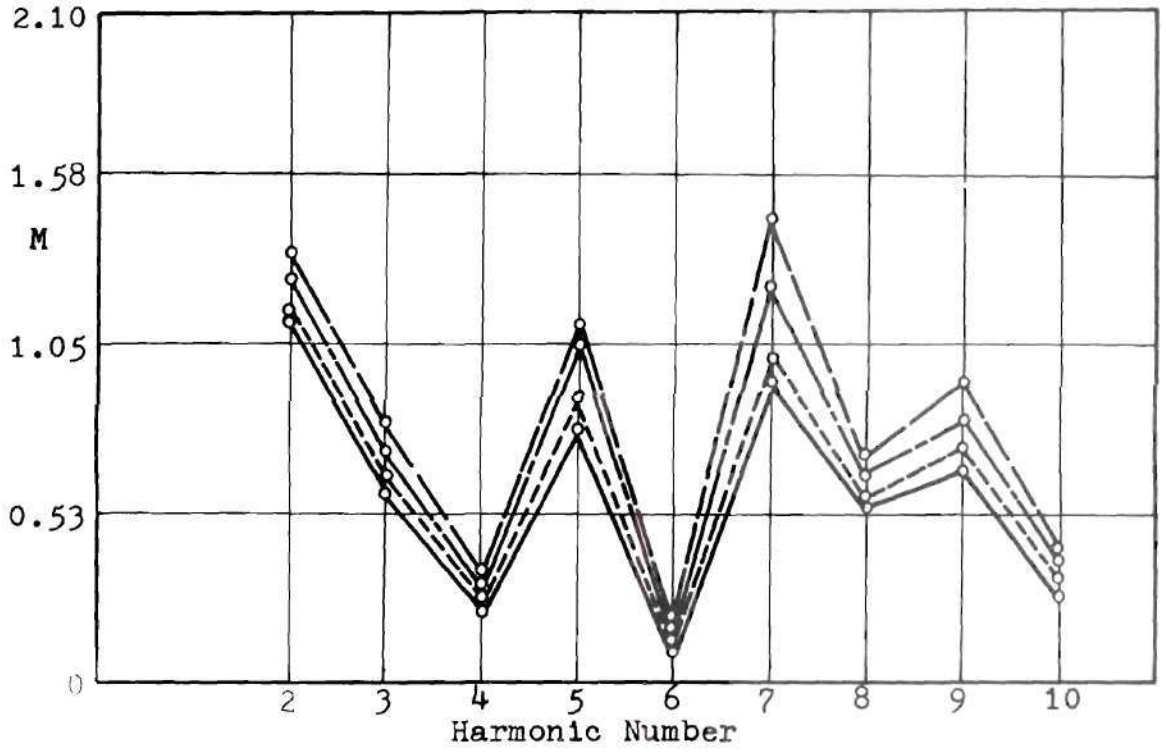

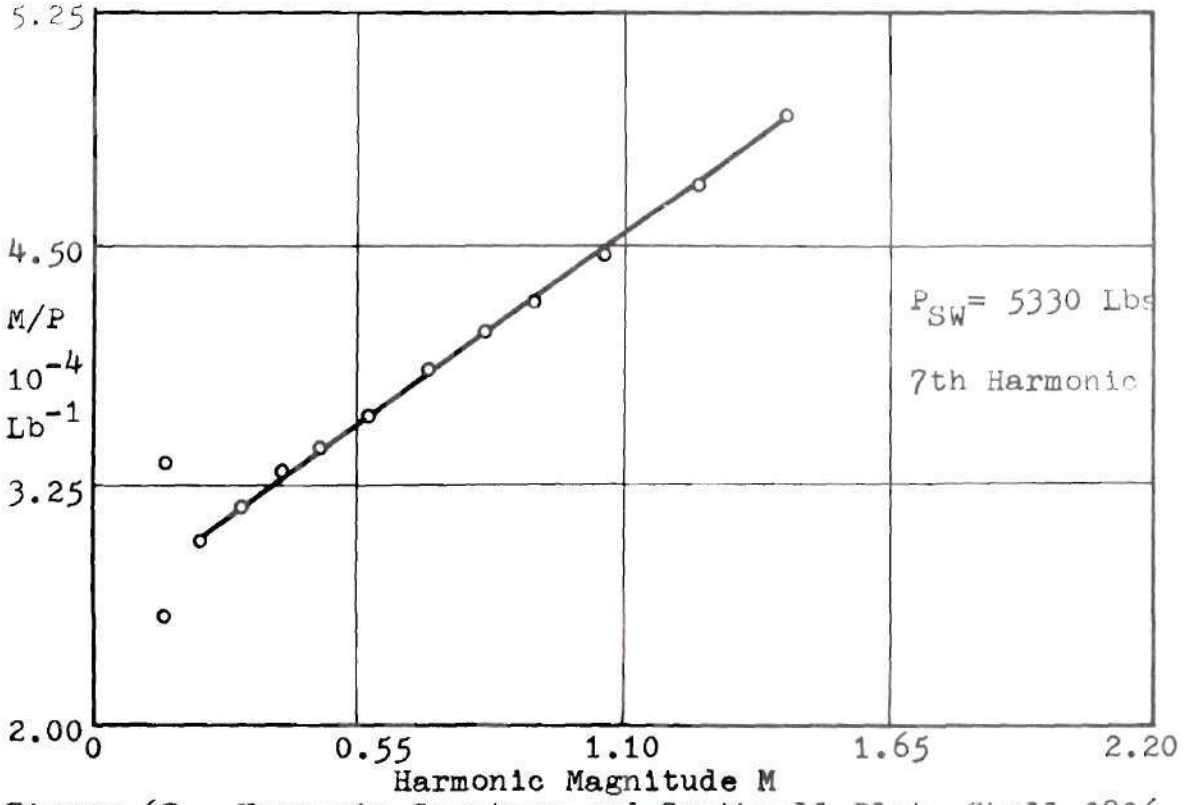

Figure 67. Harmonic Spectrum and Southwell Plot, Shell 0806.

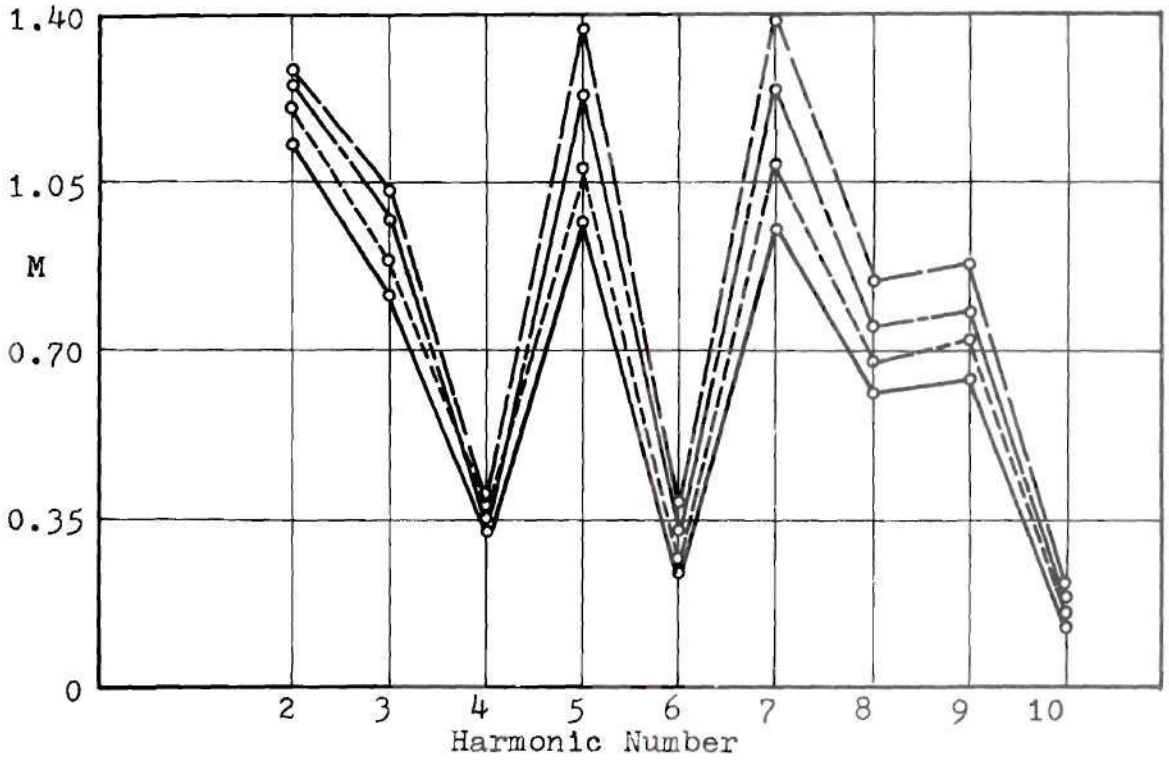

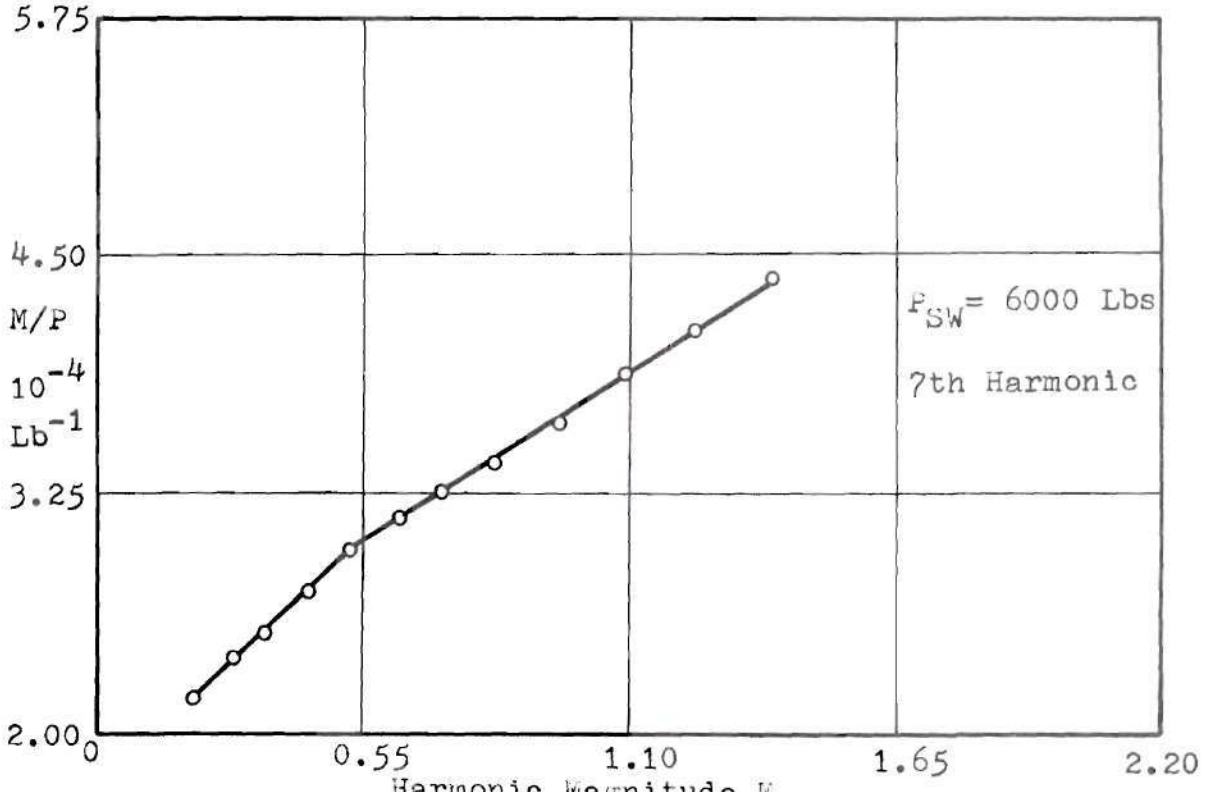

Figure 68. Harmonic Spectrum and Southwell Plot, Shell 0807.

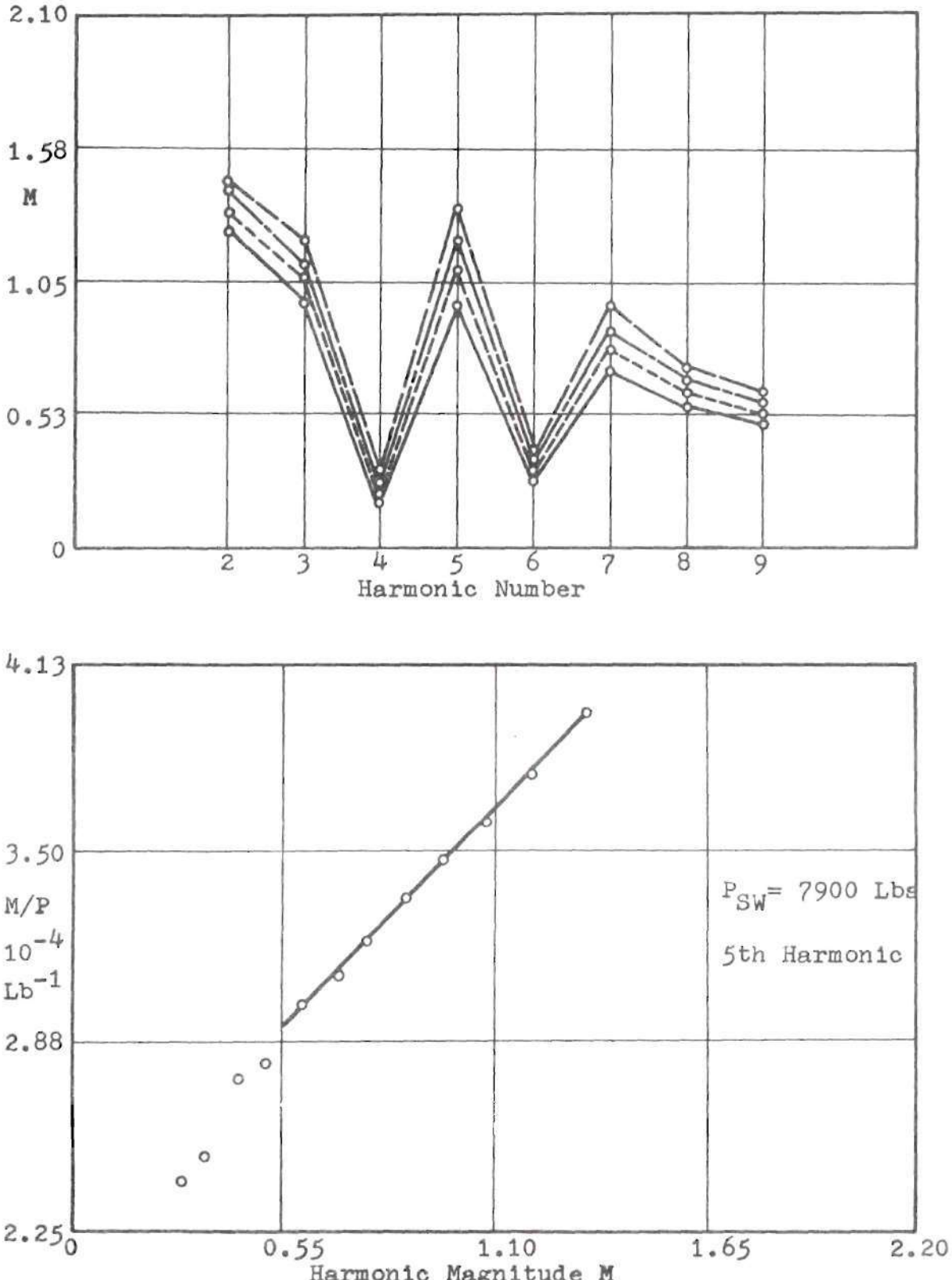

Figure 69. Harmonic Spectrum and Southwell Plot, Shell 0808.

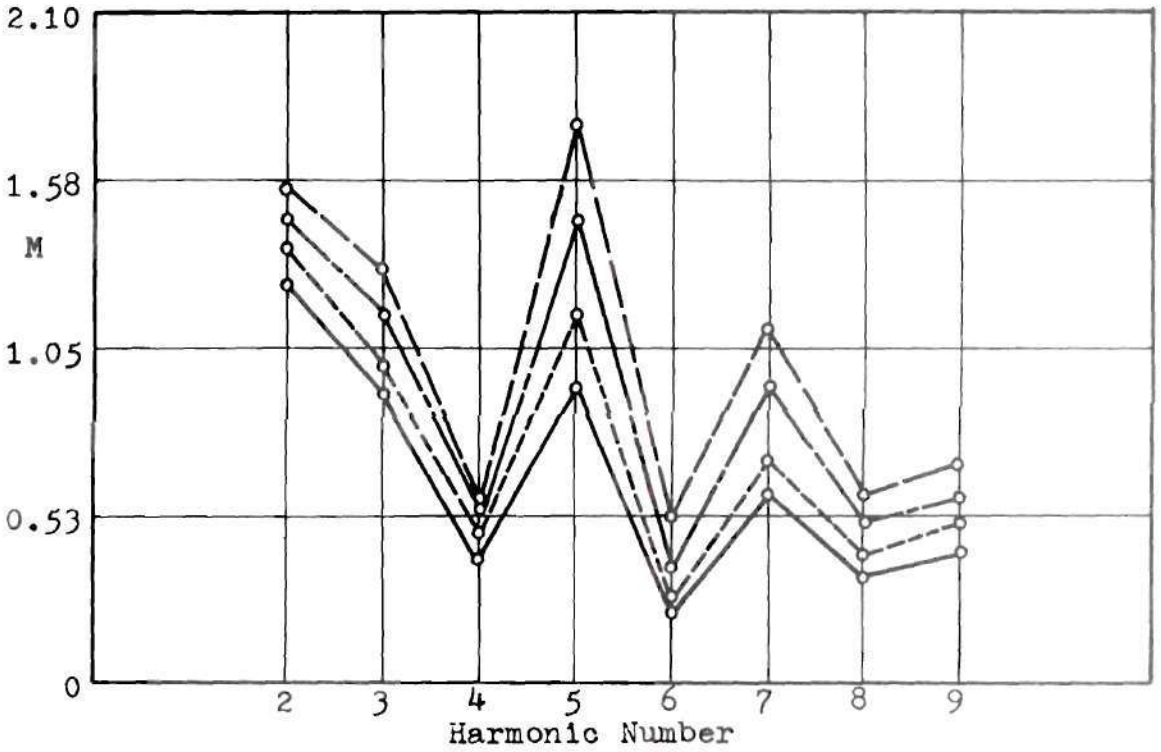

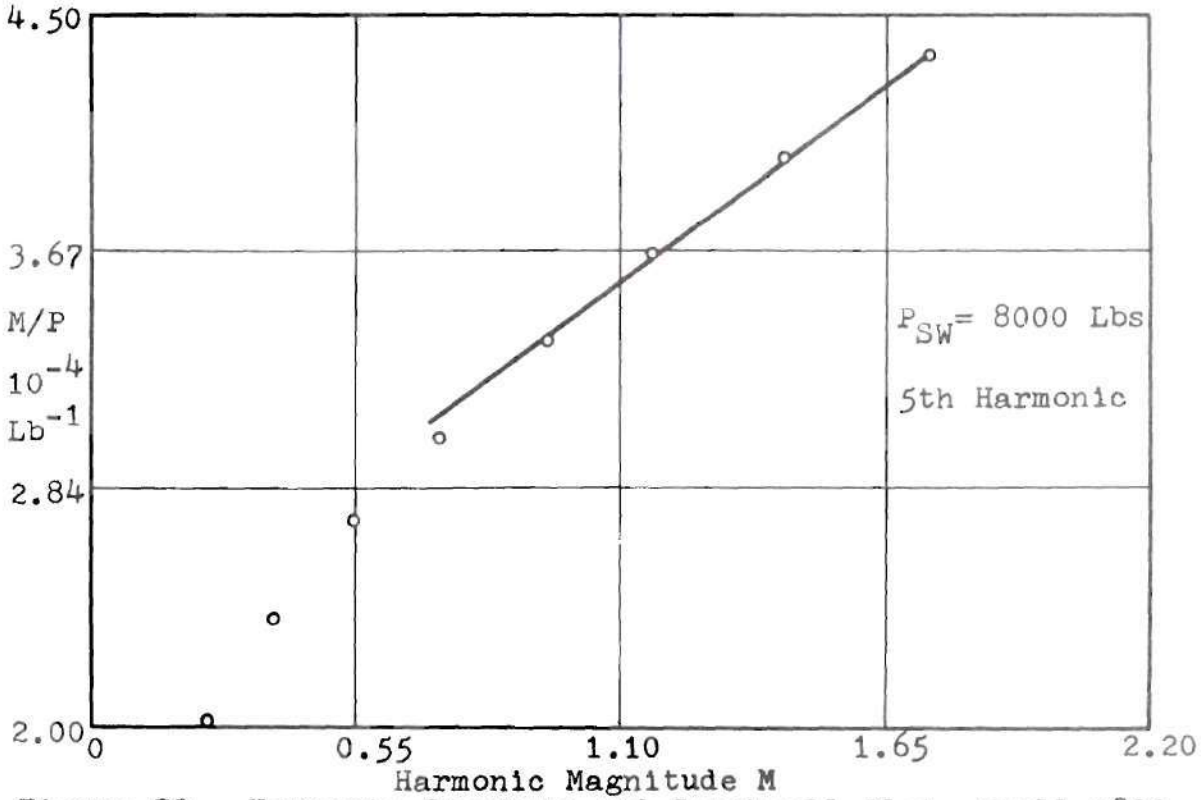

Figure 70. Harmonic Spectrum and Southwell Plot, Shell 0809.

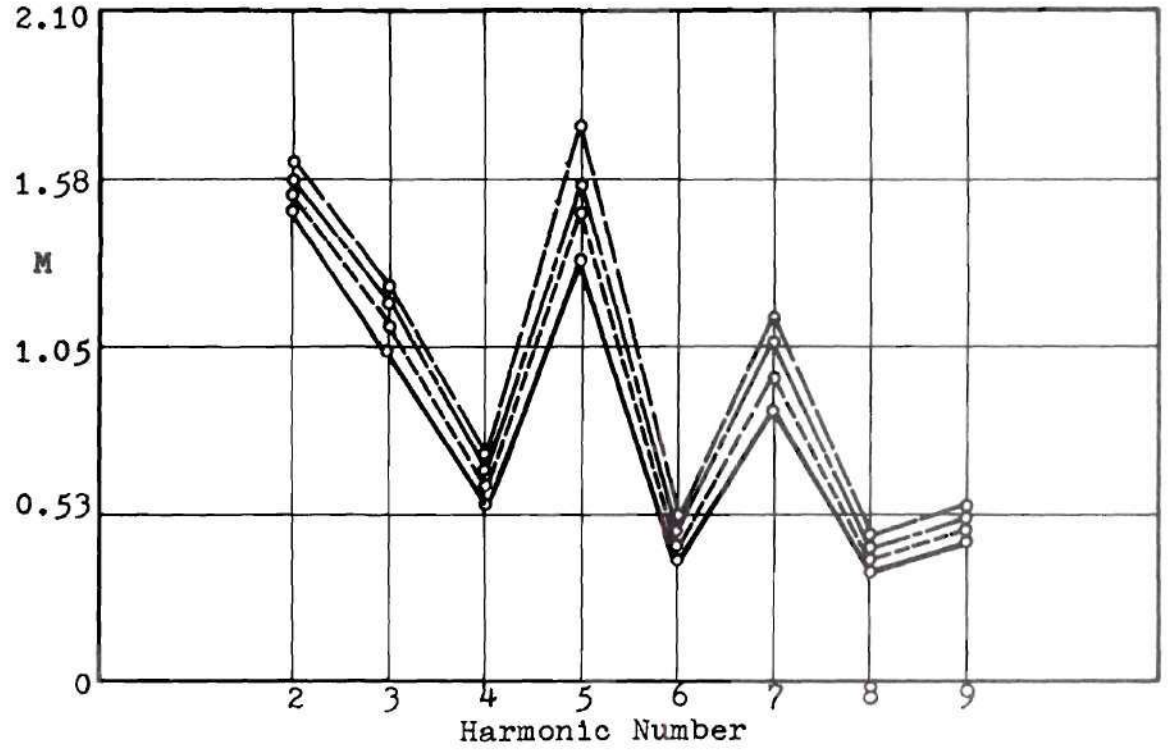

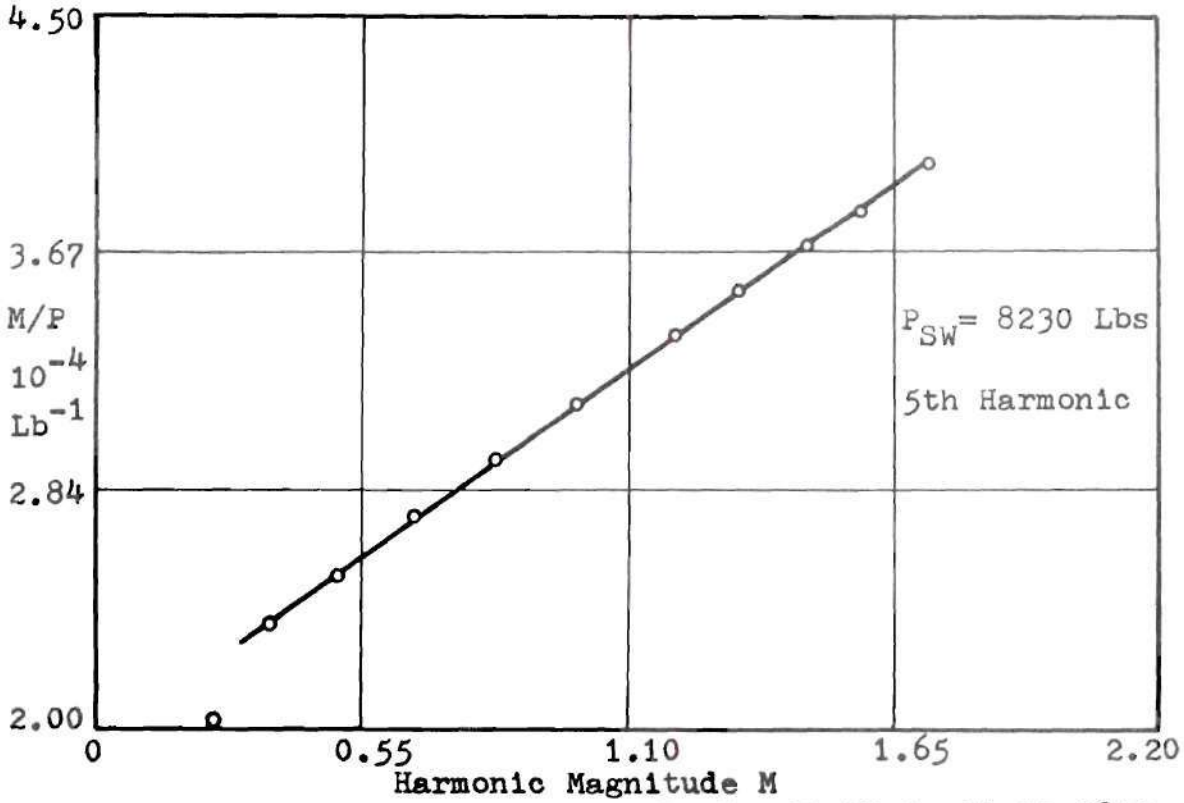

Figure 71. Harmonic Spectrum and Southwell Plot, Shell 0810.

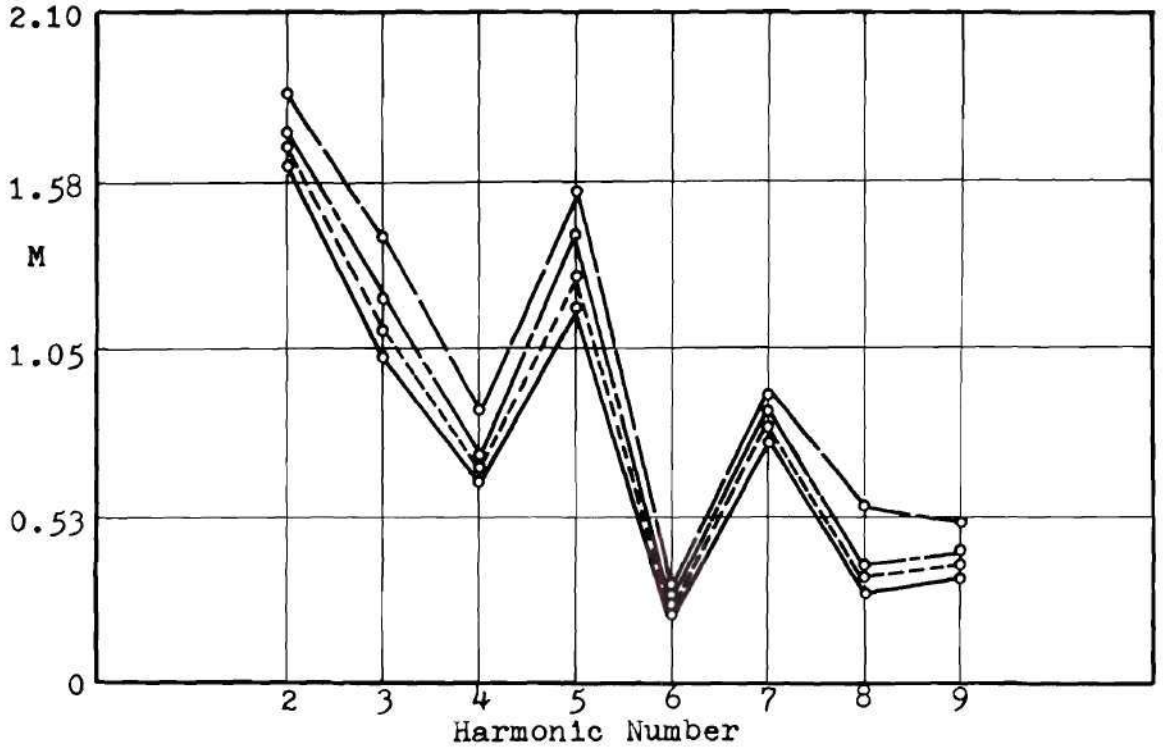

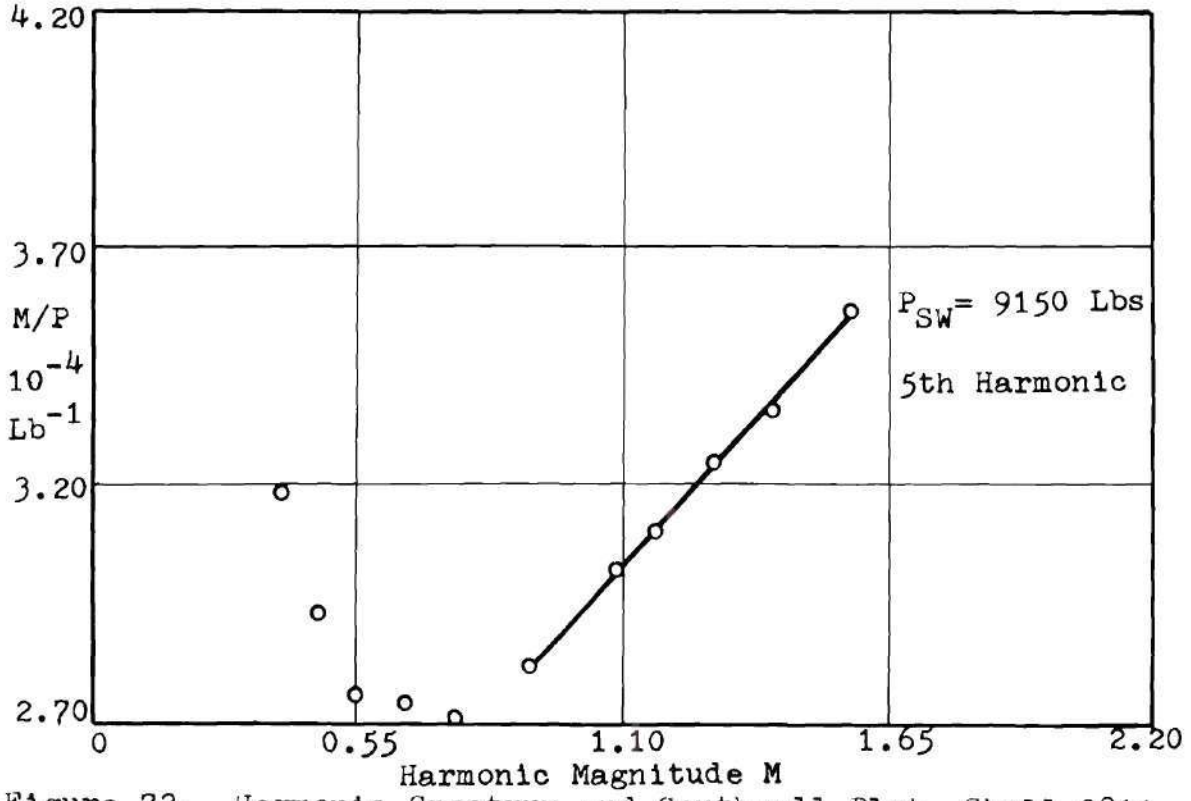

Figure 72. Harmonic Spectrum and Southwell Plot, Shell 0811.

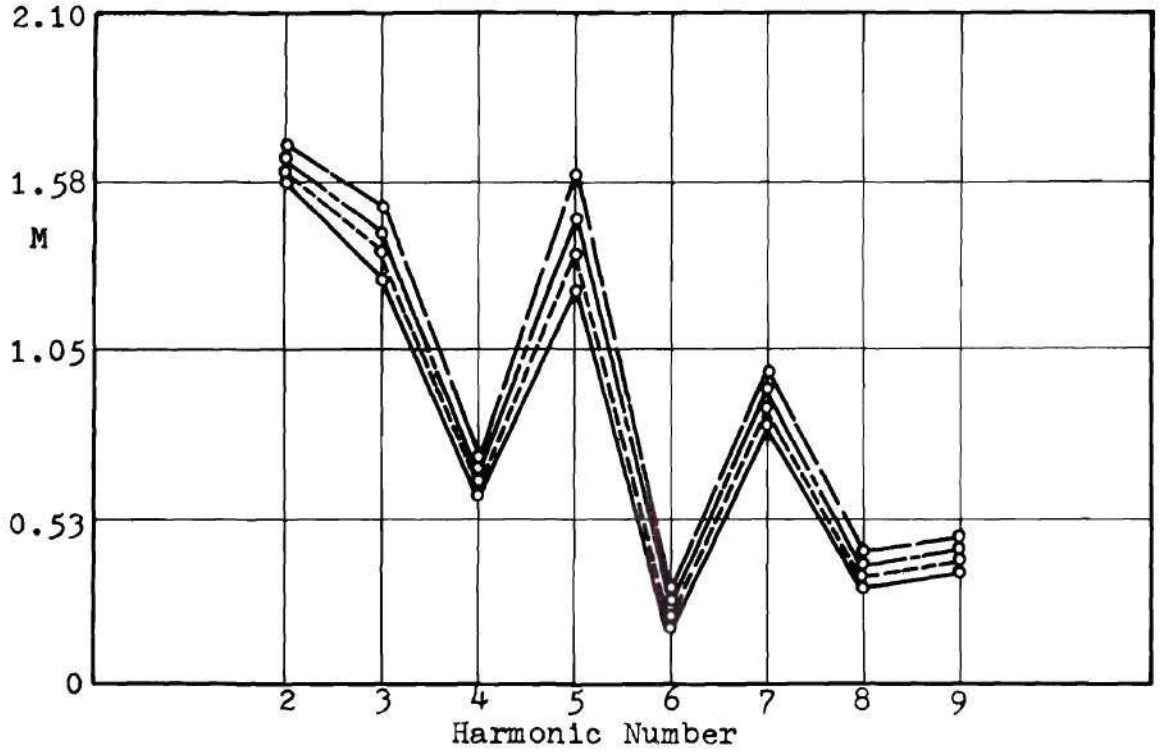

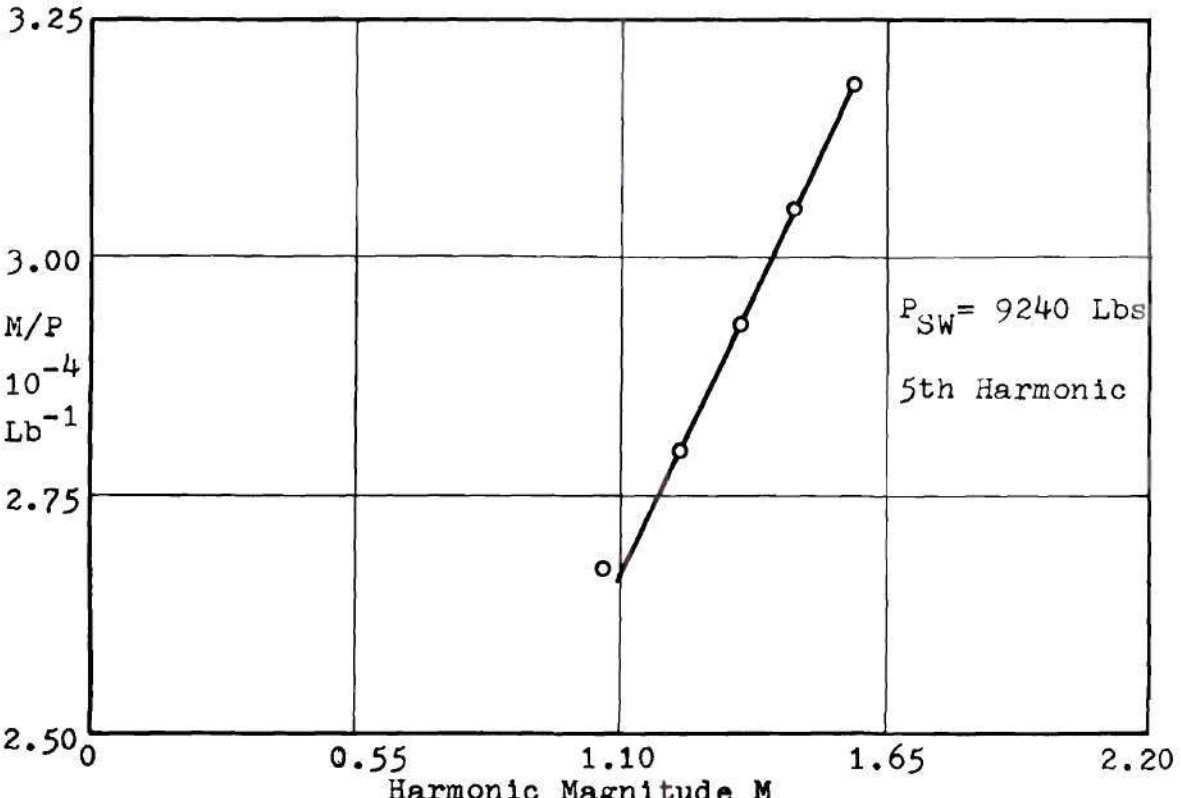

Figure 73. Harmonic Spectrum and Southwell Plot, Shell 0812.

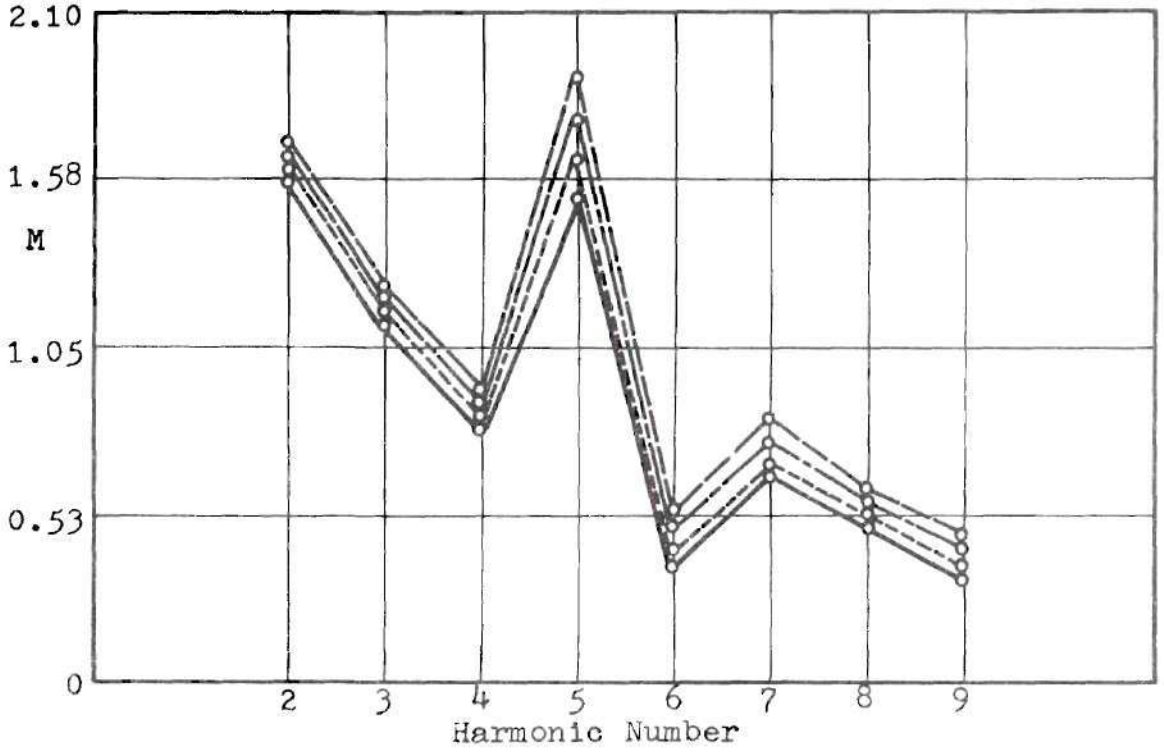

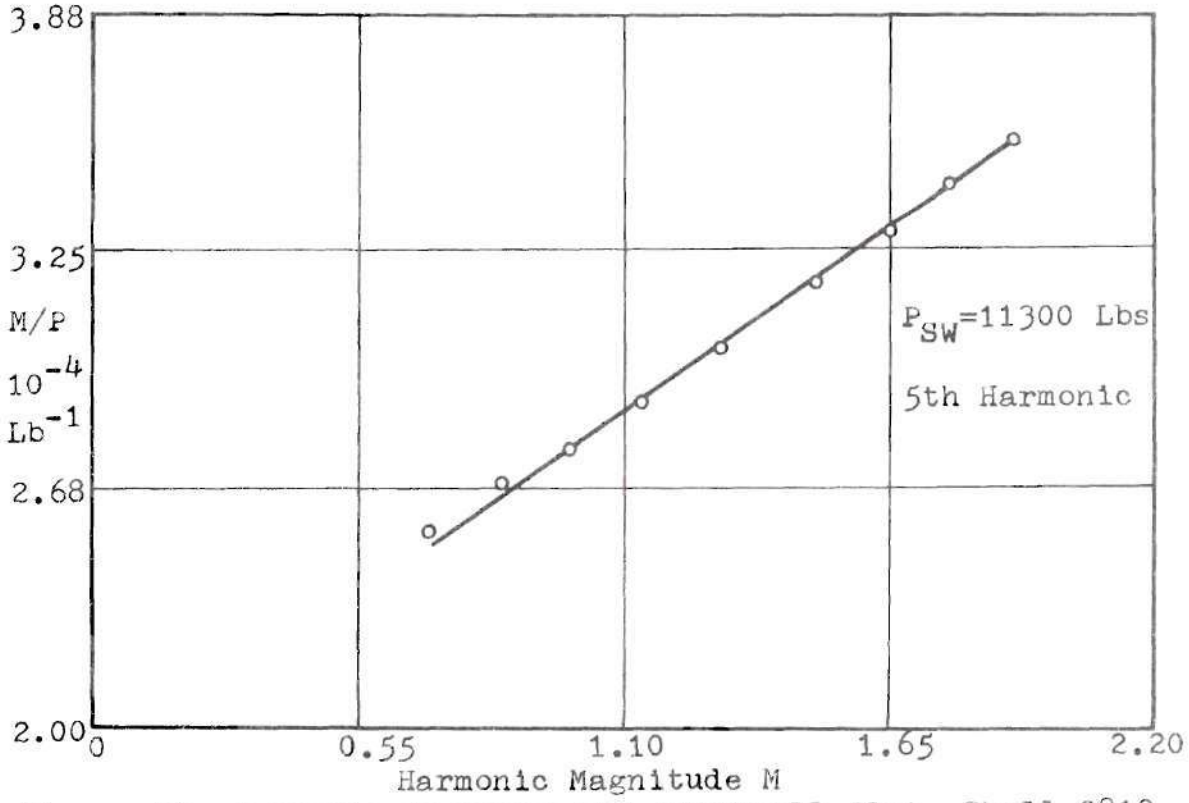

Figure 74. Harmonic Spectrum and Southwell Plot, Shell 0813.

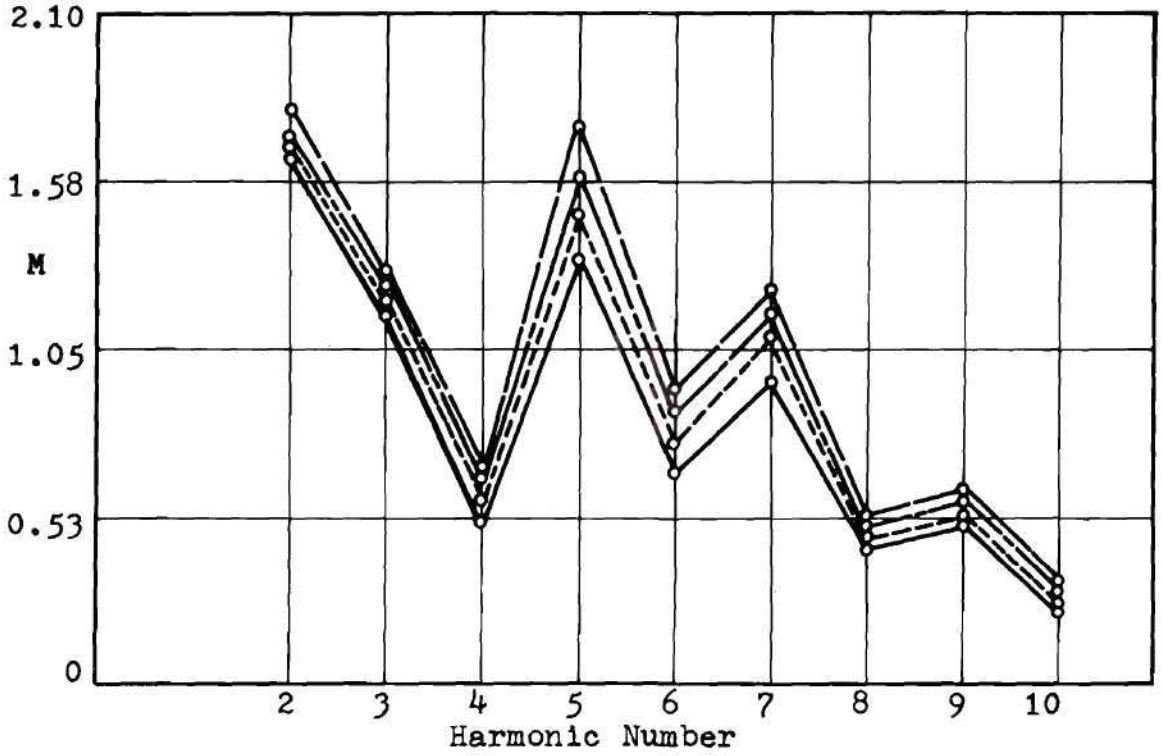

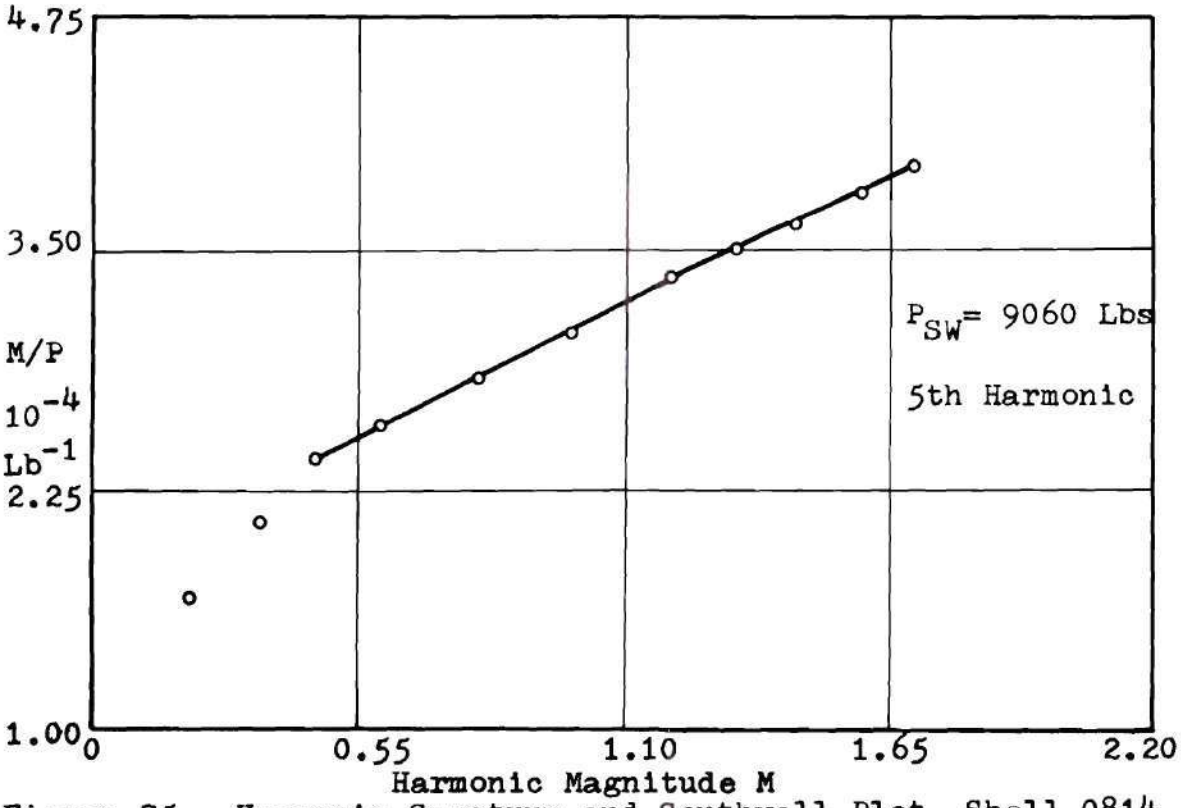

Figure 75. Harmonic Spectrum and Southwell Plot, Shell 0814.

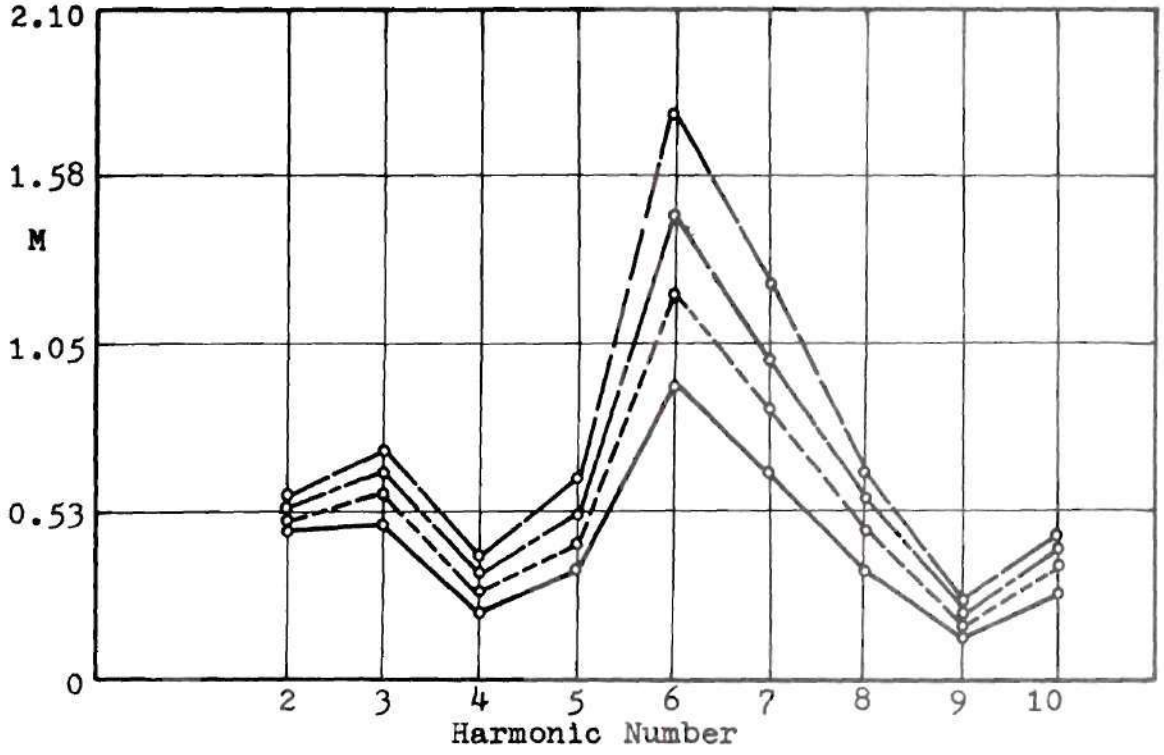

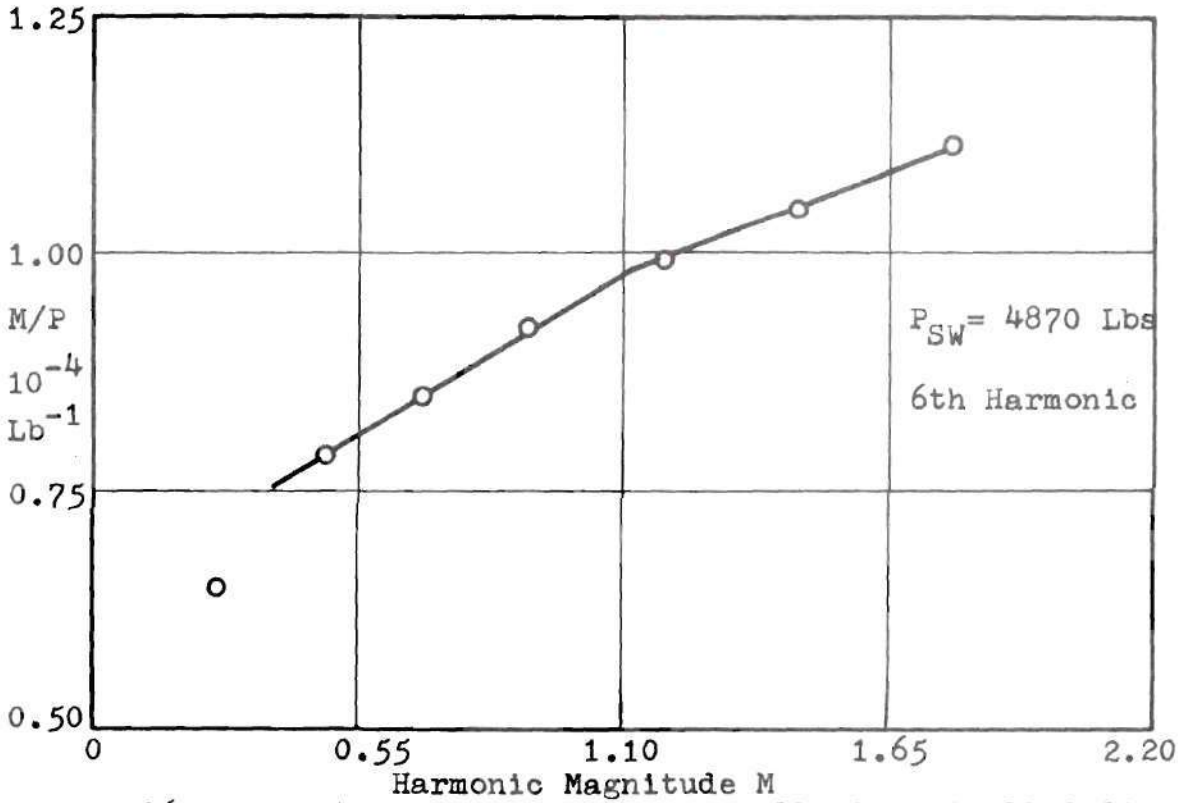

Figure 76. Harmonic Spectrum and Southwell Plot, Shell 0901.

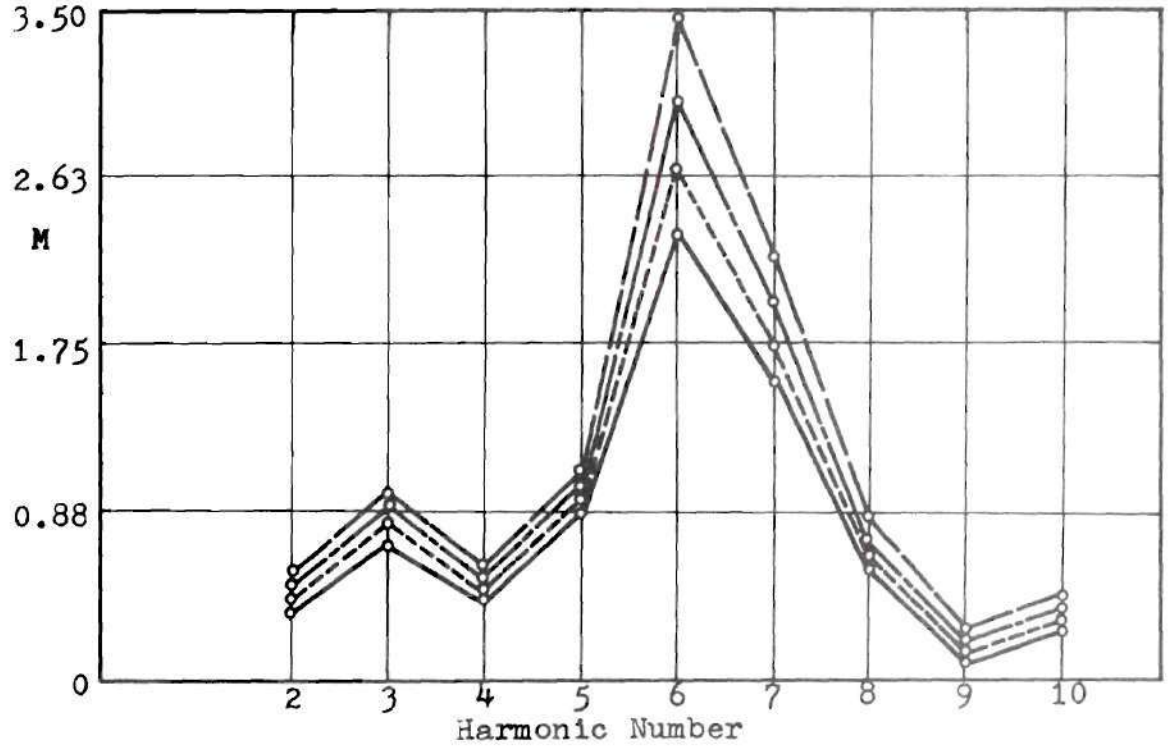

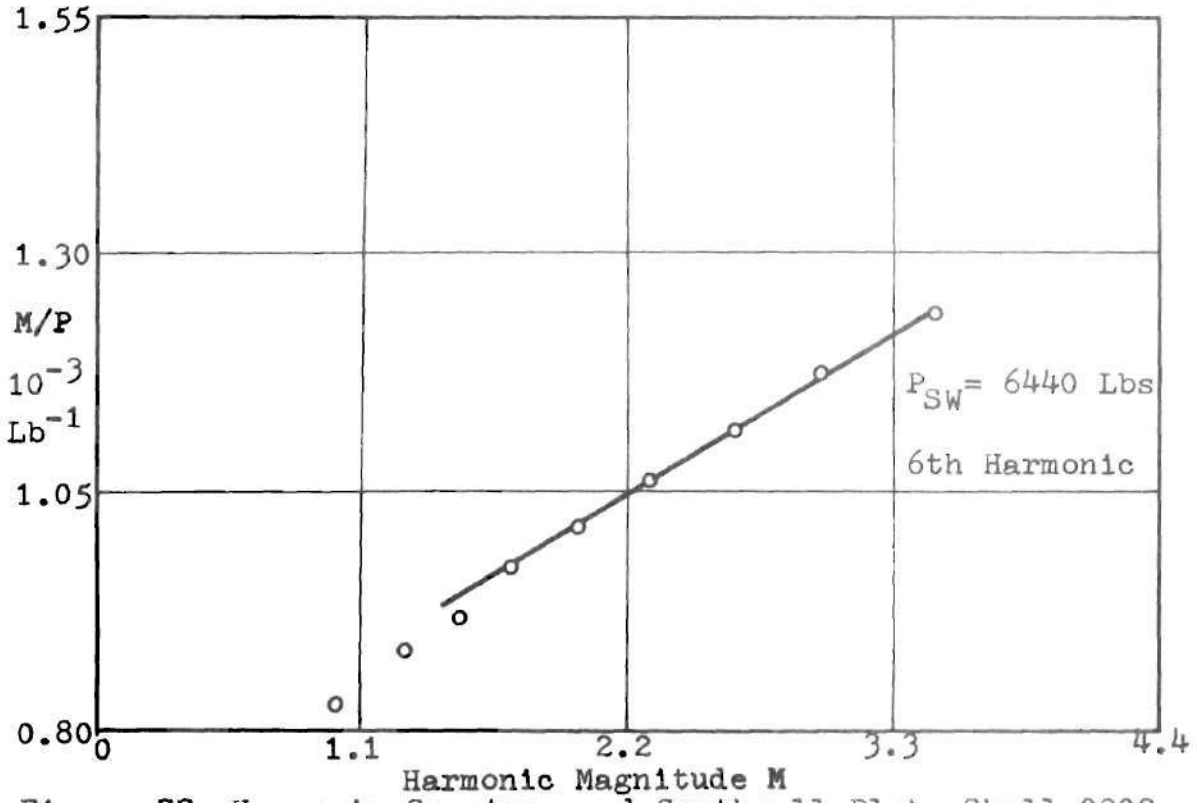

Figure 77. Harmonic Spectrum and Southwell Plot, Shell 0902.

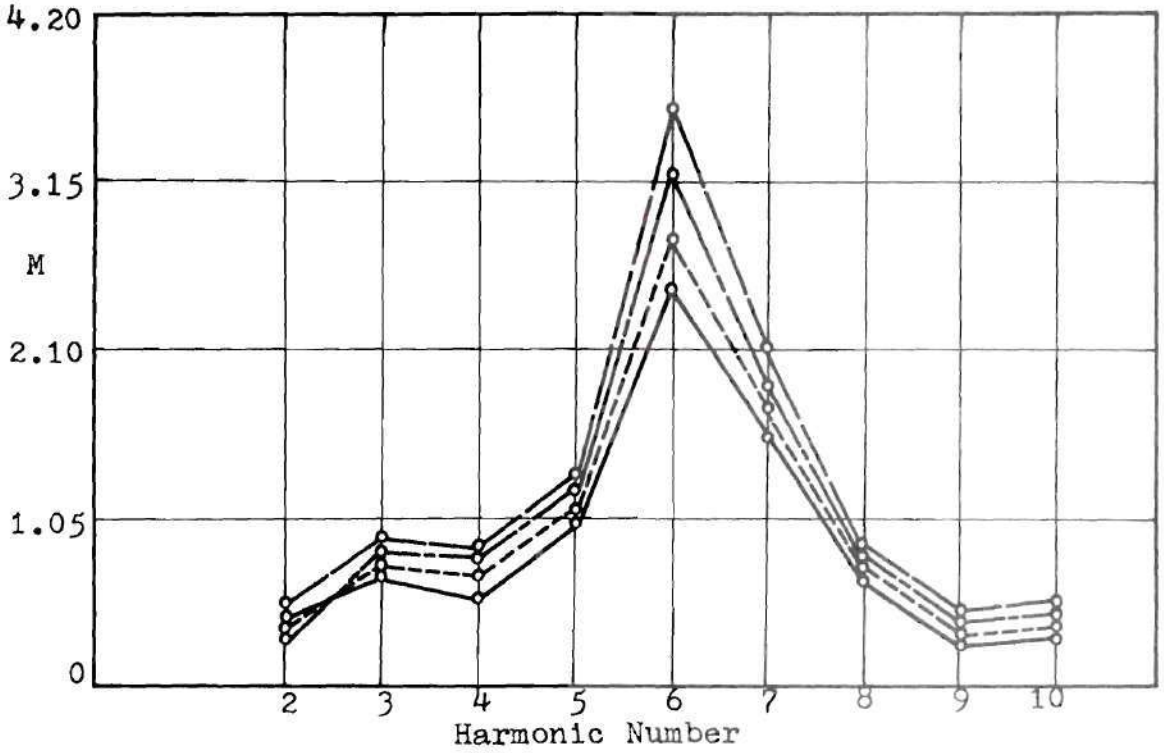

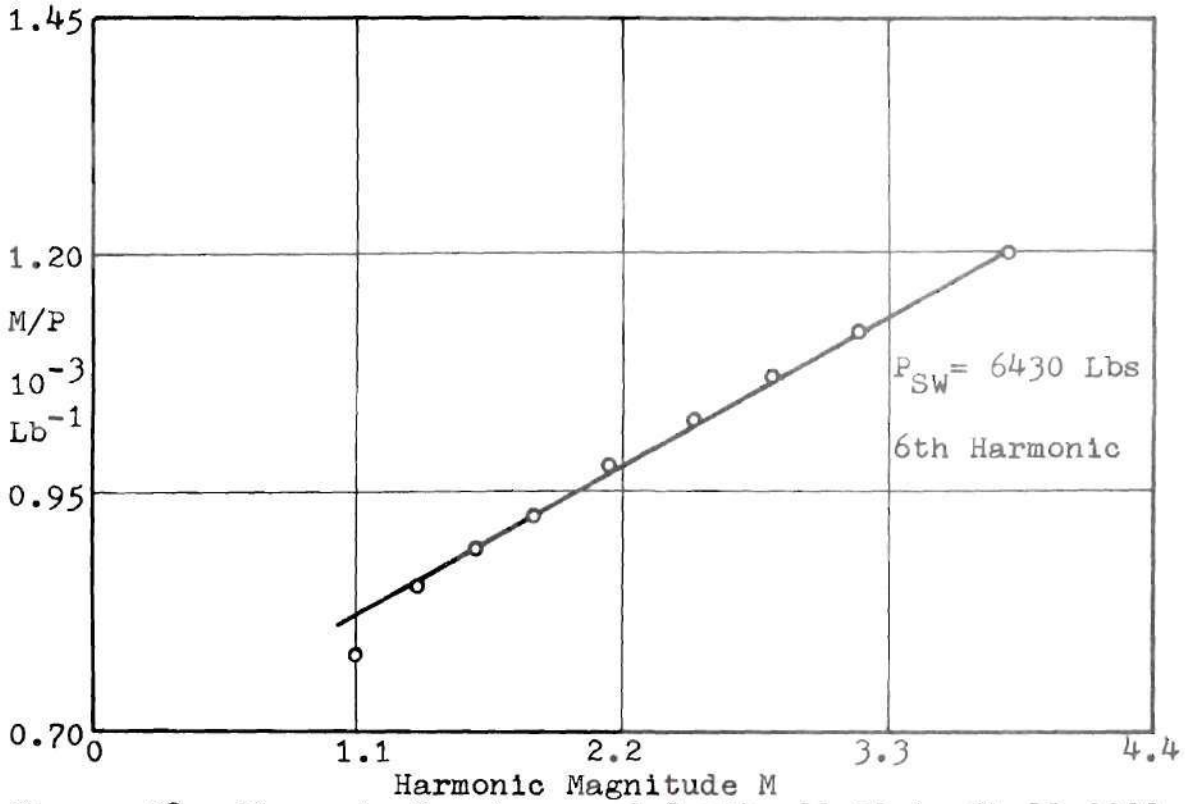

Figure 78. Harmonic Spectrum and Southwell Plot, Shell 0903.

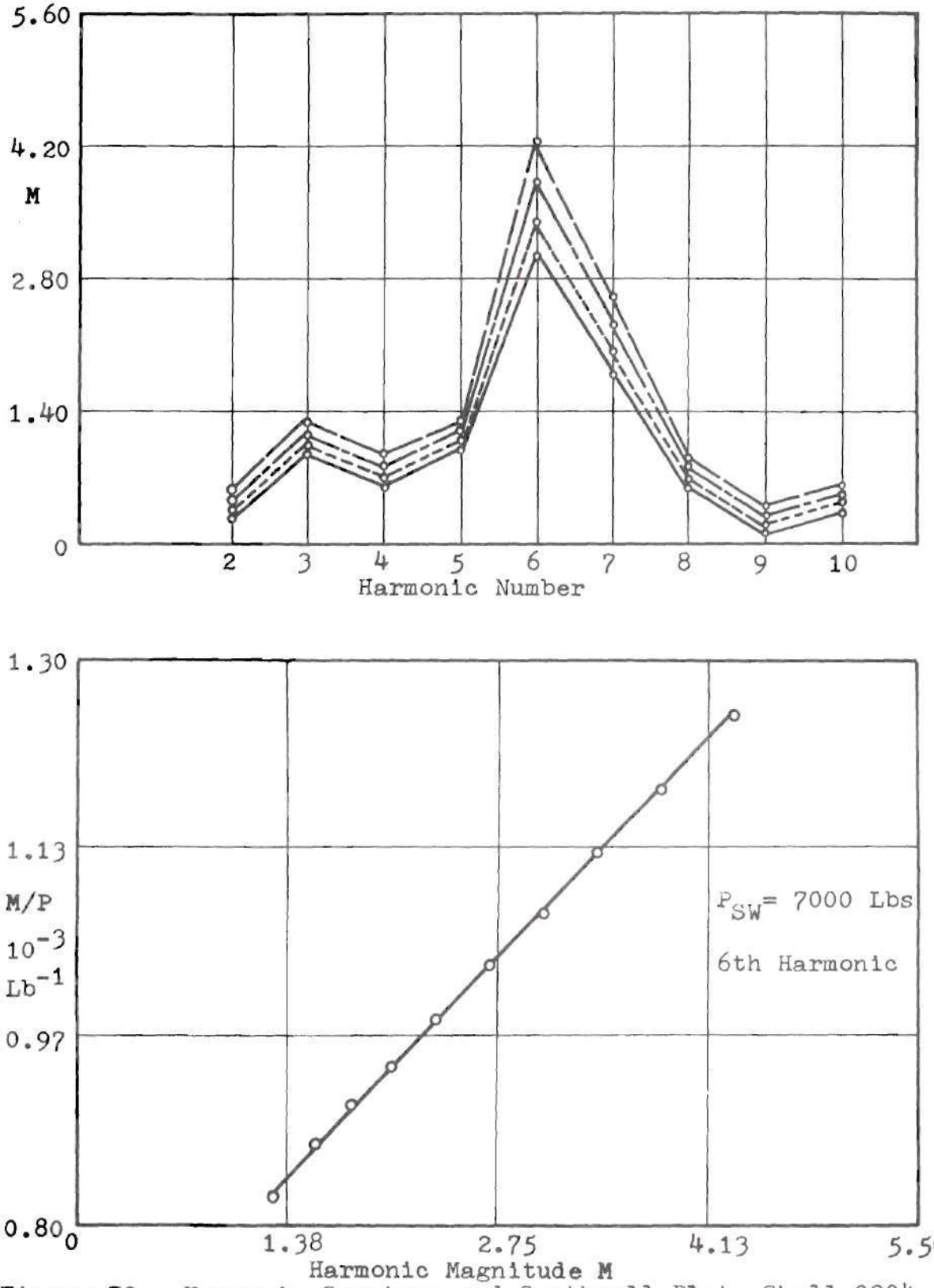

Figure 79. Harmonic Spectrum and Southwell Plot, Shell 0904.

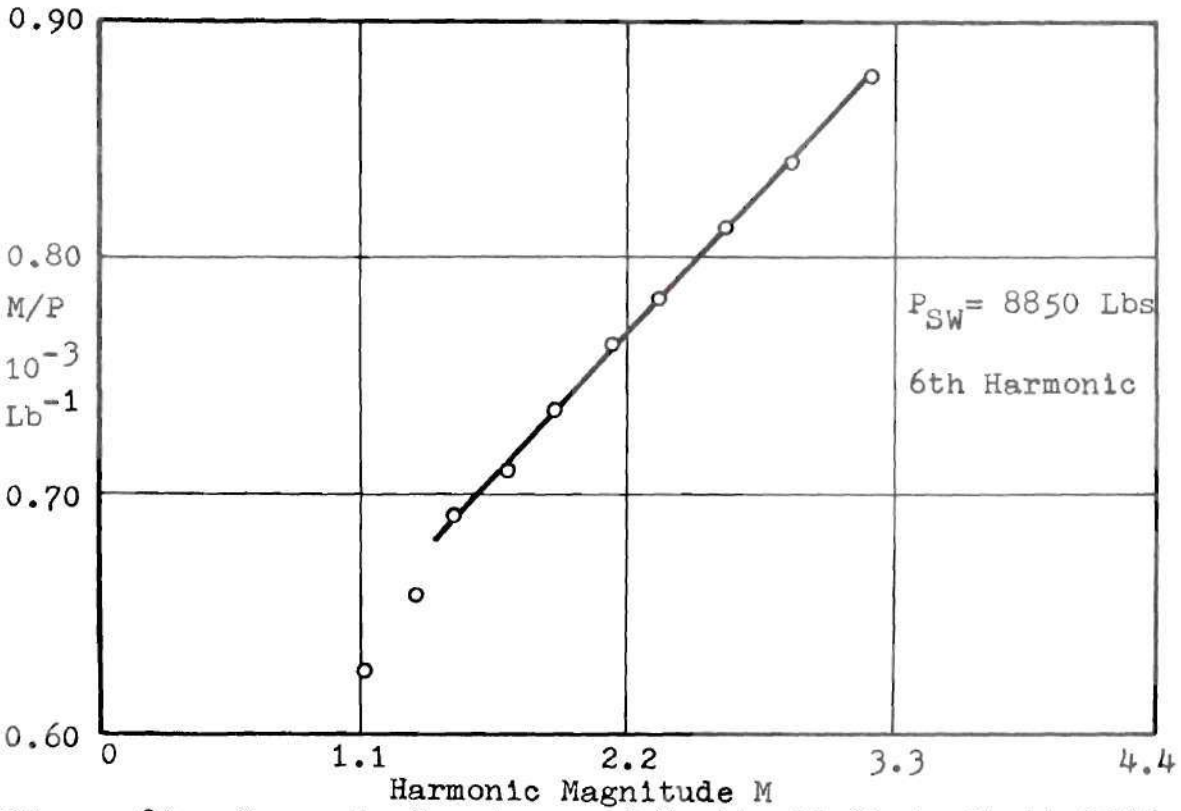

Figure 80. Harmonic Spectrum and Southwell Plot, Shell 0905.

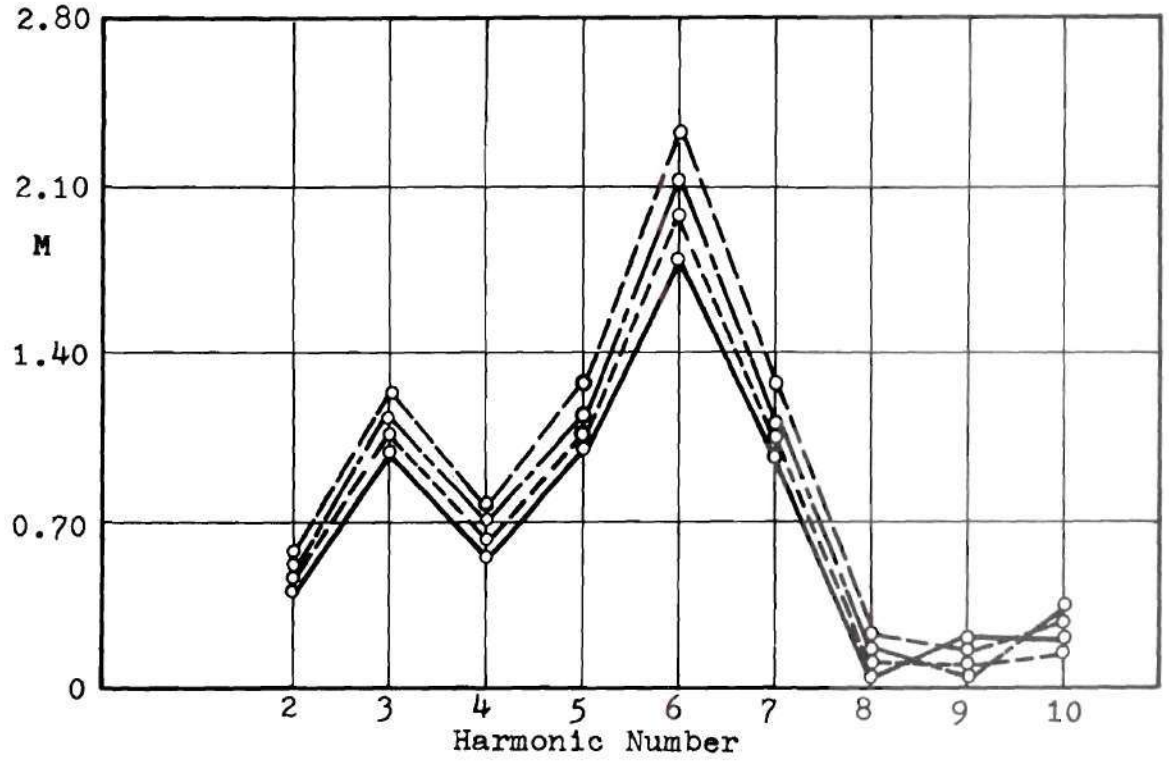

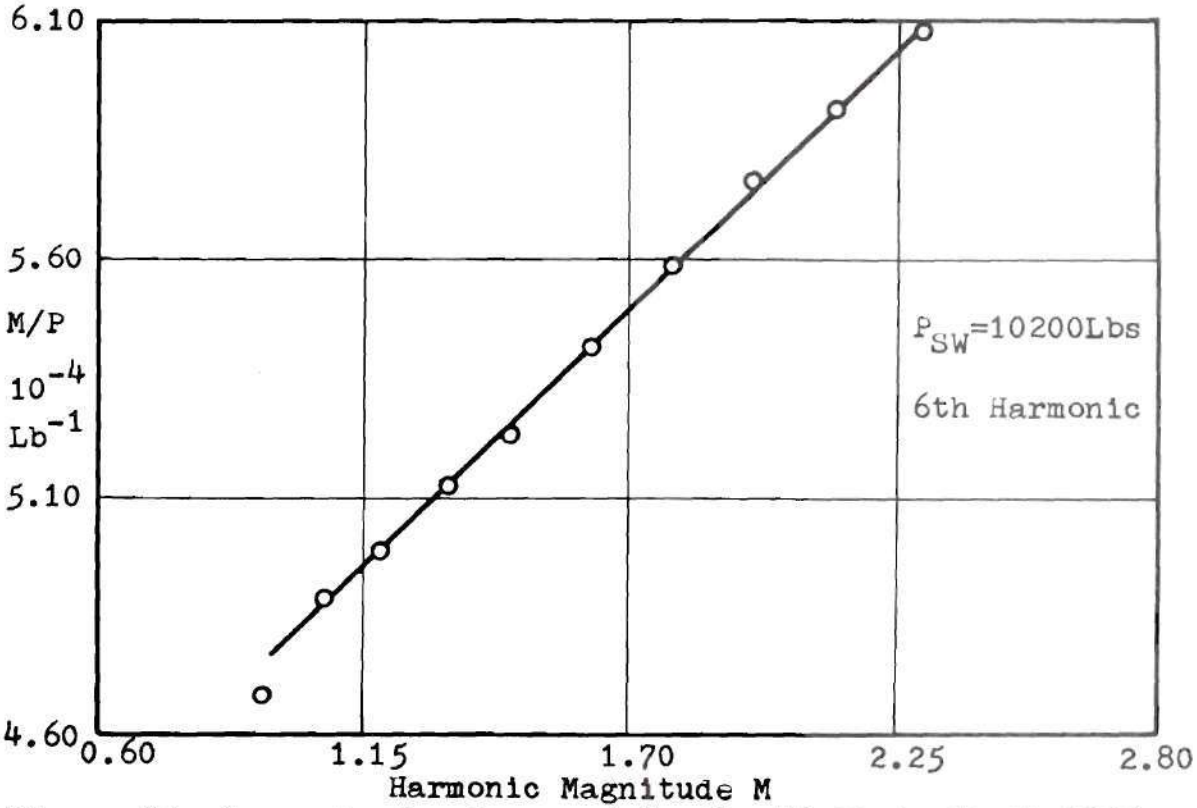

Figure 81. Harmonic Spectrum and Southwell Plot, Shell 0906.

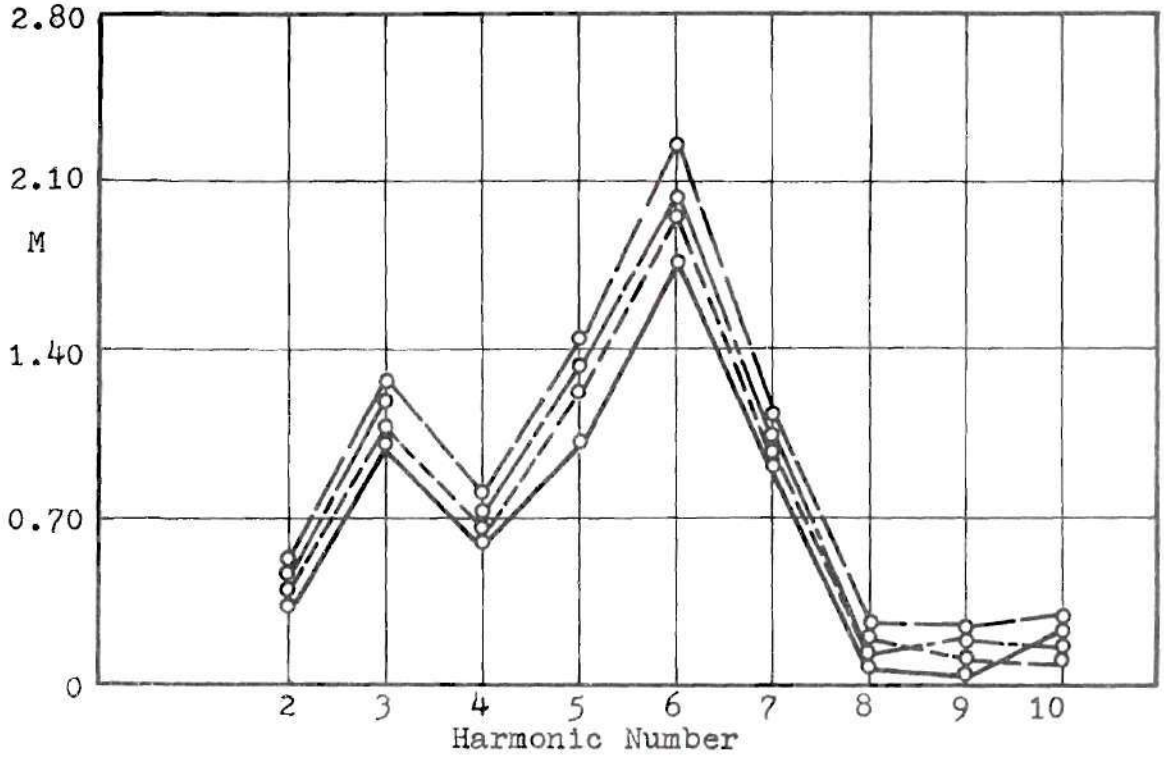

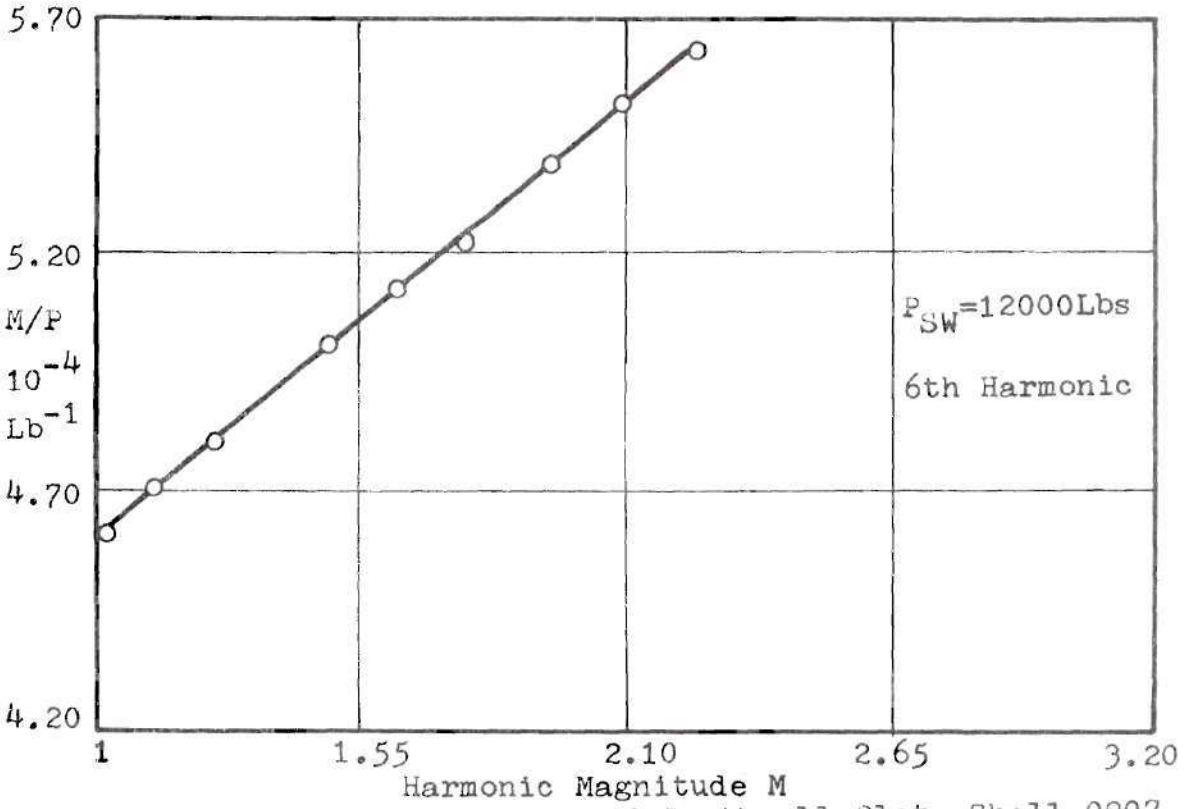

Figure 82. Harmonic Spectrum and Southwell Plot, Shell 0907.

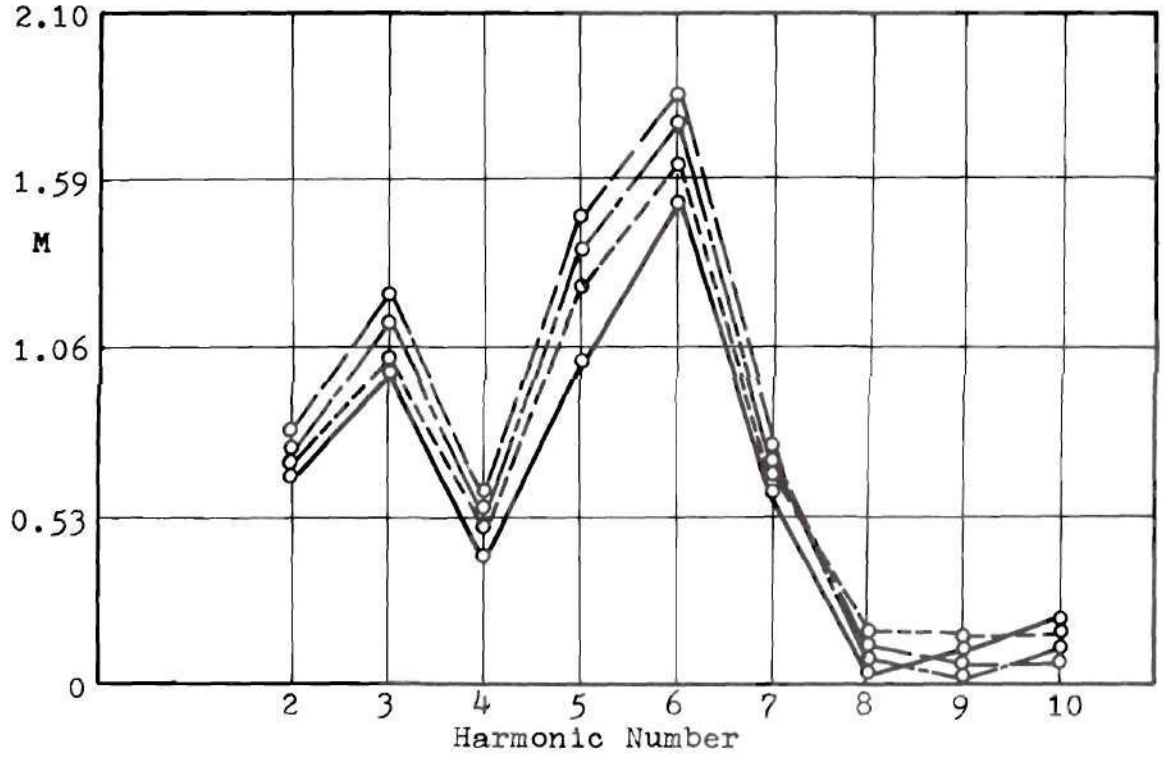

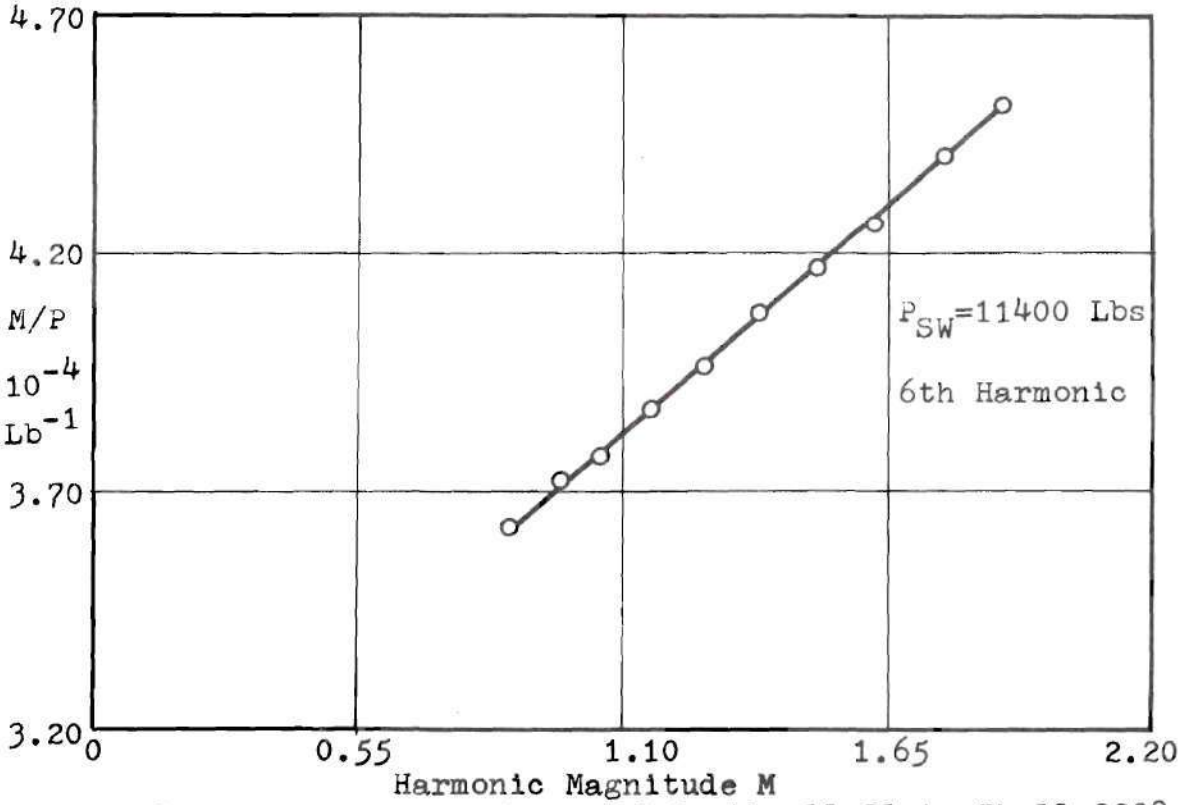

Figure 83. Harmonic Spectrum and Southwell Plot, Shell 0908.

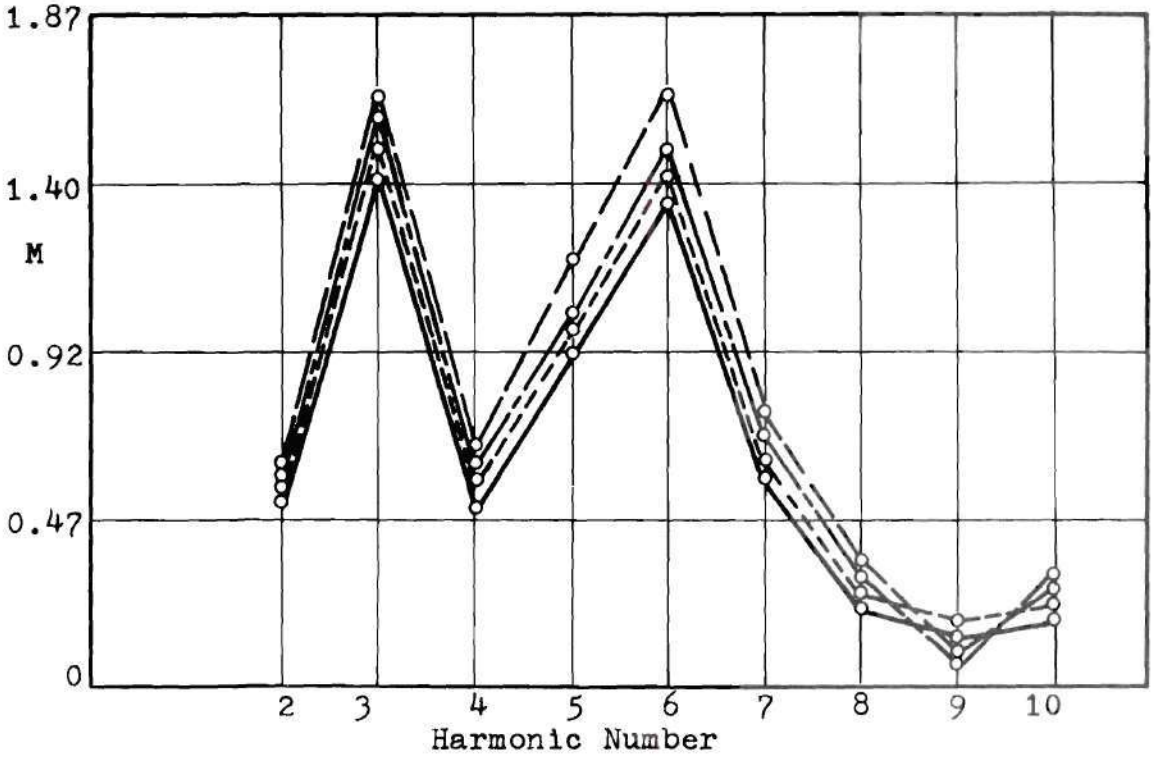

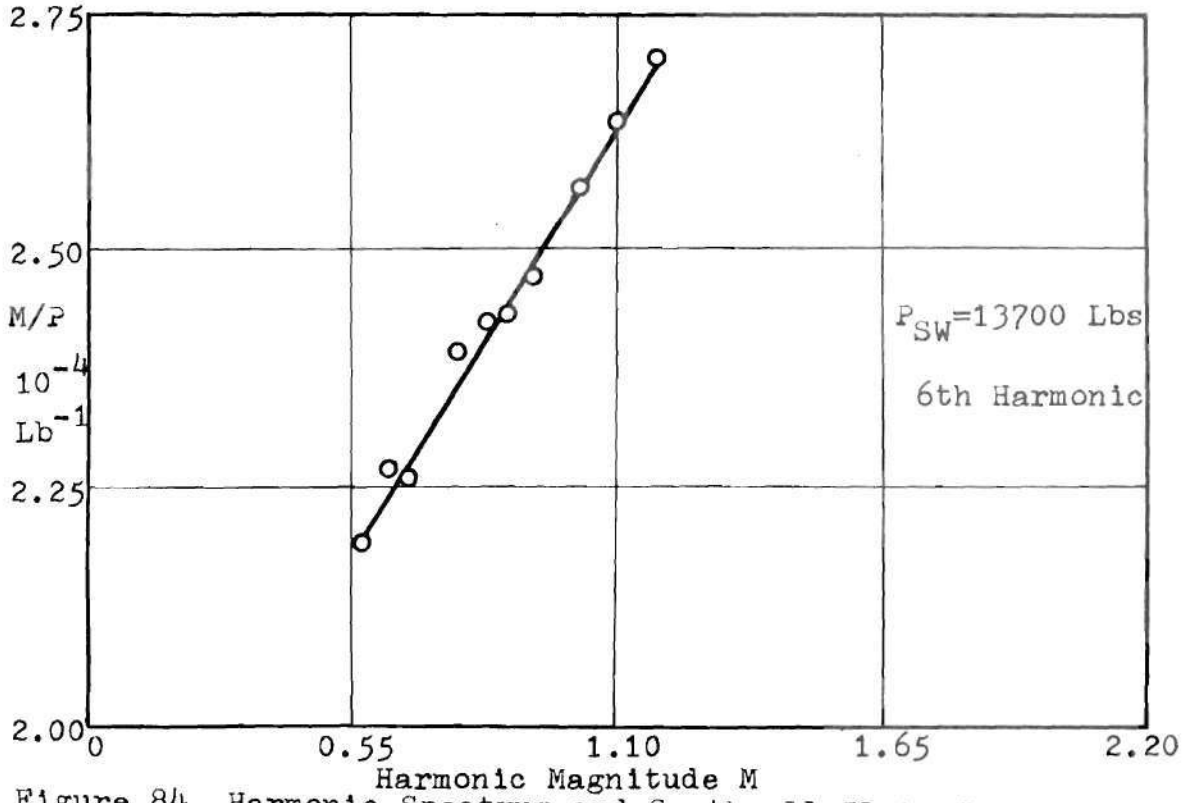

Figure 84. Harmonic Spectrum and Southwell Plot, Shell 0909.

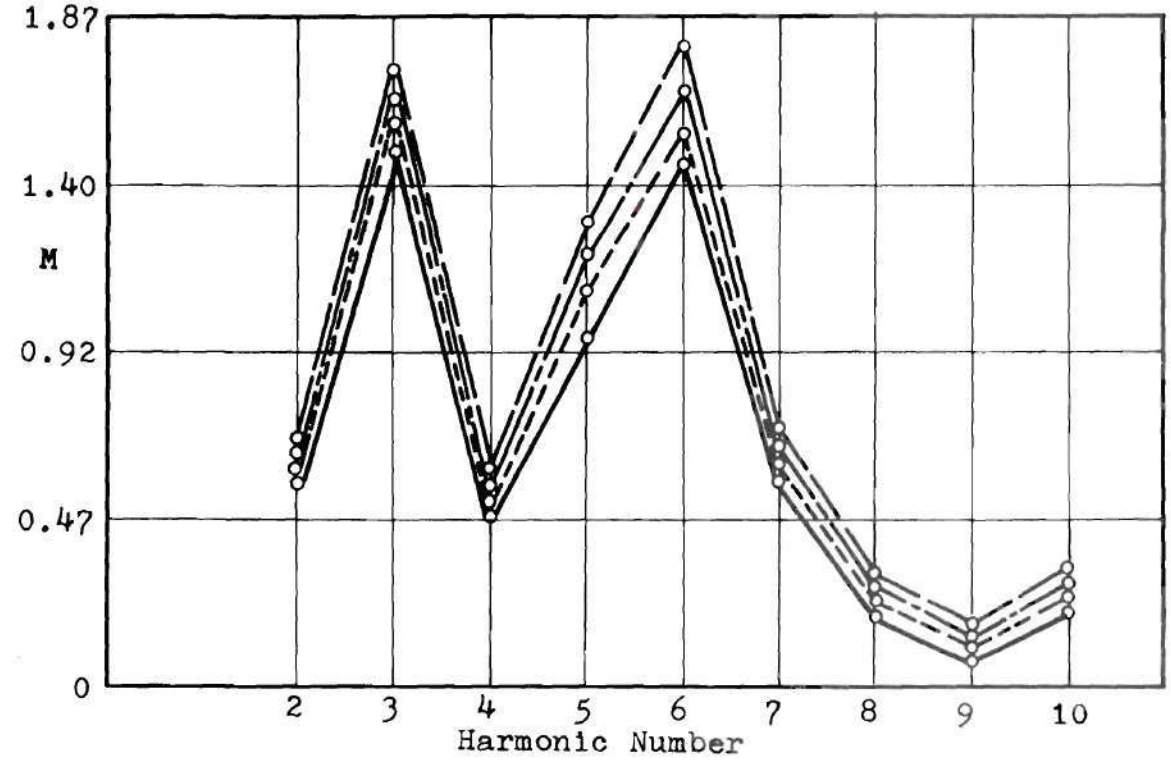

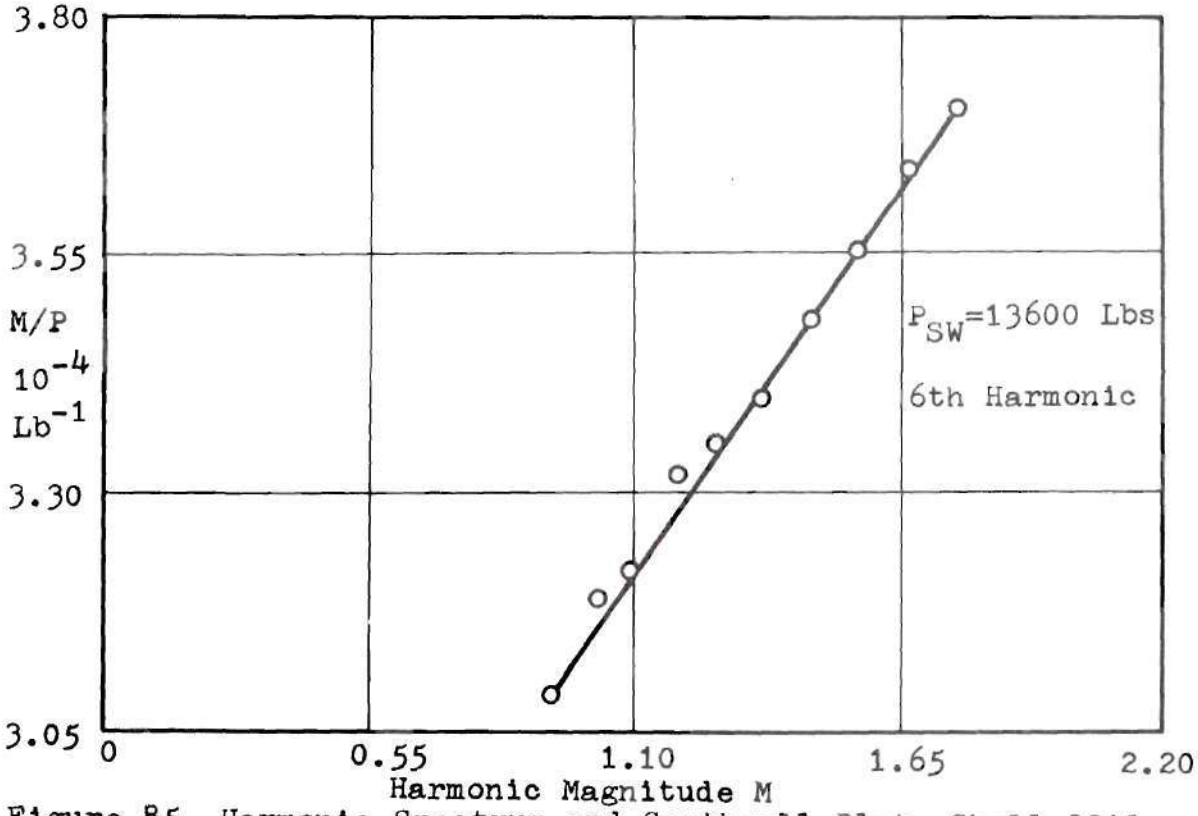

Figure.85. Harmonic Spectrum and Southwell Plot, Shell 0910.

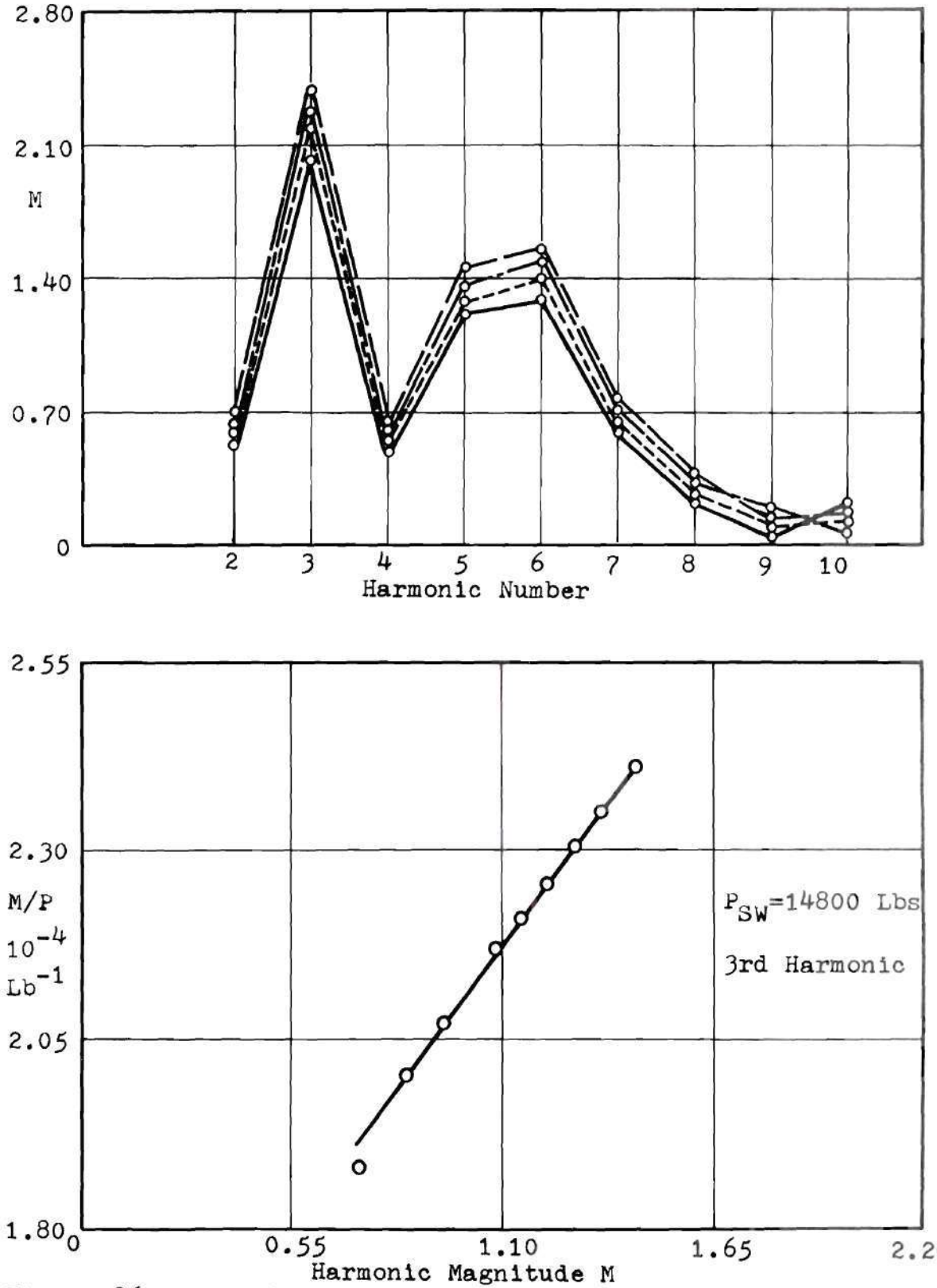

Figure 86. Harmonic Spectrum and Southwell Plot, Shell 0911.

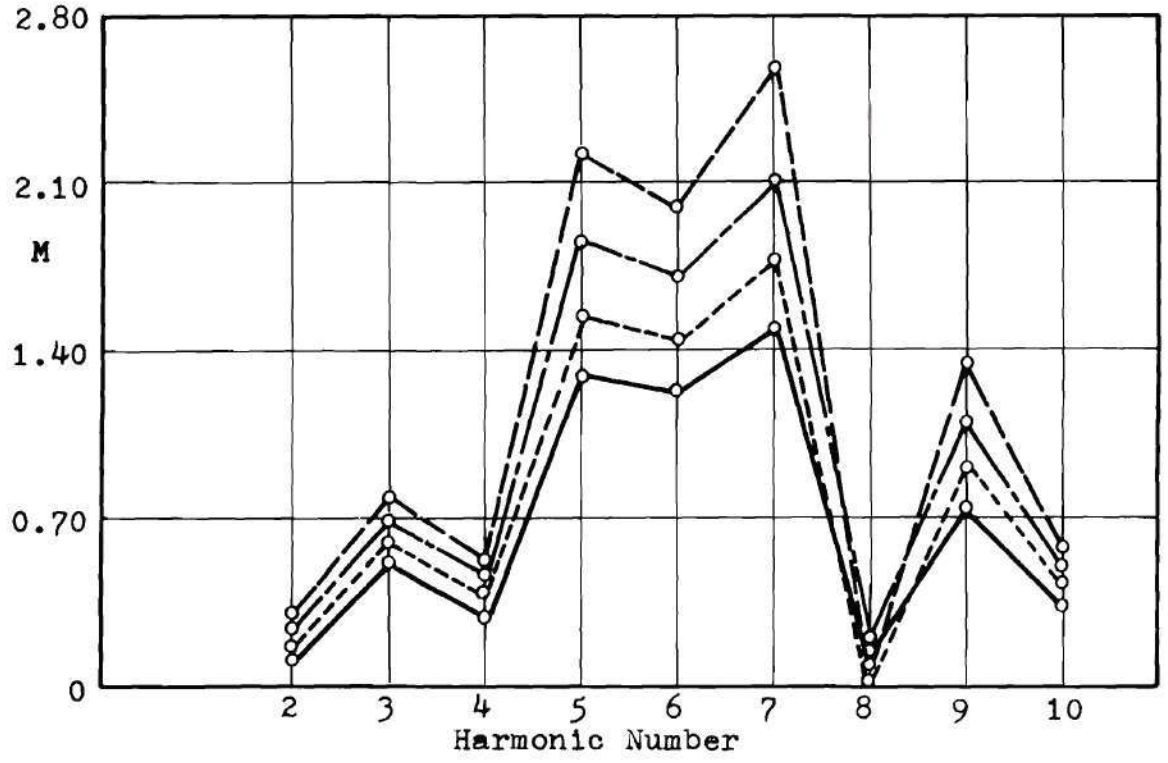

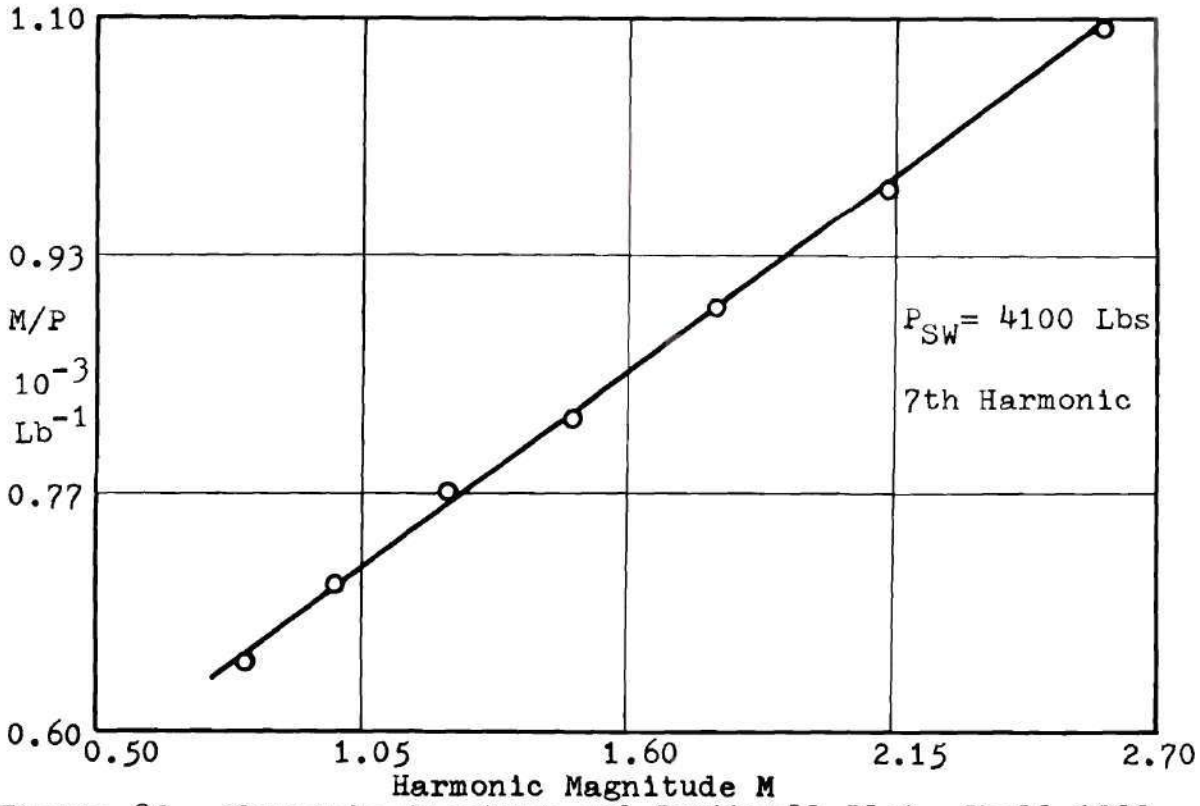

Figure 87. Harmonic Spectrum and Southwell Plot, Shell 1000.

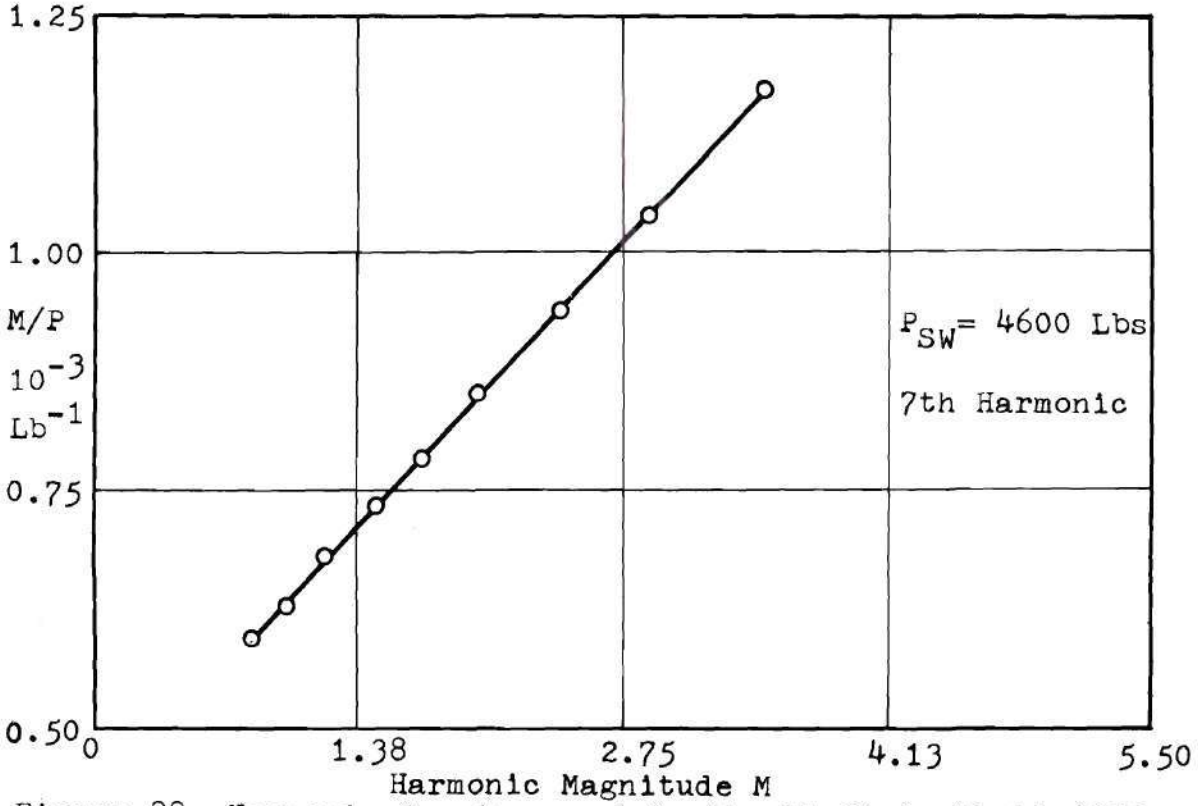

Figure 88. Harmonic Specturm and Southwell Plot, Shell 1002.

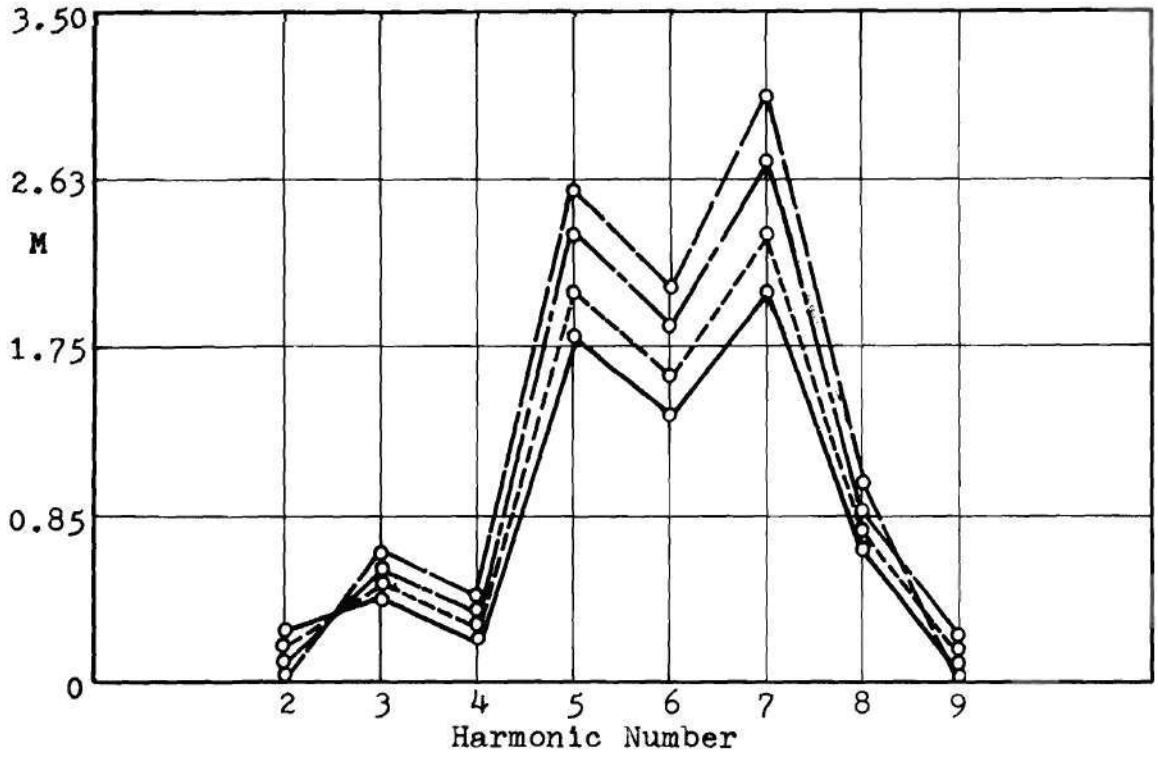

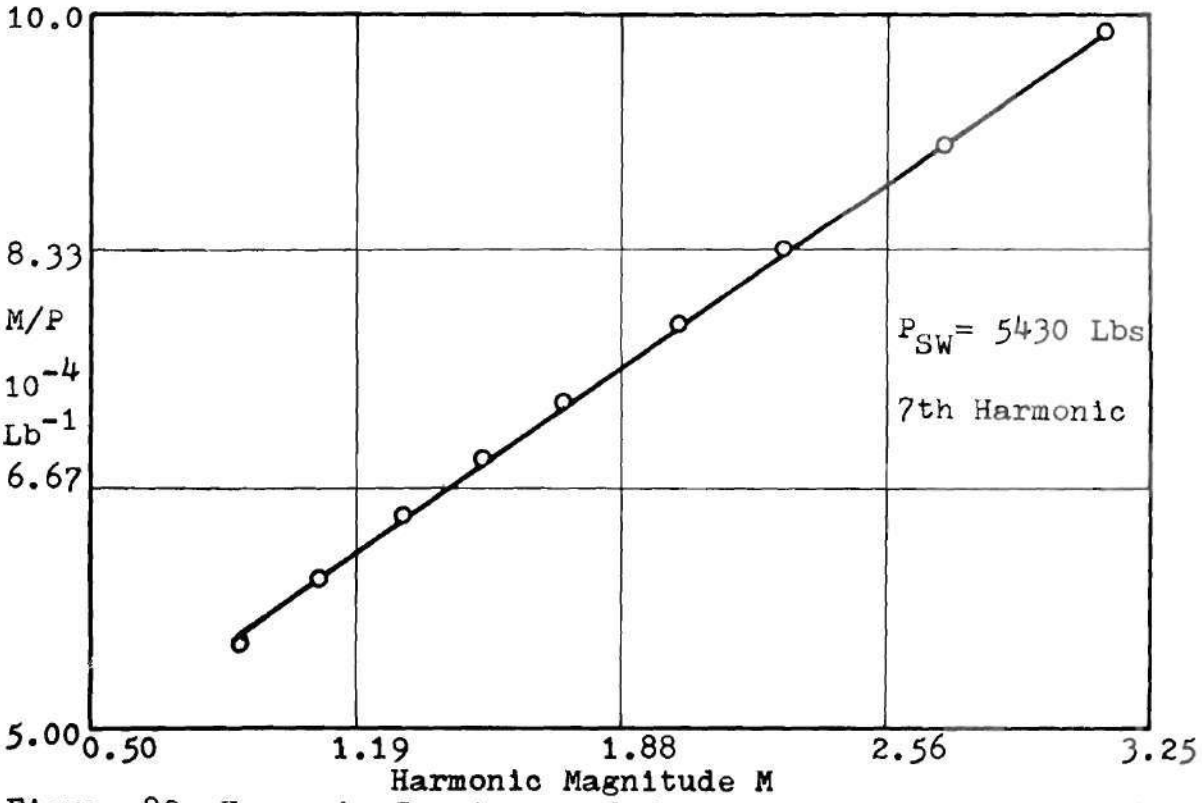

Figure 89. Harmonic Spectrum and Southwell Plot, Shell 1006.

LITERATURE CITED

1. Guggenheim Aeronautical Laboratory, California Institute of Technology, "Some Investigations of the General Instability of Stiffened Metal Cylinders, I, - Review of Theory and Bibliography," NACA TN 905, 1943.

2. Becker, H., "Handbook of Structural Stability, Part VI, Strength of Stiffened Curved Plates and Shells," NACA TN 3786,1958.

3. Flügge, W., "Die Stabilität des Kreiszylindershale," Ingenieur-Archiv, Vol. 3, No. 5, Dec. 1932, p. 463.

4. Van der Neut, A., "The General Instability of Stiffened Cylindrical Shells Under Axial Compression," Report S-314, National Luchvaart-Laboratorium, Amsterdam, Report and Transactions, Vol. 13, 1947, p. 57.

5. Baruch, M., and Singer, J., "Effect of Eccentricity of Stiffeners on the General Instability of Stiffened Cylindrical Shells Under Hydrostatic Pressure," Journal of Mechanical Engineering Sciences, Vol. 5, No. 1, March 1963, p. 23.

6. Block, David L., Card, Michael F., and Mikulas, Martin M. Jr., "Buckling of Eccentrically Stiffened Orthotropic Cylinders," NASA TN D-2960, 1965.

7. Singer, J., "The Influence of Stiffener Geometry and Spacing on the Buckling of Axially Compressed Cylindrical Shells," IUTAM Symposium Copenhagen, Theory of Thin Shells, Editor, F. I. Niordson, 1967.

8. Block, D. L., "Influence of Discrete Ring Stiffeners and Prebuckle Deformations on the Buckling of Eccentrically Stiffened Orthotropic Cylinders," NASA TN D-4283, January 1968.

9. Baruch, M., "Equilibrium and Stability Equations for Discretely Stiffened Shells," Israel Journal of Technology, Vol. 3, No. 2, June 1965, pp. 138-146.

10. Peterson, James P., "Bending Tests of Ring Stiffened Circular Cylinders," NACA TN 3735, 1956.

11. Tenerelli, D. J., and Horton, W. H., "An Experimental Study of the Local Buckling of Ring Stiffened Cylinders Subject to Axial Compression," Israel Journal of Technology, Vol. 7, No. 1-2, 1969, pp. 181-194.

12. Singer, Josef, Arbocz, Johann, and Babcock, Charles D. Jr., "Buckling of Imperfect Stiffened Cylindrical Shells Under Axial Compression, "Proceedings of the AIAA/ASME 11th Structures, Structural Dynamics, and Materials Conference, April, 1970.

13. Dickson, John N., Broillar, Richard H., "The General Instability of Ring Stiffened Corrugated Cylinders Under Axial Compression," NASA TN D-3089, 1966.

14. Peterson, James P., and Anderson, J. K., "Bending Tests of Large Diameter Ring Stiffened Corrugated Cylinders," NASA TN D-3336, 1966.

15. Anderson, James Kent, "Bending Test of Two Large Diameter Corrugated Cylinders with Eccentric Ring Stiffeners," NASA TN D-3702, 1966.

16. Peterson, James P., Dow, Marvin B., "Compression Tests on Circular Cylinders Stiffened Longitudinally by Closely Spaced Z-Section Stringers," NASA Memo 2-12-59L, 1959.

17. Peterson, James P., Whitley, Ralph G., Deaton, Jerry W., Structural Behavior and Compressive Strength of Circular Cylinders with Longitudinal Stiffening," NASA TN D-1251, 1962.

18. Card, Michael F., Jones, Robert M., "Experimental and Theoretical Results for Buckling of Eccentrically Stiffened Cylinders," NASA TN D-3639, 1966.

19. Weller, Tanchum, Singer, Josef, and Nachmani, Shimon, "Recent Experimental Studies on the Buckling of Integrally Stringer Stiffened Cylidrical Shells," TAE Report No. 100, Technion, Israel Institute of Technology, April 1970.

20. Card, Michael F., "Bending Tests on Large Diameter Stiffened Cylinders Susceptible to General Instability," NASA TN D-2200, 1964.

21. Anon, "Tests on Integral Stiffened Ring and Stringer Reinforced Cylindrical Shells," Internal Report, Lockheed Missiles and Space Company, Sunnyvale California, 1963.

22. Milligan, Roger, Gerard, George, Lakshmikantham, C., Becker, Herbert, "General Instability of Orthotropically Stiffened Cylinders," Technical Report AFFDL-TR-65-161, Part I, July 1965.

23. Lakshmikantham, C., Gerard, George, Milligan, Roger, "General Instability of Orthotropically Stiffened Cylinders," Technical Report AFFDL-TR-65-161, Part II, August 1965.

24. Katz, Lester, "Compression Tests on Integrally Stiffened Cylinders," NASA TM-X-53315, 1965.

25. Hoff, N. J., Fuchs, S. J., Cirillo, Adam J., "The Inward Bulge Type Buckling of Monocoque Cylinders II - Experimental investigation of the Buckling in Combined Bending and Compression," NACA TN 939, 1944.

26. Dunn, Louis G., "Some Investigations of the General Instability of Stiffened Metal Cylinders IX - Criterions for the Design of Stiffened Metal Cylinders Subject to General Instability Failures," NACA TN 1198, 1947.

27. Peterson, James P., "Buckling of Stiffened Clinders in Axial Compression and Bending - A review of Test Data," NASA TN-5561, 1970.

28. Shanley, F. R., "Simplified Analysis of General Instability of Stiffened Shells in Pure Bending," Journal of the Aeronautical Sciences, Vol. 16, 1949, pp. 590-592.

29. Young, T., A Course of Lectures on Natural Philosophy and the Mechanical Arts, 1st ed., Vol. II Sect. IX, London, 1807, p. 47.

30. Ayrton, W. E., and Perry, John, "On Struts," The Engineer, Vol. 62, December 10, 1866, pp. 464-465, and December 24, 1886, pp. 513-515.

31. Westergaard, H. M., "Buckling of Elastic Structures," Transactions of the American Society of Civil Engineers, Vol. 85, 1922, pp. 576-654.

32, Horton, W. H., Cundari, F. L., and Johnson, R. W., "A Review of the Applicability of the 'Southwell Plot' to the Interpretation of Test Data Obtained from Stability Studies of Elastic Column and Plate Structures," SUDAAR No. 296, Stanford University, Department of Aeronautics and Astronautics, December 1967.

33. Flügge, W., Stresses in Shells, Springer-Verlag, Berlin, 1960, p. 466.

34. Galletly, G. D., and Reynolds, T. E., "A Simple Extension of Southwell's Method for Determining the Elastic General Instability of Ring Reinforced Cylinders Subjected to External Pressure," Proceedings of SESA, XIII, No. 2, 1956, pp. 141-151.

35. Donnell, L. H., "On the Application of Southwell's Method for the analysis of Buckling Tests," Stephen Timoshenko 60th Anniversary Volumn, McGraw-Hill Book Co., 1938, pp. 27-30.

36. Tuckerman, L. B., "Hetrostatic Loading and Critical Astatic Loads," National Bureau of Standards Research Paper RP 1163, Journal of Research, N.B.S., 22, 1939, pp. 27-38.

37. Craig, J. I. II, "An Experimental Study of Wall Motions in Circular Cylindrical Shells Under Combined Loadings," Doctoral Thesis, 1969, Stanford University.

38. Hamming, Richard W., Numerical Methods for Scientist and Engineers, McGraw-Hill Book Company Inc., New York, 1962.

39. Ralston, A., and Wilf, H., Mathematical Methods for Digital Computers, John Wiley and Sons Inc., New York, 1960.

40. Meyer, R. R., "Buckling of 45 Degree Eccentric-Stiffened Waffle Cylinders," Journal of the Royal Aeronautical Society, Vol. 71, July 1967, pp. 516-520.

41. Modern Plastics Encyclopedia for 1968-69, Vol. 45, Number 14A, October 1968, McGraw Hill Inc., New York, 1968.

42. Arbocz, J., and Babcock, C. D., "The Effect of General Imperfections on the Buckling of Cylindrical Shells," Journal of Applied Mechanics, Vol. 36, Series E., No. 1, 1969, p. 28.

43. Tennyson, D. B., Muggeridge, D. B., and Caswell, R. D., "The Effect of Axisymmetric Imperfection Distributions on the Buckling of Circular Cylindrical Shells Under Axial Compression," Proceedings of the AIAA/ASME 11th Structures, Structural Dynamics, and Materials Conference, April 1970.

VITA

Joseph Scott Ford II was born June 23, 1935, the son of Joseph S. and Ellen B. Ford. He attended high school in Mecklingburg County, North Carolina, graduating in June 1953. He entered the Georgia Institute of Technology in the Fall of that year and completed the requirements for the degree of Bachelor of Aeronautical Engineering in June 1957.

Upon graduation he entered the United States Air Force, serving in the Strategic Air Command as a structural engineer. In June 1961 he entered Stanford University under Air Force sponsorship and received the Master of Science Degree and the Degree of Engineer in Aeronautics and Astronautics in March 1963. After an assignment as an Air Force engineering representative with the Northrup Corporation, he was appointed an Instructor in the Engineering Mechanics Department of the United States Air Force Academy in Colorado in 1966.

He returned to the Georgia Institute of Technology in May 1968 for further study under the faculty enrichment program of the United States Air Force Academy.

Major Ford is married to the former Sandra Torrey and they have one son, Christopher.